CRYSTAL GROWTH OF $KTiOPO_4$

FROM HIGH-TEMPERATURE SOLUTION

by

PETER FRANK BORDUI

S.B., Materials Science & Engineering
Massachusetts Institute of Technology (1983)

S.M., Materials Science
Massachusetts Institute of Technology (1983)

SUBMITTED TO THE DEPARTMENT OF
MATERIALS SCIENCE & ENGINEERING
IN PARTIAL FULFULLMENT OF THE
REQUIREMENTS FOR THE DEGREE OF

DOCTOR OF PHILOSPHY IN CERAMICS

at the

MASSACHUSETTS INSTITUTE OF TECHNOLOGY

February, 1987

Signature of Author _____
Department of Materials Science and Engineering
January 9, 1987

Certified by _____
Gabriel M. Loiacono
Thesis Supervisor

Certified by _____
August F. Witt
Thesis Supervisor

Accepted by _____
Samuel M. Allen
Chairman, Departmental Graduate Committee

Crystal Growth of $KTiOPO_4$ from High-Temperature Solution

by

Peter Frank Bordui

Submitted to the Department of Materials Science and Engineering on January 9, 1987 in partial fulfillment of the requirements for the Degree of Doctor of Philosophy in Ceramics

Abstract

The development of a practical production process for single crystals of the important nonlinear optical material $KTiOPO_4$ was undertaken as a case study in crystal growth from high-temperature solution. Following selection of the previously-reported high-temperature solvent composition $K_6P_4O_{13}$, a preliminary analysis was performed of the expected growth process kinetics. The results of the analysis were applied in establishing design criteria for a furnace system for growth of $KTiOPO_4$ from its solution in $K_6P_4O_{13}$.

Two identical furnace systems were built. They enabled top-seeded growth of $KTiOPO_4$ by a slow cooling process and each featured an annular heat pipe liner providing for a high degree of spatial temperature uniformity in the central furnace cavity. The achieved thermal field enabled avoidance of copious spurious nucleation, a common problem with other furnace systems used in previous attempts to grow $KTiOPO_4$ from solution.

A series of high-temperature viscosity and density measurements was made on $KTiOPO_4$-$K_6P_4O_{13}$ growth solutions employing one of the heat pipe based furnace systems. The gathered data were used in establishing a room-temperature flow visualization facility for experimental analysis of fluid convection patterns prevailing in the crystal growth process. Due to the high degree of spatial temperature uniformity throughout the growing crystal and surrounding solution in using the heat pipe based furnace systems, the possibility of natural buoyancy-driven convection could be neglected with the dynamic similarity flow visualization based strictly on forced convection effects due to imposed crystal rotation.

An extensive set of experiments was devoted to investigation of the effects of seed orientation and attachment, fluid convection, and bulk supersaturation on initial seeded growth using the furnace systems. The preferred seed attachment technique involved ultrasonically drilling and threading a small $KTiOPO_4$ crystal and screwing it onto the end of a threaded platinum seed rod. The achievement of initially uniform and flaw-free growth off a seed crystal was determined to require the controlled dissolution of the original seed surfaces prior to initiation of supersaturation and consequent growth.

An additional set of experiments was devoted to treatment of a chronic flawing problem whereby volumes of growth solution would become trapped and included in growing crystals. Room-temperature flow visualization analyses and crystal growth experiments in the heat pipe based furnace system were correlated through application of a recently-developed qualitative

model of interfacial instability in crystal growth from solution. A crystal orientation configuration was thereby established enabling flaw-free growth of $KTiOPO_4$ crystals to sizes limited only by the dimensions of the furnace cavity.

The overall process developed through the project enables production of the largest flaw-free crystals of $KTiOPO_4$ growable on a routine basis from high-temperature solution. Crystalline plates 10 x 10 x 7 mm^3 oriented in the optimal direction for second-harmonic generation can be fabricated from crystals produced in 10-day growth runs with properties measured to be at least as good as $KTiOPO_4$ crystals grown by other methods.

Thesis Supervisor: Gabriel M. Loiacono
Senior Member of Research Staff, Philips Laboratories

Thesis Supervisor: August F. Witt
Professor of Materials Science

Foreword

The work presented herein was carried out at North American Philips Laboratories, Briarcliff Manor, New York, from June of 1984 through December of 1986. It was performed under the combined auspices of Philips Laboratories and the Department of Materials Science and Engineering of the Massachusetts Institute of Technology, Cambridge, Massachusetts. It is being submitted to the Department in partial fulfillment of the requirements for the Degree of Doctor of Philosophy in Ceramics.

The following presentations, publications, and patent application involve work performed in this thesis project:

"Studies on the Growth of $KTiOPO_4$ from High-Temperature Solution", P.F. Bordui, J.C. Jacco, G.M. Loiacono, J.J. Zola, and R.A. Stolzenberger, ACCG-East, Atlantic City, NJ, October, 1986.

"Viscosity and Density of Solutions Used in High-Temperature Solution Growth of $KTiOPO_4$ (KTP)", P.F. Bordui and J.C. Jacco, accepted for publication by J. Crystal Growth.

"Growth and Properties of Large Single Crystals of $KTiOPO_4$ (KTP) from High-Temperature Solution Using Heat Pipe Based Furnace System", P.F. Bordui, J.C. Jacco, G.M. Loiacono, J.J. Zola, and R.A. Stolzenberger, submitted to J. Crystal Growth.

"Second Harmonic Generation Using Flux-Grown KTP", R.A. Stolzenberger, P.F. Bordui, G.M. Loiacono, and J.C. Jacco, to be presented at CLEO-87, Baltimore, MD, April, 1987.

"Process for Crystal Growth of $KTiOPO_4$ from Solution", P.F. Bordui and G.M. Loiacono, U.S. Patent Application filed, June, 1986.

Acknowledgements

One of the greatest sources of enjoyment for me over the past three years has been my interaction with the many people who have guided, assisted, and supported me in carrying out the research project reported in this thesis. It is with pleasure that I take this opportunity in formally extending my gratitude.

I wish to thank Professor Witt for eight years of guidance and inspiration, dating back to my original decision to pursue the study of materials science. My thanks to Professor Motakef for assistance in dealing with the many transport-related issues encountered in this project. Also, my thanks to Professor Kingery for graciously reviewing my manuscript and serving on my review committee.

I gratefully acknowledge the management of Philips Laboratories for financial support of the entirety of my doctoral program.

I wish to thank the staff of the Philips Laboratories Instrument Shop for their expert work in constructing many of the furnace system components. Also, my thanks to Mike Athanas, Kevin Salotti, Kevin McKeon, and Tony Pink for their expert assistance in preparing seed crystals and in fabricating and polishing grown specimens for testing.

Myron Frommer and Tom McGee deserve thanks for their surface analytical work in attempting to track down the seed degradation problem.

Thanks to George "The Baron" Kostecky for technical assistance at various stages of the project and for putting up with an enormous amount of good-natured abuse. Also, my thanks to Dick Stolzenberger for performing the optical characterization experiments on the grown crystals.

My thanks to John Zola for his expert but patient guidance and assistance, particularly in the design of the furnace system and in addressing various issues regarding seed fabrication.

I owe a great deal of thanks to John Jacco with whom I have been fortunate to associate as both a personal friend and a professional colleague. At numerous stages in the project, his input and assistance proved critical to its final successful completion.

My greatest debt is to Gabriel Loiacono for inspiration, support, and guidance that have influenced all aspects of my professional life, including this thesis project but extending far beyond it. I hope I may one day be able to help someone else the way he has helped me.

On a personal level, my parents deserve a large fraction of the credit for anything I might ever accomplish. Also, my thanks to Carol Tate for her friendship and backing over the past several years. Finally, my thanks to Anja for her inspiration and patient support.

Peter Bordui
Briarcliff Manor, New York
December, 1986

Table of Contents

List of Figures

List of Tables

Chapter 1

Background & Introduction

1.1 Crystal Growth from High-Temperature Solution

In the growth of single crystals from high-temperature solution (HTS), the material to be crystallized is dissolved in a suitable solvent and crystal growth occurs as a result of induced supersaturation. Growth may occur on a seed crystal or following induced nucleation. Supersaturation may be effected by solvent evaporation, slow cooling of the solution, establishment of a transport process in which solution flows from a hotter to a cooler region, or a combination of these methods. Although "HTS crystal growth" is not precisely defined, normal process temperatures range between 300° and 1800°C and solute concentration values usually range between 10 and 80 mole%. Most HTS growth processes result in facetted crystals. Typical linear growth rates are on the order of several millimeters per day.

As discussed by Elwell and Scheel [1], probably the greatest strength of HTS crystal growth is its broad applicability. For producing single crystals of a desired phase, a potential high-temperature solvent can usually be found. Also noted in the same reference is the fact that, in some cases, crystals of more desirable quality can be grown from HTS than by any other feasible method.

Typically, however, growth from HTS is considered a "last resort" technique. In only few cases have intensive efforts been made to grow crystals larger than a few grams in weight [1]. Process conditions for HTS growth are normally chosen by intuition or experience based on trial and error [2]. Not surprisingly, the results of HTS growth processes are often less than satisfactory, with copious spontaneous nucleation in supersaturated solutions and solution inclusions in grown crystals being particularly common problems.

The basis for its lowly status can probably be best illustrated by comparing HTS growth with other crystal growth methods. Considering the various melt growth techniques, although they commonly involve technical difficulties associated with the typically high operating temperatures, in the area of growth mechanistics they are generally relatively simple. Most melt growth processes may be characterized as dominated by heat transfer. As such, to a large extent, controlling a melt growth process amounts to controlling the heat transfer. Temperature is the single most important dependent process variable, and the growth interface can be taken to be the melting point isotherm.

Considering the contrasting case of crystal growth from aqueous solution, here the growth mechanistics are usually much more complex. Although the heat transfer process is often negligible in determining the growth rate, both the bulk mass transfer process and the network of interface attachment steps play important roles. Here, however, because of the low operating temperatures, relatively sophisticated experimental techniques can be brought to bear to aid in controlling a fundamentally subtle and sensitive process. Thus, accurate solution monitoring schemes can be set up, elaborate stirring and seed-holding mechanisms can be employed, and, to investigate directly the interface attachment processes, complementary interference microscopy experiments can be carried out. Perhaps most important is the fact that an operator can usually see clearly into a crystallizer, enabling direct feedback on the effect of varying process conditions.

Crystal growth from HTS may be thought of as featuring the combined disadvantages of melt growth and aqueous solution growth. As with aqueous solution growth, the kinetics of growth from HTS tend to depend critically on several different but interrelated sub-processes. Thus, understanding, modelling, and controlling an HTS growth process is fundamentally challenging. With operating temperatures as high as or higher than those commonly encountered in melt growth, however, there are severe restrictions placed on the range of experimental techniques that can be used to help address the challenge. With hot and often highly corrosive

solutions, in situ solution monitoring techniques are in many cases all but impossible. Seed holding and stirring techniques must be mechanically simple. Operating above 500 °C, the ±0.005 °C temperature control band common to aqueous solution growth systems is, at present, experimentally unattainable. Visual inspection of a growth process is always restricted and often impossible.

Nevertheless, because of its potential usefulness, general development of both theoretical understanding and technical facility in HTS crystal growth is desirable. Consensus among those who have commented on the subject is that, at present, such development requires the establishment of model systems where novel techniques are explored and prevailing theory is meaningfully tested. Such systems should presumably involve both recent advances in process technology and relevant theoretical insights developed in other areas to aid in establishment of experiments with definable boundary conditions. Also cited as important is the acquisition of physical property data requisite to meaningful modelling and analysis.

1.2 History of $KTiOPO_4$ and Its Growth as a Single Crystal

Potassium titanyl phosphate, $KTiOPO_4$ (often referred to as "KTP"), was discovered in 1890 [3]. Its structure was analyzed in the early 1970s [4,5]. In 1976, property measurements were reported that identified $KTiOPO_4$ as an attractive non-linear optical material, particularly for frequency doubling of 1060 nm radiation from the Nd:YAG laser [6]. Recently, further data have been reported that indicate the suitability of $KTiOPO_4$ for both electro-optic modulation and integrated optic applications as well [7].

The structure of $KTiOPO_4$ belongs to the acentric orthorhombic point group m2m and the space group $Pn2_1a$. Single crystals of $KTiOPO_4$ exhibit high non-linear optical coefficients, high optical damage threshold, and low phase matching temperature sensitivity. Uncontaminated crystals are optically transparent from 350 nm to 4500 nm. Crystals may be relatively easily

machined and polished, and are both insensitive to moisture and chemically stable under typical application conditions.

Large-scale application of $KTiOPO_4$ has been prevented mainly by the scarcity of high-quality single crystals. $KTiOPO_4$ decomposes to TiO_2(s) and KPO_3(l) at roughly 1160 °C, precluding the possibility of crystal growth from the melt. Initial patents covering $KTiOPO_4$ production involve both HTS and hydrothermal crystal growth methods [8,9]. Although several embodiments of each of these two approaches have been pursued, no other general crystal growth method has ever been reported for production of $KTiOPO_4$.

Initial attention focused mainly on hydrothermal growth. Most of the early measurements on $KTiOPO_4$ were performed on hydrothermally grown crystals. To date, the only commercially available $KTiOPO_4$ crystals are grown by a hydrothermal process. In this process, nutrient made by reaction of KH_2PO_4 and TiO_2 is combined with water and sealed in a gold-lined autoclave. Crystal growth takes place at an autoclave pressure of about 25 kpsi and a temperature around 600 °C with an internal temperature gradient of roughly 50 °C. Details of the process are covered in the reference by Gashurov and Belt [10].

As is clear from the continued scarcity of high-quality $KTiOPO_4$ crystals, this hydrothermal process currently in use for $KTiOPO_4$ production is less than satisfactory. Six weeks are required for production of crystals yielding flaw-free cubes no larger than 5 mm on an edge. Moreover, due to inherent mechanical problems in scaling up the size of the high-pressure growth vessels, the prospects for greatly increasing the achievable crystal size are not good [11]. A new hydrothermal $KTiOPO_4$ growth process was recently reported by Laudise et. al. [12]. Due to higher solubilities at lower pressures, the maximum achievable crystal size may be increased. Remaining, however, with any hydrothermal process is the problem of slow growth rate if large crystals are needed. Also, OH^- ions are incorporated into all hydrothermally-grown

crystals. The problems this may cause have not yet been fully examined. Further, in regard to potential future application of $KTiOPO_4$ in integrated optical structures, hydrothermal growth methods do not lend themselves well to production of epitaxial crystalline films.

Including one of the patents on $KTiOPO_4$ production, as of the start in 1984 of the work reported herein, there were but two reports on the subject of $KTiOPO_4$ growth from HTS [8,13]. Both reports concerned the growth of $KTiOPO_4$ from its solution in potassium phosphate melts at temperatures between 750° and 1050°C. Seeded growth and growth following induced nucleation were reported. Preliminary work on a variety of slow cooling and gradient transport techniques was discussed. The largest clear crystals obtained were several millimeters on edge. Report was made of initial attempts to grow $KTiOPO_4$ in a rotatable spherical platinum crucible equipped with an accelerated rotation capability. The system followed an earlier design reported by Tolksdorf and Welz [14]. The best crystals grown measured 5 x 7 x 12 mm^3 and contained solution inclusion flaws. Spurious nucleation was identified as a serious difficulty.

In the several years that the present work has been in progress, further work on HTS growth of $KTiOPO_4$ has been reported. Experiments using the spherical crucible technique have continued [15]. Although the size and quality of the grown crystals have improved, both spurious nucleation and solution inclusions in grown crystals continue to plague the process. Moreover, due to the near impossibility of satisfactorily understanding the thermal boundary conditions in the system, modelling and analysis essential to efficiently addressing these problems are severely hampered.

So-called "top-seeded" solution growth techniques whereby a seed is lowered into the growth solution from above have been reported by groups in both the Soviet Union [16,17] and the People's Republic of China [18,19]. All groups report use of potassium phosphate as a solvent. Although details are sketchy, it appears that the largest flaw-free single-crystalline volumes obtained in any of these works measure less than 5 x 5 x 5 mm^3.

Also notable is the recently reported work by Ballman et. al. [20] in which $KTiOPO_4$ is grown from its solution in a melt consisting of a solution of potassium phosphate and potassium tungstate. It is claimed that the lower viscosity of the tungstate-based solution relative to the pure potassium phosphate is a benefit to crystal growth. So far, only small crystals have been reported. They have been measured to contain significant concentrations of tungsten [21]. Although the effect of tungsten on relevant material properties is not yet known, this must be considered a potential problem.

1.3 Scope of Research and Organization of this Report

The research presented in this thesis consisted of the development, analysis, and improvement of a practical process for crystal growth of $KTiOPO_4$ from high-temperature solution. The goal of the work has been to address issues presented in both Sections 1.1 and 1.2. On one hand, it is hoped that the present project will serve as a well-developed case study, shedding desired light on the nature and development of HTS crystal growth processes in general. On the other hand, it is expected that the information acquired and techniques established will lead to an improved technological capacity for producing high-quality single crystals of this important optical material.

Chapter 2 presents a furnace system specifically designed and constructed for crystal growth of $KTiOPO_4$ from its solution in $K_6P_4O_{13}$ within a temperature range of 900° to 1000°C. The basis for the design, construction details, and thermal characteristics are presented, along with discussion of advantages offered by the system over other systems previously used for HTS growth of $KTiOPO_4$. Chapter 3 presents some of the secondary apparatus and techniques attendant to growing $KTiOPO_4$ using this furnace system.

Chapter 4 covers viscosity and density measurements performed on solutions encountered in the growth process. The measurements were performed in the same furnace system used for

growth. Viscosity and density data serve the dual roles of first, elucidating the solution structure and, thus, the growth mechanism, and, second, enabling accurate modelling of transport phenomena occurring during the growth process.

Chapter 5 presents the details of a room-temperature flow visualization process established to aid in investigating fluid convection patterns prevailing during crystal growth. Chapter 6 considers the initial stages of seeded growth in the system. Results of investigations into the influence of seed orientation and attachment, fluid convection, and bulk supersaturation are presented.

A chronic undesirable flawing phenomenon was encountered during the growth experiments. Specifically, interfacial instability led to formation of bands of occluded solution in crystals in advanced stages of growth. Chapter 7 presents work devoted to analysis and avoidance of this problem, involving correlation between crystal growth experiments and flow visualization studies.

Chapter 8 presents characterization data from standard analyses performed on single-crystalline $KTiOPO_4$ material grown over the course of the project. The analyses include IR and UV/visible spectroscopy, spark source mass spectroscopy, and measurement of conversion efficiency for frequency doubling of 1.06 μm Nd:YAG laser output.

Chapter 9 is an attempt to summarize the present work and put it in perspective in the context of both HTS crystal growth in general and $KTiOPO_4$ production in particular.

Chapter 2

Furnace System

2.1 Introduction

In developing a crystal growth process for a given material, the design or selection of the furnace system is generally the single most important step. This is primarily because the nature of the furnace system determines both the achievable ranges of and the degree of controllability over all the basic process parameters. No furnace system can be infinitely flexible in providing for an unlimited range of tightly controllable process conditions. Consequently, compromises are necessarily embodied in the furnace system design even prior to the start of the first growth experiments. An inappropriate set of compromises corresponding to an ill-suited furnace design can doom a project to failure.

In cases where the ability to model or quantitatively analyze some aspect of a growth process is critical to further development of that process, it is particularly important that the furnace system allow for the definability of boundary conditions relevant to such modelling or analysis. Following the considerations of Section 1.1, this is especially significant for furnace systems developed for crystal growth from HTS, where modelling and analysis take on added importance due to inherent limitations on experimental techniques for more direct measurement or control.

Secondary to the above considerations but worthy of note is the fact that a furnace system must be relatively easy and efficient to operate and not prone to chronic breakdown. Given a necessarily finite amount of effort budgeted for development of any crystal growth process, the less effort spent on routine operation and maintenance, the greater the likelihood of success.

This Chapter presents a furnace system developed specifically for HTS crystal growth of

$KTiOPO_4$. Following a brief discussion of the chosen high-temperature solvent, the general requirements that led to the furnace system design are considered. Design and construction details are then presented followed by discussion of operating characteristics and performance features.

2.2 Selection of $K_6P_4O_{13}$ as Solvent

The high-temperature solvent selected for the growth of $KTiOPO_4$ in this work was a potassium phosphate melt denotable as the composition $K_6P_4O_{13}$. The formula $K_6P_4O_{13}$ as used here denotes strictly a liquid composition; no crystalline $K_6P_4O_{13}$ phase is implied or even suspected to exist. $K_6P_4O_{13}$ can be thought of as a liquid solution of KPO_3 and $K_4P_2O_7$. It can be made by heating together an equimolar ratio of KH_2PO_4 and K_2HPO_4. The liquidus for the $K_6P_4O_{13}$ composition occurs at roughly 815 °C [22].

The choice of a potassium phosphate solvent was based on the desire for a relatively low melting point solvent containing no species foreign to $KTiOPO_4$. The particular choice of the composition $K_6P_4O_{13}$ was based on preliminary work involving a range of potassium phosphate compositions between KPO_3 and $K_4P_2O_7$ [23]. Despite initial reports of difficulties encountered in crystal growth experiments involving this solvent [13,15], none of the data indicated clear and unavoidable problems inherent in the use of the solvent itself.

The choice of $K_6P_4O_{13}$ as the high-temperature solvent largely defined the properties of the $KTiOPO_4$ growth solutions. A number of these properties were particularly relevant to the furnace system design. First, the volatility of the growth solutions in air was known to be low but measureable at temperatures of 1000 °C or less. Specifically, volatilization of the same growth solution from open crucibles held at 1000 °C was reported to be about 1% by weight after 5 days [24]. The volatile species was KPO_3. It was thus felt that the growth solutions need not

be contained in sealed crucibles but that at the same time, furnace components that could suffer from corrosion due to long-term exposure to the volatilization product should be protected. Second, the glassy solid formed along with $KTiOPO_4$ upon cooling a growth solution to room temperature is water soluble. Thus, no provision needed to be made for a way to jettison the hot solution in separating it from grown crystals or emptying crucibles. Third, the only practical material for crucibles and submersible hardware was found to be pure (99+%) platinum. All other materials tested indicated an unacceptable degree of chemical attack by the growth solution, implying contamination of grown crystals at the very least. Fourth, the solubility of $KTiOPO_4$ in $K_6P_4O_{13}$ was known to range between roughly 0.5 and 0.8 grams solute per gram solvent between 900° and 1000°C, respectively [24]. Finally, based on previously estimated values for density and Newtonian viscosity [24], the kinematic viscosity of a saturated solution could be estimated to be approximately 0.25 cm^2/sec at 1000°C. The role of these solubility and viscosity data in designing the furnace system will be seen in the next Section.

2.3 Development of Furnace System Design Criteria

To be effective, a furnace system must be tailored to the kinetics of the crystal growth process to be developed. However, since development of the growth process is the very objective, there are necessary limits on what can be known at the outset concerning its kinetics. Nevertheless, armed with background physical data, basic crystallization principles, and information from related efforts, insights can be drawn concerning the nature of the kinetics of a proposed process. These insights can in turn be used to guide the design of the furnace system.

In their most general form, the kinetics of any process of crystallization from a fluid phase involve three steps in series, the second of which consists of one or more of three parallel steps, specifically:

1. Bulk mass transport of "growth units" (atoms, molecules, or ions)

through the fluid to the growing interface by convection, diffusion, or both.

2. Interface attachment which can include adsorption, surface diffusion, and desolvation, and which, with simplifying assumptions, is usually considered to take place by one or more of the following mechanisms:
   a. Normal (Wilson-Frenkel) growth on an atomically rough surface.
   b. Surface nucleation on an atomically smooth surface.
   c. Growth on spiral surface steps generated by screw dislocations intersecting an otherwise atomically smooth surface.

3. Removal of the heat of crystallization by conduction, convection, or radiation.

This general process of crystallization from a fluid can be represented by an electrical circuit analog, as shown in Figure 1. Here, the kinetic steps listed above are represented as resistances, with the more complex interface attachment mechanisms being represented by small resistive networks. The bulk supersaturation, the driving force for the crystallization process, is represented as the voltage source in the circuit analog. The possibility of nucleation and growth of undesired spurious crystals is represented in the circuit by a Zener diode, allowing a low resistance short-circuiting of the voltage source, should the voltage exceed some threshold level. The crystal growth rate is represented as the current through the circuit.

Understanding the kinetics of a proposed crystallization process to the extent necessary to guide the design of an effective furnace system amounts to being able to ascribe values, or at least relative values, to the resistances in the circuit analog. In the case of the interface attachment process, it is generally sufficient to treat the network shown in Figure 1 as a single equivalent resistance to be compared with the resistances associated with the mass transport

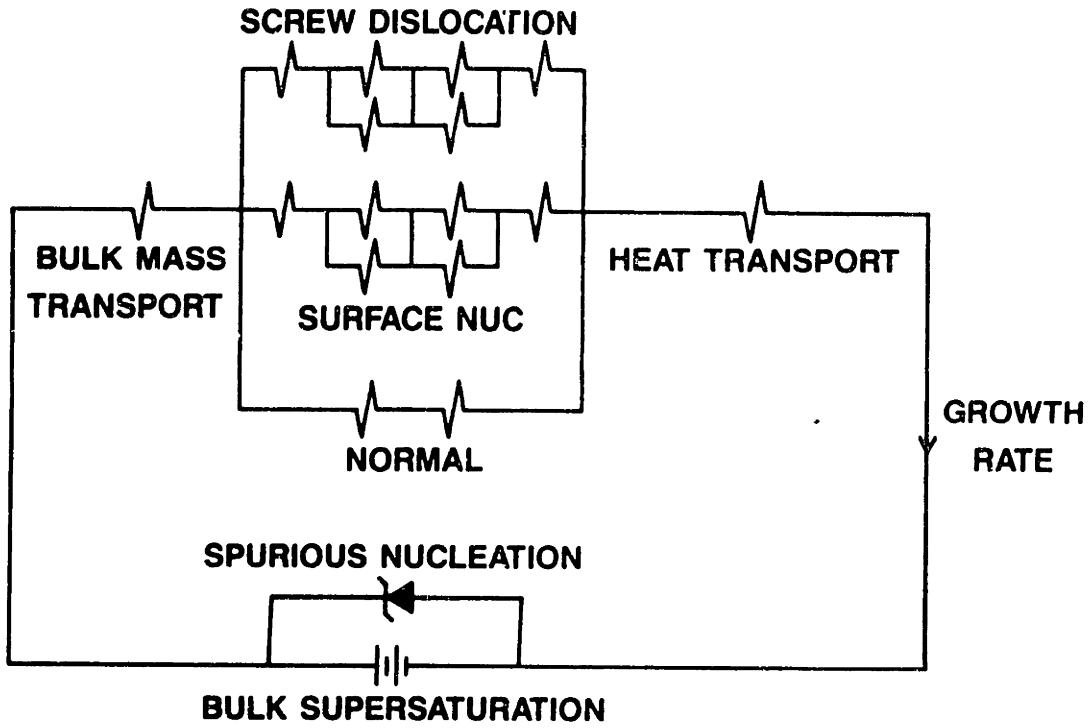

Figure 1. Electrical circuit analog of generalized crystallization kinetics

and heat transport processes.

Ideally, one could write a single equation representing the generalized growth kinetics, insert known values of physical property parameters, and determine directly by inspection the nature of the kinetics of a proposed growth process. Unfortunately, this is impossible at present. Although such equations have been derived, albeit involving numerous simplifying assumptions (see, for example, the work by Gilmer, Ghez, and Cabrera [25]), much of the physical data required for numerical evaluation are typically hard to specify within an order of magnitude. Insight into kinetics must therefore be gained through a much more approximate intuitive approach.

Considering in this fashion the kinetics of $KTiOPO_4$ crystallization from its solution in $K_6P_4O_{13}$, it was at the outset reasonable to suppose that the kinetic resistance associated with the interface attachment process would be significant. Initial work on HTS growth of $KTiOPO_4$ using potassium phosphate solvents resulted in the formation of strictly facetted crystals [13,15]. In general, formation of macroscopically facetted crystals indicates that the corresponding interface attachment process involves atomically smooth surfaces and presents a kinetic resistance of at least the same order as the resistances associated with heat transport and mass transport. By way of explanation, it may be considered that if the interface attachment resistance were not significant in comparison to either the mass transport or heat transport resistances, the solid/liquid interface corresponding at any time to the macroscopic shape of the growing crystal would reflect the form of the thermal or concentration fields. That either of these would assume the regular, polygonized form corresponding to the growth habit of a facetted crystal would be most unlikely.

Regarding the kinetic resistances associated with the mass transport and heat transport processes, it has been shown by Nielsen [26] that these can be compared through estimating the value of the expression kRT^2/ CDL^2, where k is the thermal conductivity of the fluid, R the gas

constant, T the absolute temperature, C the bulk concentration in the fluid of the crystallizing species, D the diffusivity of the crystallizing species through the fluid, and L the heat of crystallization. If the expression is much less than 1, then heat transport kinetic resistance is much greater than the mass transport kinetic resistance. If the expression is much greater than 1, then the reverse is the case. For a value of the expression within an order of magnitude equal to 1, the two kinetic resistances are approximately equal. Substitution of a combination of reported and estimated values for $KTiOPO_4$ crystallization from solution in $K_6P_4O_{13}$ into the expression yielded a value of roughly 1000, indicating mass transport dominance. A second calculation involving extreme values purposely chosen to favor the significance of the heat transfer process yielded a value of roughly 500. It was thus reasonable to suppose that the kinetic resistance associated with heat transport could be safely ignored.

A further question concerned the significance of the mass transport process relative to the interface attachment process. Based on the considerations so far presented, the interface attachment kinetic resistance is clearly significant while the kinetic resistance associated with mass transport has merely been shown to be much greater than that associated with heat transport. The question remained as to whether the mass transport kinetic resistance would itself be of a great enough magnitude to be considered along with that of interface attachment in considering the overall process kinetics.

Here insight was gained from work reported in the area of crystal growth from aqueous solution. There were a number of studies reported on aqueous solution crystal growth systems in which direct comparison was made between the kinetic resistances associated with the interface attachment and mass transport processes [27-30]. It was found in these studies that the two resistances were usually roughly equal in magnitude and therefore both significant in considering overall process kinetics. The only condition under which one of the two was clearly dominant was that of a very high Reynolds number, where then the mass transport kinetic resistance decreased to a negligible level.

In the case of $KTiOPO_4$ crystallization from $K_6P_4O_{13}$, the kinematic viscosity of the growth solution was known to be at least 25 times greater than that typical of aqueous solutions. Also, in an HTS process, due to limitations on the sizes and design complexity of stirring and seed rotation devices, the relative crystal/solution flow velocities typically achievable are much less than those in aqueous solution growth. Thus, the highest Reynolds numbers achievable in $KTiOPO_4$ crystallization would most likely be much smaller than those found necesary in the aqueous solution growth studies to reduce mass transport kinetic resistance to a negligible level. It might therefore be supposed that the mass transport kinetic resistance in the proposed $KTiOPO_4$ crystallization process would have to be assumed at the outset to be significant.

For this conclusion by analogy between HTS and aqueous solution growth to be strictly valid, however, it would be necessary for the interface attachment kinetic resistance in the HTS process to be of comparable or lesser magnitude than that for the cited aqueous solution growth examples. Otherwise, the inferred higher mass transport resistance in the HTS process might be swamped out by an even greater difference in the interface attachment resistances, with the overall HTS growth kinetics still dominated by interface attachment.

It was unfortunately difficult to draw meaningful comparisons here between the aqueous solution growth interface attachment kinetics and those for the $KTiOPO_4$ growth process under consideration. The argument might be advanced that, since any interface attachment process involves a number of thermally activated steps, the process occurring at higher temperature, in this case $KTiOPO_4$ growth, is likely to feature lower interface attachment kinetic resistance. Irrespective of the validity of such an argument, no evidence was found suggesting that the $KTiOPO_4$ interface attachment kinetics should be supposed to be higher than that for the aqueous solution growth experiments. It was thus reasoned that, in the absence of further data, the crystallization of $KTiOPO_4$ from its solution in $K_6P_4O_{13}$ should be taken for purposes of furnace design as representing a case of mixed interface attachment and mass transfer kinetic control.

The final step to be made in the kinetic analysis of $KTiOPO_4$ crystallization was an estimate of its overall kinetic resistance relative to some other previously studied crystallization system, for example, growth of single crystalline silicon from its melt. Melt growth of silicon is well known to be dominated by heat transfer. Thus, in the simplified circuit analog for the overall silicon crystallization process, the only resistance is that associated with heat transfer. The absolute magnitude of this resistance, however, must be supposed for several reasons to be less than or at most equal to the heat transfer kinetic resistance associated with HTS growth of $KTiOPO_4$. First, the oxide solution can be assumed to have a lower thermal conductivity than liquid silicon. Second, with much higher kinematic viscosity, convective heat transfer would presumably be slower in the HTS process. Finally, radiative heat transfer should be less effective in the lower temperature HTS process. Thus, the dominant kinetic resistance in silicon crystallization is smaller than a resistance supposed to be negligibly small in determining the overall kinetic resistance of the proposed $KTiOPO_4$ growth process. Therefore, the overall kinetic resistance in the proposed growth of $KTiOPO_4$ could be expected to be vastly greater than that typically encountered in silicon melt growth.

To summarize the preliminary considerations of the kinetics of the proposed $KTiOPO_4$ crystallization process, they were expected to be dominated by a combination of interface attachment and mass transport control, and the overall kinetic resistance to growth was expected to be relatively large. Combining these findings with knowledge of the earlier-mentioned growth solution properties, furnace system design criteria were readily forthcoming. First, in light of the magnitude of the overall kinetic resistance to growth, it was clear that in order to achieve a viable linear crystal growth rate on the order of millimeters per day, the process would need to be driven by a significant bulk supersaturation level.

Due to the high kinetic resistance associated with the interface attachment process, it was reasonable to assume that, although in violation of the constitutional supersaturation criterion

[31], a bulk supersaturation condition could be tolerated without catastrophic interfacial breakdown, and the growing crystal could be totally submerged in solution. Further, the high viscosity and glass forming tendencies of the growth solution indicated that the kinetic barrier to spurious nucleation should be high enough to allow a bulk supersaturation condition to be successfully maintained.

As in the case of crystal growth from aqueous solution where the attainment and maintenance of a significant bulk supersaturation level is common, it was clear that spatial temperature uniformity throughout the region of the growing crystal would be desirable for avoiding spurious nucleation. In a supersaturated solution, spatial temperature variations are well known to lead tc spatially local supersaturation variations which, upon reaching a critical level, result in nucleation of undesirable spurious crystals. Temporal temperature stability was also seen to be desirable. Sharp temporal fluctuations in temperature effect spatial variations and, further, are known to promote interfacial instability when growing with a significant bulk supersaturation level [31].

It was clear from both preliminary solubility data on the chosen growth solution and previously reported growth experiments that the thermal variation of $KTiOPO_4$ solubility in $K_6P_4O_{13}$ could be adequately exploited in establishing the desired bulk supersaturation condition. Due to the high kinematic viscosity of the growth solution and the supposed technical difficulty in spatial temperature control, it was decided that a cooling process would likely be more effective than a gradient transport process for controlling the supersaturation level.

To lower the supposedly significant mass transport kinetic resistance, relative motion between the growing crystal and the growth solution was thought to be a necessity. Thanks to the possibility of leaving the solution uncovered, it was decided that such motion could be effected through use of a "top-seeded" technique, whereby the growing crystal would be supported in the growth solution from above on a translatable and rotatable mechanism. Such a

growth process would be initiated by affixing a small previously-formed seed crystal to the mechanism and lowering it into the solution. It was believed that such a top-seeded technique would result in more effective and more controllable bulk mass transport than would an accelerated crucible rotation technique. It was also noted that spatial temperature uniformity already cited as desirable should greatly aid in modelling and analysis of the bulk mass transport profile since natural thermal convection would be essentially eliminated. A final assumption concerning the desire to lower the mass transport kinetic resistance was that, consistent with other technical considerations, the growth temperature should be as high as possible in order to lower the kinematic viscosity of the growth solution.

To summarize this lengthy but key Section, preliminary kinetic analysis combined with knowledge of growth solution properties indicated that the preferred furnace system for HTS growth of $KTiOPO_4$ from $K_6P_4O_{13}$ should feature slow cooling, spatial temperature uniformity throughout the growth solution, tight temporal temperature control, and a "top-seeded" seed-holding and stirring configuration.

2.4 Furnace System Design and Construction

The furnace system developed for crystal growth of $KTiOPO_4$ from its solution in $K_6P_4O_{13}$ is represented in Figures 2, 3, and 4. The key component in the furnace system is a sodium-filled Inconel heat pipe. The pipe, made by Dynatherm, Inc. [32], is 61 cm long with a 10.2 cm inner diameter and a 14.1 cm outer diameter. Within the partially hollow walls of the heat pipe is contained an open channelled wicking structure filled with metallic sodium. Within the operating temperature range of the heat pipe, the sodium exists in both the liquid and vapor phases. Highly efficient heat transfer is effected through vaporization of the sodium liquid in locally hot regions and pressure-driven flow of the vapor to relatively cool regions where condensation occurs. Continuous passive operation is effected by an opposed surface tension driven flow of the liquid through the wicking structure. A number of references may be consulted for further

general information on heat pipe operation [33]. Resultant effective thermal conductivities are several orders of magnitude higher than the best metallic conductors. The net effect is that the central cavity within such a heat pipe heated from the outside exhibits high degrees of spatial temperature uniformity and stability, largely independent of the heating geometry.

The use of heat pipes to achieve improved thermal field control has been reported in crystal growth from the melt [34-35] and by liquid phase epitaxy. As of the start of this project, there was no previous report of the use of heat pipes in bulk crystal growth from HTS.

As shown in Figure 2, the heat pipe is oriented vertically and supported by a stainless steel stand-off, 12.7 cm long with a 9.5 cm inner diameter and a 14.0 cm outer diameter. The stand-off is in turn supported on a circular base plate 41 cm in diameter by 1.3 cm thick and made of fused silica [36]. Machined ceramic spacers provide thermal barriers above and below the stand-off. Silica cloth cut-outs provide evenly distributed bearing surfaces at all regions of contact. The silica base plate rests on an aluminum support plate, 46 cm in diameter by 1.3 cm thick.

A cylindrical silica glass pedestal supported by the upper ceramic spacer extends up into roughly the center of the heat pipe cavity, as shown in the figure. The pedestal is 25 cm in length with an 8.0 cm inner diameter and an 8.5 cm outer diameter.A machined ceramic crucible support plate fits into the top of the cylindrical silica pedestal. Three Type S platinum-sheathed thermocouples are mounted flush with the top of the crucible support plate, one in the center, one at a 1.8 cm radius, and the third at a 3.2 cm radius opposed to the second. The leads for the three thermocouples exit through the bottom of the furnace, as shown. Both the silica pedestal and the stainless steel stand-off are filled with coiled blankets of insulation.

A silica glass cylinder, 60 cm long with a 9.0 cm inner diameter and a 9.5 cm outer diameter, serves as a liner to protect the inner wall of the heat pipe from potentially corrosive volatilization products from the growth solution. It has a flanged upper end allowing it to be directly

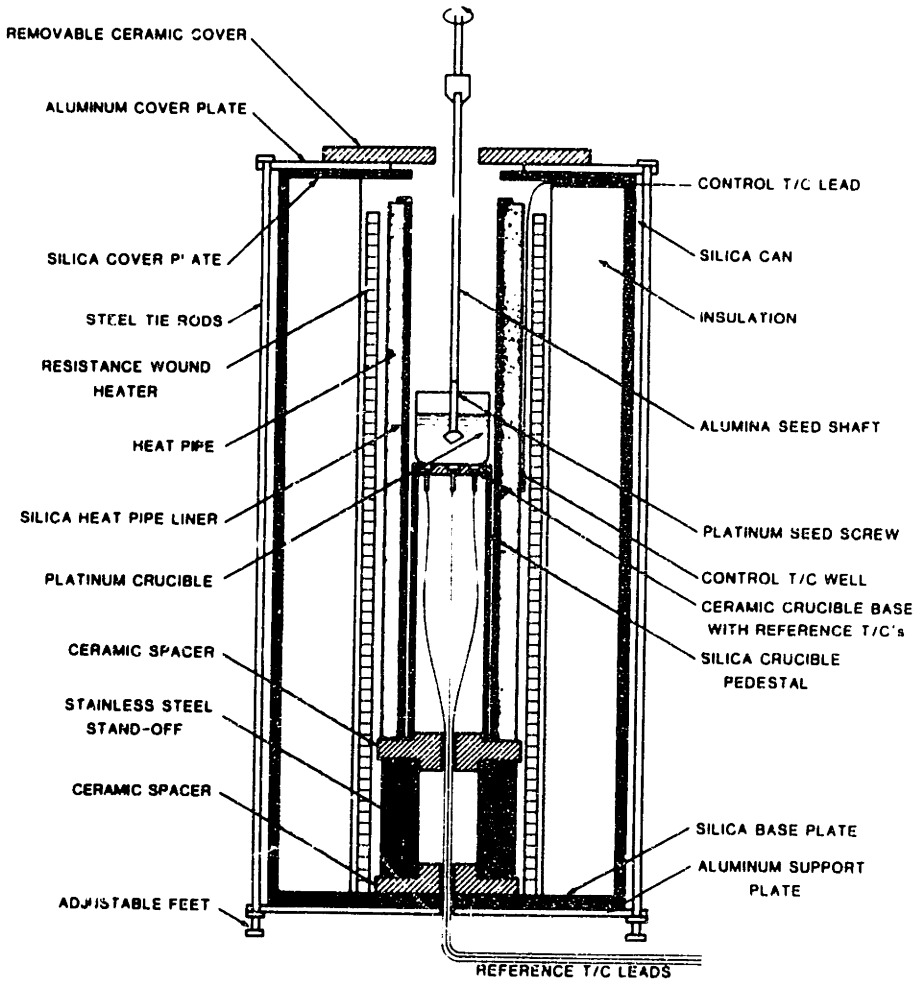

Figure 2. Heat pipe based furnace system (schematic)

supported by the upper end of the heat pipe.

A pair of resistance wound clam-shell heaters [37], 46 cm long with a 15 cm inner diameter are positioned immediately adjacent to the outside of the heat pipe. The heating elements are Super-Kanthal, held in place in the channelled inner walls of the ceramic shells by ceramic packing cement. The heaters are supported by two 15 cm long unheated ceramic half-shells of the same diameter which in turn rest on the silica base plate.

Six nested cylinders of alumino-silicate insulation [38] are positioned immediately adjacent to the outside of the clam-shell heaters. The total cylindrical insulation package measures 81 cm in height with a 16.5 cm inner diameter and a 37 cm outer diameter and is supported by the silica base plate.

A fused silica can [39], 81 cm in height with a 38 cm inner diameter and a 41 cm outer diameter, serves as the outer wall of the furnace. It rests on the silica base plate. Resting on the silica can is an annular fused silica cover plate [36], 6.4 mm thick and 41 cm in diameter with a 13 cm diameter hole through its center. A set of notches cut 5 mm deep into the upper edge of the silica can and spaced evenly around its circumference allows for the passage of the heater leads between the can and the silica cover plate.

An annular aluminum cover plate, 6.4 mm thick and 46 cm in diameter with a 26 cm diameter hole through its center, rests on the silica cover plate. Four stainless steel tie rods, each 91 cm long and 9.5 mm in diameter, secure the cover plate to the aluminum base plate and, extending through the base plate, serve as support columns for adjustable steel feet. For the purpose of moving the furnace, four retractable ball casters, mounted to the support plate and not shown in the figure, can be brought down to take the load off the steel feet.

Serving as the top surface of the furnace, resting on the aluminum cover plate, is a removable ceramic cover [38]. The ceramic cover consists of the halves of a 28 cm square by 2.5 cm

thick plate with a 2.5 cm diameter circular hole through its center, cut in two through the central hole along a line parallel to two of the sides.

The puller system used to perform the top-seeding and stirring functions was designed and built at Philips Laboratories. It features 40 cm of total axial travel and rotation at rates continuously adjustable from 0 to 100 RPM. To allow for sufficient working space above the furnace, the vertically-mounted puller unit is positioned with its lower end roughly 90 cm above the furnace cover. An adjustable Jacobs chuck couples a 65 cm long by 1.3 cm diameter aluminum extension shaft to the lower end of the puller shaft. An Albrecht chuck is mounted to the lower end of the aluminum extension shaft. Ceramic seed rods and stir paddle shafts are held in the Albrecht chuck.

A tubular steel frame structure provides support for both the furnace and the puller unit mounted above. The furnace rests directly on a heavy-duty adjustable X-Y table in turn mounted to the bottom cross-members of the steel frame. The puller is supported by a 25 cm square aluminum plate with a 5.2 cm diameter hole through its center mounted to the top cross-members of the steel frame. The frame was welded from tubular 5 cm (2 inch) square Type 1020 steel. It is supported by four heavy-duty adjustable steel feet on a 1.2 m by 1.8 m by 30 cm high pneumatic base plate [40].

Power to the resistance heaters is provided by a 5.2 kW zero-crossover SCR [41]. The SCR is controlled by a Eurotherm Model 990 temperature controller [42]. The control thermocouple for the Model 990 is Type S and platinum-sheathed, positioned in a small Inconel well mounted roughly halfway along the outer wall of the heat pipe, as shown in Figure 2. The control thermocouple lead exits the furnace through a notch in the silica can similar to the ones used for the heater leads.

The temperature set-point programming scheme is shown in Figure 3. A Hewlett-Packard HP-85 desktop computer [43] is programmed to control a Keithley Model 230 voltage supply

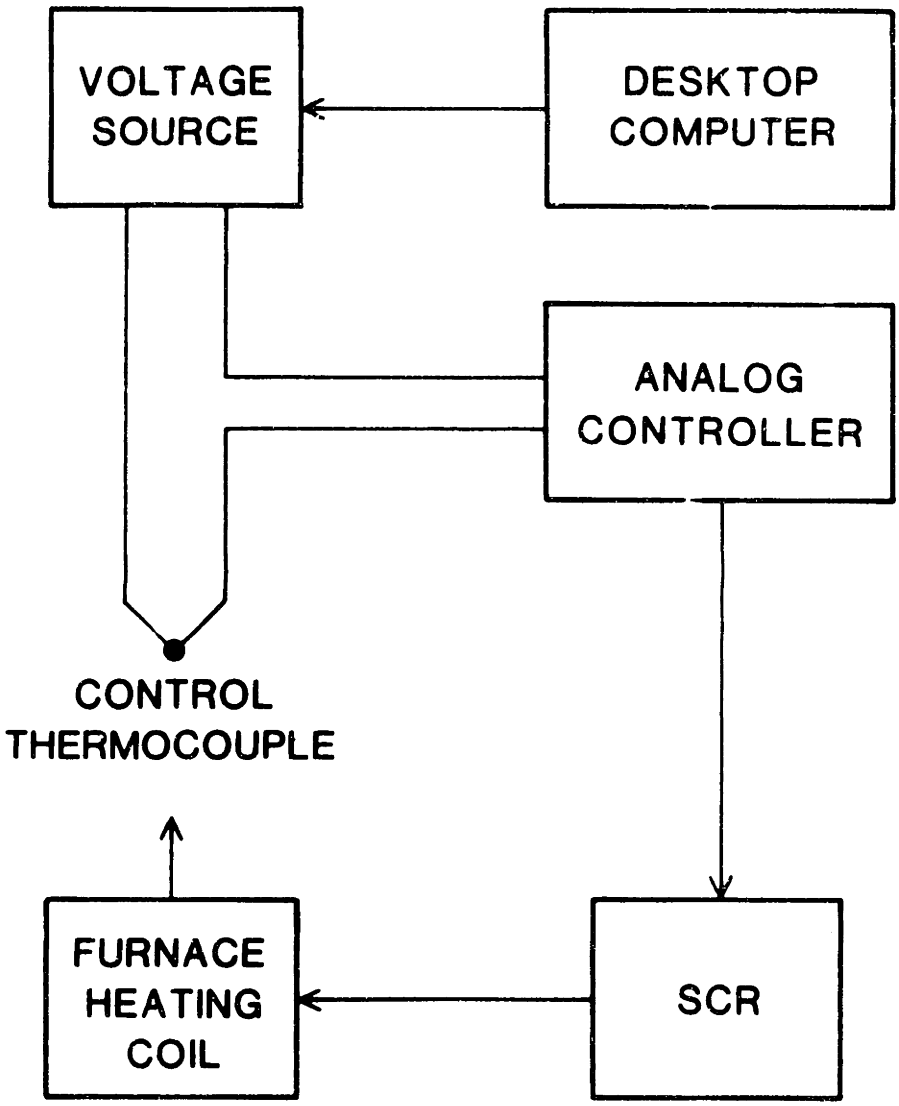

Figure 3. Temperature programming and control system (schematic)

[44]. The signal from the Model 230 is appropriately scaled through a voltage divider and used to bias the signal from the control thermocouple. The reference thermocouples mounted in the crucible support plate are read by the HP-85 using a Keithley Model 181 nanovoltmeter accessed through a Keithley Model 705 scanner. The Model 705 is equipped with a thermistor-monitored thermocouple connection plate enabling software compensation. The HP-85 is programmable in BASIC and coordinates both temperature programming and data acquisition. It is interfaced to a Hewlett-Packard disc drive memory storage system. All digital communications between system components are carried over an IEEE-488 interface bus.

The puller unit is coupled to a control box. Attendant to this control box is a second control box facilitating programmable stoppage and reversal of puller rotation.

Two identical furnace systems were built. As shown in Figure 4, the furnaces are positioned on either end of the pneumatic base plate. The measurement and control equipment for each furnace including the SCR and the HP-85 is mounted in a portable instrument positioned adjacent to the furnace itself. Rolling steps and a catwalk spanning the pneumatic base plate provide access to the top furnace openings and the puller units.

2.5 Thermal Characterization of Furnace System

As presented in Section 2.3, among the desired furnace system performance features were that a high degree of spatial temperature uniformity be attainable throughout the volume of growth solution and that the temperature at any location in the solution be stable and controllable over time. After completion of construction, a number of initial thermal characterization experiments were performed investigating the extent to which the furnace system met these design objectives.

Spatial profiling was approached through a combination of experimental and analytical techniques. A calibrated Type S thermocouple with a platinum sheath was positioned at

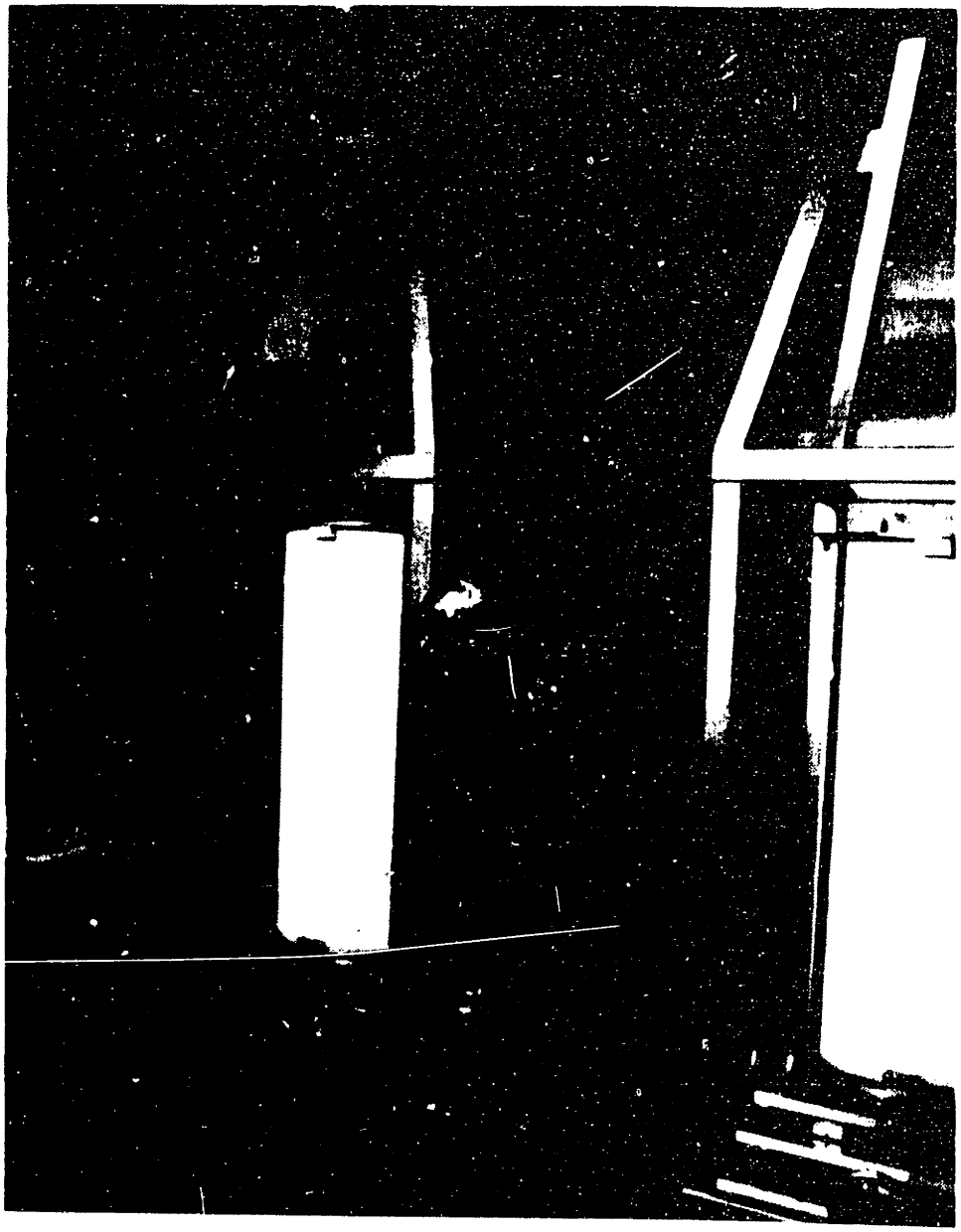

Figure 4. Heat pipe based furnace system

various locations in an unstirred growth solution and in the air space above this solution. Simplified heat transfer calculations were then performed to establish the validity and accuracy of considering these thermocouple measurements as representing the actual thermal conditions that would exist within and around the growth solution in a $KTiOPO_4$ growth operation.

Figure 5 shows the thermocouple assembly used in the profiling. The 80 cm long by 1.6 mm diameter sheathed thermocouple lead was brought through the bore of an alumina tube. The tube was 43 cm long with a 6 mm outer diameter and a 3.5 mm inner bore diameter. Roughly 35 cm of the sheathed lead nearest the junction was coiled to form a roughly 1.5 cm diameter by 5 cm long helix. This was done to increase the exposure of the lead to the furnace environment. A 3.5 cm long by 2 mm wide slot cut axially through the wall at the upper end of the alumina tube allowed the opposite end of the thermocouple lead to be brought out to a connection without interfering with the mounting of the alumina tube in the Albrecht chuck at the end of the puller extension shaft. Axial motion of the thermocouple assembly relative to the furnace was controlled through the puller unit. Radial motion was controlled through the adjustable X-Y table supporting the furnace. The calibration of the profiling thermocouple is traceable to NBS standards. The absolute accuracy of the thermocouple was better than $\pm 0.5\,^{\circ}C$ over the range of the measurements. The thermocouple was read with the same equipment used to monitor the thermocouples in the crucible support plate.

A roughly 230 cm^3 volume of $KTiOPO_4$-$K_6P_4O_{13}$ growth solution was contained in a 7 cm high by 8 cm diameter cylindrical platinum crucible. The crucible was positioned on the support plate at the top of the pedestal. The solution had a concentration of 0.6 g $KTiOPO_4$/g $K_6P_4O_{13}$, corresponding to a saturation point of $968 \pm 0.5\,^{\circ}C$, and was prepared according to procedures discussed in Section 3.2. For all the profiling measurements, the halves of the ceramic furnace cover were in a closed position, thereby allowing a 2.5 cm diameter hole for passage of the thermocouple assembly.

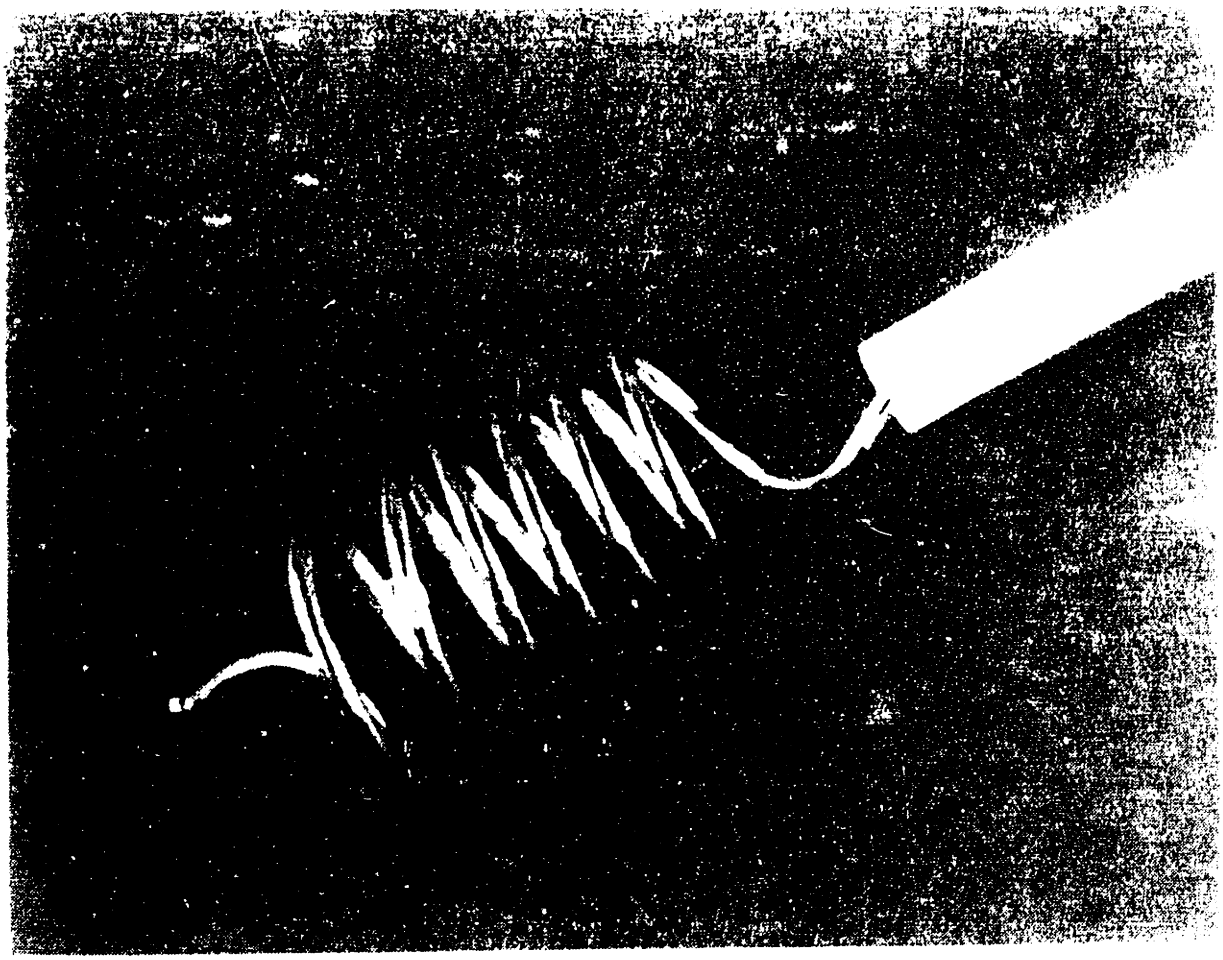

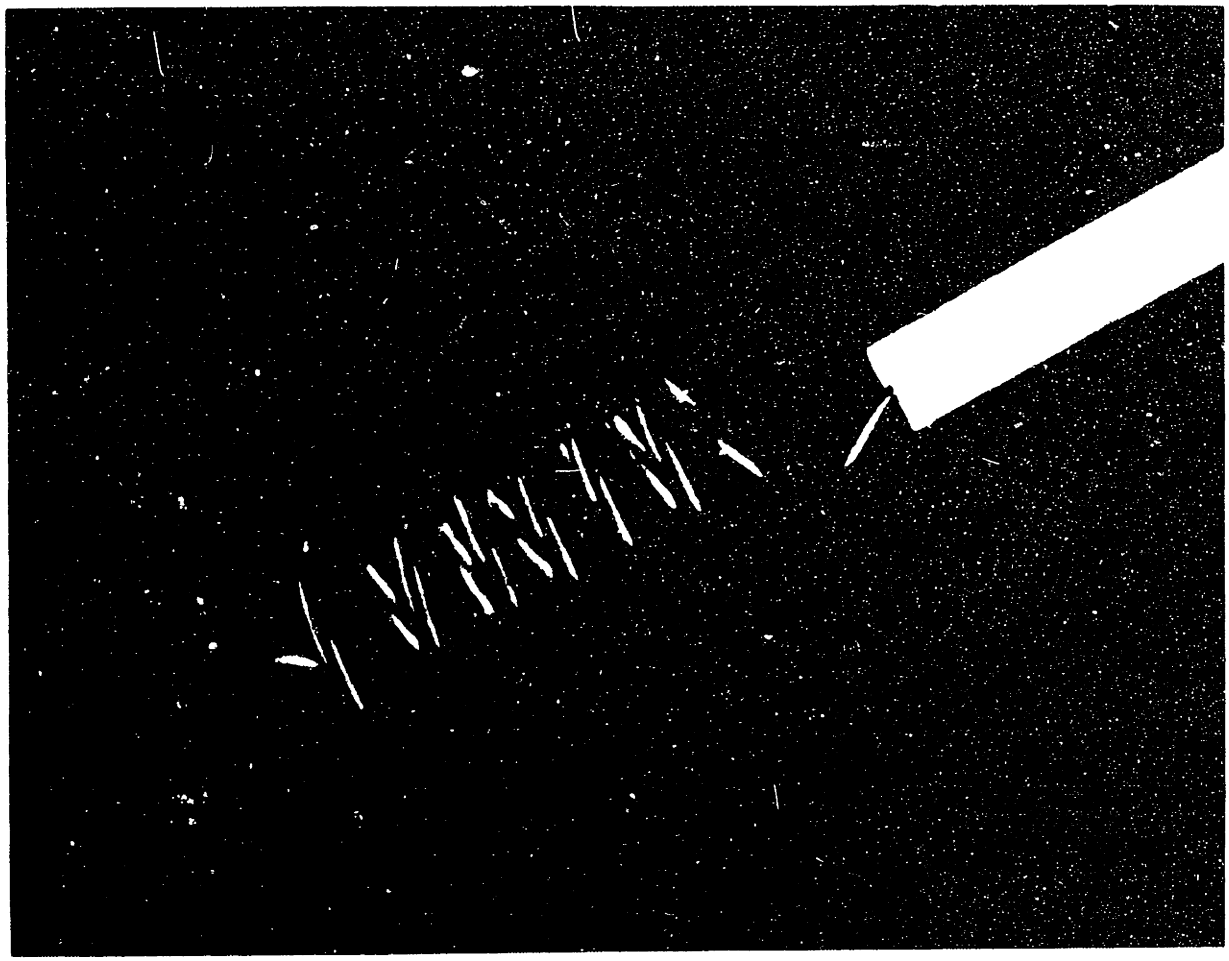

Figure 5. Thermocouple assembly for furnace profiling

Profiling data are represented by Table 1. Initial profiling actually consisted of a series of measurements at each of a variety of furnace temperature set-points. Such measurements were repeated periodically over the course of the project, in each of the two furnace systems. The profiling data shown in the Table represent a typical but actual case.

There were two primary issues to be addressed in determining the extent to which the thermocouple data represented the actual furnace temperature profile of interest. First, it had to be determined to what extent conductive heat transfer out the furnace through the thermocouple assembly itself would cause an artificially low temperature reading to be registered at the thermocouple junction. Second, it had to be determined to what extent the optical properties of the thermocouple assembly being different from that of the growth solution or the air in the furnace cavity might cause spurious radiative heat transfer effects resulting in artificial junction temperature readings.

Analysis of the thermal conductive loss through the thermocouple assembly was straightforward, treatable as a fin problem. Consider the thermocouple assembly to be a fin of uniform cross section transferring heat from the air inside the heat pipe furnace cavity to the air outside the furnace at room temperature. Assume steady-state conditions with the thermal conductivity of the platinum sheathed thermocouple and the heat transfer coefficient between the thermocouple and the furnace air both constant. Assume that the temperature profile radially across the sheathed thermocouple lead is flat. The following equation is then valid [45] for the relationship between the temperature of the thermocouple tip, T_T, the air temperature in the furnace cavity, T_A, and room temperature, T_R:

$$\frac{T_A - T_T}{T_A - T_R} = \frac{1}{\cosh(BL)} \quad \text{where} \quad B = (h_A P/kS)^{1/2}. \tag{2.1}$$

Here L represents the length of the thermocouple assembly within the heated furnace cavity, h_A the thermocouple/furnace air heat transfer coefficient, P and S the perimeter and cross-sectional

POSITION	RADIUS (mm)	DEPTH (mm)	TEMPERATURE (° C)
1	0	1	969.3
2	"	6	968.9
3	"	11	969.0
4	"	16	969.1
5	"	21	969.1
6	"	26	969.1
7	"	31	969.1
8	"	36	969.2
9	"	41	969.6
10	5	36	969.5
11	10	"	969.6
12	15	"	969.8
13	20	"	970.3
14	25	"	970.4
15	5	6	969.0
16	10	"	969.2
17	15	"	970.0
18	20	"	970.5
19	25	"	970.8
20	0	-20	970.7
21	"	-40	971.5
22	"	-60	971.9
23	"	-80	971.5
24	"	-100	971.0
25	"	-120	970.2

Table 1. Furnace system temperature profiling data (Depth coordinate of 0 at melt surface increasing downward, radius coordinate of 0 at crucible centerline increasing outward)

area of the sheathed thermocouple lead, and k the thermal conductivity of platinum. Appropriate values for L, P and S are 60 cm, 5 mm, and 2 mm^2, respectively. A conservatively high value for k is 45 W/m °K. A conservatively low value for h_A is 5 W/m^2 °K [46]. Substitution into the equation yields a value of $(T_A - T_T)/(T_A - T_R)$ equal to roughly 3×10^{-5}. Thus, for a furnace air temperature of 975 °C and room temperature of 25 °C, the error due to conductive loss effects in considering the thermocouple measurement to equal the furnace air temperature is less than 0.08 °C. For the case of the coiled end of the thermocouple assembly being submerged in the growth solution, the error is even less due to more efficient heat transfer between the thermocouple and the liquid solution. Clearly, such a conductive heat loss effect is negligible in influencing the extent to which the thermocouple profiling data represent the actual furnace temperature profile of interest.

Analysis of the radiative heat transfer problem was somewhat more challenging. The furnace cavity is heated by the inner walls of the heat pipe through the silica heat pipe liner. Heat is presumably transported out of the cavity in an upward direction toward the unheated cover area. The radiative absorbtivity of the platinum thermocouple assembly is higher than that of the air in the furnace cavity. The issue to be considered was thus to what extent would radiative heating of the thermocouple assembly by the hotter furnace walls produce a higher junction temperature at a given location than would exist at that location in the absence of the thermocouple.

Consider the situation where the very tip of the coiled thermocouple assembly, containing the junction, is just piercing the surface of the liquid solution. This corresponds to Position 1 in Table 1. Presumably, of all the thermocouple measurements made with the sheathed junction submerged in the solution, the measurement at Position 1 is the most likely to be influenced by spurious radiation effects. This is because Position 1 involves at the same time both the smallest contact area for convective or conductive heat transfer between the thermocouple assembly

and the growth solution and the largest area for radiative heat transfer between the assembly and the hotter furnace walls. Thus, the error value determined from a conservative analysis of this problem can clearly serve as an upper bound to the error in taking any of the thermocouple data in Table 1 for positions within the solution as representing the temperature values that would exist in the absence of the thermocouple.

The first step in the analysis was an estimate of the radiative heat transfer coefficient through the air between the thermocouple assembly and its surrounding environment. A value can be estimated from the following equation:

$$h_R = 4\epsilon\sigma(T_{AVG})^3. \tag{2.2}$$

Taking T_{AVG} as 970 °C and ϵ, the emissivity of the platinum-sheathed thermocouple assembly, as 0.14 [47], h_R is estimated to be 61.3 W/m^2 °K.

The second step was the determination of the length of the thermocouple assembly up from the junction that could influence the junction through conduction. Treatable as a fin problem, with h_R of 61.3 W/ m^2 °K, P of 2 mm, S of 5 mm^2, and k of 45 W/m °K, B given by $(h_R P/kS)^{1/2}$ equals 18, and tanh(BL) equals 0.99 for L of 4.5 cm. Thus, only the roughly 4.5 cm of the thermocouple assembly nearest the tip need be considered in the analysis.

The third step was a conservative estimate of the effective temperature "seen" by this 4.5 cm length of coiled platinum lead. Because of its coiled geometry, all of the 4.5 cm length is within roughly 1.5 cm of the 8 cm diameter liquid surface. It was thus felt reasonable to take the liquid surface view factor as 0.5, with the remaining 0.5 contributed by the furnace wall. The effective temperature radiating to the extreme 4.5 cm of the thermocouple assembly could then be expressed as

$$(T_{EFF})^4 = 0.5(T_W)^4 + 0.5(T_S)^4 \tag{2.3}$$

where T_W is the temperature of the inner surface of the furnace cavity wall and T_S that of the

liquid surface. Both these values would be difficult to specify exactly, but conservative upper bounds could be easily established. T_W was taken as the temperature of the control thermocouple mounted in the well on the outer surface of the heat pipe. Including a cross-correlation performed to eliminate inconsistencies between the control thermocouple and the calibrated profiling thermocouple, T_W was taken conservatively to be 977.0 ° C. An upper bound on T_S was provided directly by the thermocouple reading at Position 1, specifically, 969.3 ° C. T_{EFF} was thus determined conservatively to be 973.0 ° C.

The fourth step was the determination of the resulting radiative heat transfer to the extreme 4.5 cm of the thermocouple assembly. This is given by the following equation:

$$Q = (h_R PkS)^{1/2} (T_{EFF} - T_T). \tag{2.4}$$

It is conservative because the use of T_T of 969.3 ° C represents an upper bound for the temperature difference driving the heat transfer. Q is calculated to be 1.9 x 10^{-2} W.

The final step was the estimate of the temperature difference between the sheathed thermocouple junction and the surrounding liquid solution at Position 1 corresponding to the transfer of this heat, Q, out the thermocouple tip into the liquid. A conservatively small value for the heat transfer coefficient between the thermocouple tip and the liquid could be established based on the assumption of the tip as an immersed sphere. The limiting lowest value for the Nusselt number of an immersed sphere is 2 [48]. Thus,

$$Nu = \frac{hD}{k} = 2 \quad \text{and} \quad h = \frac{2k}{D} \tag{2.5}$$

where here D is the diameter of the tip, k the thermal conductivity of the liquid solution, and h the heat transfer coefficient of interest. Given, by definition of h,

$$Q = Ah\Delta T, \tag{2.6}$$

substitution of the area of a sphere and rearrangement yields

$$\Delta T = \frac{Q}{2\pi k D.} \tag{2.7}$$

This represents the maximum error due to taking the thermocouple reading at Position 1 as representing the liquid solution temperature at Position 1 in the absence of the thermocouple. Q is 1.9 x 10^{-2} W, as determined in the previous step. D is the tip diameter, 1.6 mm. The thermal conductivity of the liquid solution can be roughly estimated as 2 W/m °K, typical of a glass-forming oxide liquid. The resultant value for ΔT is 1.0 °C.

A simple but conservative heat transfer analysis thus shows that the temperature in the liquid solution at Position 1 in the absence of the measuring thermocouple is at most 1 °C cooler than the measured value of 969.3 °C reported in Table 1. Moreover, as already noted, due to the effect of increased contact area between the thermocouple assembly and the solution, the other values in the Table for locations within the solution are even more directly indicative of the actual thermal profile existent in the absence of the thermocouple. Details of the solution thermal profile can thus be determined more or less directly from inspection of the data in Table 1.

Linear extrapolation from the data represented in Table 1 yields the conclusion that the spatial temperature variation throughout the 230 cm^3 volume of solution is less than ±1.9 °C. Considering the general difficulty of thermal field control in the neighborhood of 1000 °C, this degree of temperature uniformity is exceptional. At a given depth, the temperature increases with proximity to the crucible wall. This is to be expected since the heat input to the solution flows laterally from the furnace walls through the crucible. Near the crucible wall, the temperature appears to be highest near the surface. This is presumably due to the additional heat input from the crucible wall extending above the liquid level. This wall area can serve as a radiatively heated fin, conducting heat to the solution near the surface near the wall. The lowest temperature in the solution is probably at the center of the liquid surface, already referred to as Position 1. Heat presumably leaves the liquid largely by radiation from its

surface, and Position 1 has the greatest radiative view factor to the unheated furnace cover.

An additional point to note is that the spatial temperature uniformity in the liquid solution must be assumed to increase even further with forced convection from an immersed and rotating crystal and seed rod. With linear crystal growth rates on the order of only mm/day, the effect of the latent heat of crystallization on the bulk temperature profile can be assumed negligible.

Although of much less concern than the readings taken in the liquid, the thermocouple measurements taken with the junction suspended in the furnace air above the liquid surface, corresponding to Positions 20 through 25 in Table 1, are difficult to correlate with air temperatures existent in the thermocouple's absence. This is due to the difficulty in establishing a reasonable value for the furnace air/thermocouple heat transfer coefficient. Although the thermocouple temperatures shown in the Table are probably higher than the corresponding air temperatures in the absence of the thermocouple, without detailed knowledge of the air convection pattern necessary to specify a heat transfer coefficient, quantitative analysis cannot yield estimates any more accurate than can be achieved by blind intuition. The main reason for routinely performing thermocouple profiling measurements in the air cavity was to check the operation of the heat pipe, as discussed in Section 3.6.

Turning now to the issue of temporal temperature stability within the liquid solution, the analysis here was much simpler than in the case of the spatial profile. A number of experiments were performed in which the thermocouple assembly was positioned with its sheathed junction immersed at a given location in the liquid solution with the furnace temperature set-point held constant. The thermocouple reading was recorded continuously over time periods ranging up to 24 hours in duration. Experiments were performed for each of a series of junction locations and furnace set-points. In all cases, the thermocouple reading at a given location was stable over time to within $\pm 0.25\,^{\circ}$C.

A final issue on the subject of thermal characterization of the furnace system concerned the

role played by the heat pipe in achieving the measured uniformity and stability of the thermal field within the growth solution. Specifically, were the measured thermal characteristics critically dependent on the operation of the heat pipe or were they merely a function of the relatively large size and thermal mass of the furnace system overall? To examine this issue, one of the furnace systems was disassembled and the heat pipe was replaced with a "dummy", made by the same manufacturer and alike in all respects except for the absence of the metallic sodium within its hollow walls. The system was reassembled around the dummy heat pipe, re-heated to within the operating temperature range of interest, and thermally characterized using the same methods reported earlier in this Section.

The results of the thermal profiling were very different from those presented for the case of the operating heat pipe. First, the difference between the average liquid solution temperature and the temperature of the control thermocouple was roughly 110 °C. This compares with a corresponding value of roughly 9 °C for the case of the operating heat pipe. Second, the maximum temperature difference across the liquid solution was measured to be roughly 18 °C, 5 times the corresponding value in the other case. Only in the degree of temporal temperature stability were the two cases similar. The temporal temperature stability using the dummy heat pipe was measured to be roughly ±0.30 °C, only slightly worse than the corresponding ±0.25 °C value determined for the working heat pipe. It was thus concluded that, although the temporal stability of the solution thermal profile may be solely a function of the overall thermal mass of the furnace, the operation of the heat pipe liner is critical to the attainment of the desired spatial temperature uniformity in the system.

It is recognized that there are potentially other methods aside from the incorporation of a heat pipe liner for effecting spatial temperature uniformity within a furnace cavity. By presenting the results of this simple experiment using a dummy heat pipe, it is not intended to imply that the use of a heat pipe is strictly necessary to achieve spatial temperature uniformity in HTS growth of $KTiOPO_4$. It remains to be seen whether other furnace system designs

incorporating different approaches to thermal field control can effect the same desirable thermal characteristics. The point to be noted is merely that the incorporation of a working heat pipe is critical to the operation of the furnace system presented here.

2.6 Advantages of Achieved Thermal Field

Before leaving this Chapter, it is worthwhile to underscore the significance of the solution temperature uniformity and stability that was sought, designed for, and experimentally confirmed in the development of the heat pipe based furnace system. As discussed in Section 1.2, prior to the start of this project, spurious nucleation had been identified as a potentially unavoidable problem in single crystal growth of $KTiOPO_4$ from HTS. From the first experiments performed in the heat pipe system, it was clear that, relative to these earlier works, the problem of spurious nucleation was largely avoided. Although with a finite level of bulk supersaturation driving the crystallization process, the possibility of spurious nucleation can never be entirely eliminated, the thermal field achieved in the heat pipe furnaces was adequate to allow most growth runs to proceed for at least 7 days without incidence of spurious nucleation. In a number of cases, growth runs continued for more than two weeks, involving a total temperature drop of roughly 70 $^{\circ}$C, without evidence of spurious nucleation.

A second point to be stressed in regard to benefits of the achieved thermal field concerns the ability to effectively model the bulk mass transport phenomena occurring during the growth process. Since the thermal gradients across the solution are very small, thermal buoyancy-driven convection does not occur. Thus, bulk fluid motion is due largely to forced convection effected by rotation of the growing crystal. Given knowledge of the kinematic viscosity of the growth solution, the bulk fluid flow profile corresponding to the forced convection can be analyzed using relatively straightforward techniques. Such analysis would be much more difficult if not impossible if buoyancy-driven convective effects were significant. This issue of flow modelling enabled by the thermal field is involved in work presented in Chapters 4, 5, and 7.

Finally, as presented in Chapter 6, the ability to effectively seed the growth of $KTiOPO_4$ was found to require the controllable slight dissolution of the original surfaces of seed crystals no larger than several millimeters on a side. The ability to reproducibly control such an operation depended critically on the high degree of temporal stability and run to run repeatability of the thermal field afforded by the furnace system.

Chapter 3

Techniques & Apparatus Attendent to Crystal Growth

3.1 Introduction

In the day to day operation of any crystal growth furnace system, numerous techniques are employed that do not vary from one growth run to the next. These are generally developed in the early stages of using a system and are aimed at reproducibility, simplicity, and effectiveness. In the interest of completeness, this Chapter presents such secondary techniques and apparatus attendent to crystal growth of $KTiOPO_4$ in the heat pipe furnace system. Although none of the material covered here is claimed to be novel, all of it is relevant to operating the furnace system and reproducing results discussed in other Chapters.

3.2 Charge Preparation

The $KTiOPO_4$ - $K_6P_4O_{13}$ growth solutions were prepared by heating mixtures of the starting materials KH_2PO_4, K_2HPO_4, and TiO_2. When combined in appropriate ratios, the following reactions occurred on heating:

$$2KH_2PO_4 + 2K_2HPO_4 = K_6P_4O_{13} + 3H_2O \tag{3.1}$$

$$KH_2PO_4 + TiO_2 = KTiOPO_4 + H_2O \tag{3.2}$$

As described elsewhere [13], the two reactions can be considered to take place simultaneously. The $KTiOPO_4$ formed dissolves in the $K_6P_4O_{13}$, yielding a single liquid phase. The water is evolved as vapor. It is possible that some of the water produced results in formation of OH^- ions dissolved in the solution. Similar phenomena have been reported to occur in formation of sodium phosphate melts from corresponding hydrogen-containing phosphate starting materials

[49]. In these sodium phosphate systems, the dissolved OH^- is volatile and its concentration decreases with soak time at high temperature. In the present work, although quantitative experiments were not performed, there was evidence that OH^- was present in grown $KTiOPO_4$ crystals (see Chapter 8).

The TiO_2 and K_2HPO_4 used were both purchased from Aldrich Chemical [50]. The TiO_2 was nominally 99.9% pure while the K_2HPO_4 was A.C.S. grade. The KH_2PO_4 was purchased from M.C.B. [51] and was A.C.S. grade. Impurity analyses were performed on each different lot of starting materials by optical emission spectroscopy and atomic absorption spectrophotometry. In all cases, the chemicals used contained at most 10 ppm of any metallic impuity with the exception of one lot of K_2HPO_4 which was measured to contain roughly 80 ppm of sodium. In addition, thermogravimetric analysis using a Perkin-Elmer TGS-2 [52] was performed on samples of each of the starting materials to investigate the possibility of water absorption. Uncontrolled and variable water absorption by the starting materials could otherwise lead to compositional inaccuracies in solution preparation. The TiO_2 and KH_2PO_4 were consistently found to contain no absorbed water, irrespective of humidity and temperature conditions in the laboratory. The K_2HPO_4 was found to be hygroscopic under conditions of high absolute humidity in the laboratory. K_2HPO_4 used in charge preparation was therefore held in a drying oven at 120 °C for at least 5 days prior to use. Additional gravimetric analysis confirmed the efficacy of such an approach for avoiding accidental water incorporation.

The chemicals were weighed out using a Sartorius Model 1204 balance [53]. A typical recipe for growth solution preparation consisted of 294.63 g KH_2PO_4, 202.90 g K_2HPO_4, and 79.90 g TiO_2. Such a mixture of starting chemicals occupied a volume of roughly 500 cm^3. The mixture was poured into a 18 cm high by 15 cm diameter alumina ball mill jar. After addition of 12 cylindrical milling balls, each 2.5 cm long by 2.5 cm in diameter, the jar was sealed and rotated on a tumbler at roughly 100 RPM for 1 hour. After removal of the milling balls, the well-mixed

powder was poured into a cylindrical platinum crucible, 8 cm high by 11 cm in diameter. The compositional accuracy of this charge preparation method can be assumed conservatively to be better then ±0.1%. Further impurity analysis of samples of milled powder confirmed the avoidance of aluminum contamination.

Heating and reaction of the milled starting materials took place in either of two muffle furnaces, one a Thermolyne Model 10500 [54], the other a Lindberg Model 51442 [55]. The furnace used was pre-heated to a nominal soak temperature of 1050 °C and the cylindrical platinum crucible containing the powder was introduced into the furnace cavity. It was found necessary to have the furnace pre-heated; slow heating of the powder resulted in foaming and overflow from the crucible due to evolution of H_2O vapor.

A charge was held for at least 16 hours at 1050 °C in the muffle-furnace, resulting in the transformation of the powder to roughly 230 cm^3 of homogeneous liquid. Using stainless steel beaker tongs, this liquid was poured into a smaller cylindrical crucible, 7 cm in height by 8 cm in diameter for immediate introduction into the heat pipe furnace.

3.3 Loading a Crystal Growth Run

Prior to introduction of a crucible containing a prepared solution, the heat pipe furnace was pre-heated to a temperature roughly 30 °C above the solution's saturation point. Access to the furnace cavity was gained by momentarily sliding open the halves of the ceramic cover plate. Each of the platinum crucibles used in the heat pipe furnace had two holes, each 2 mm in diameter, centered 5 mm below the rim and diametrically opposed about the circumference. Into these holes fit the end pins of a pair of specially made 60 cm long tongs. The arms of the tongs would open up to lock the end pins into the crucible holes from within. Squeezing the arms together would withdraw the pins, releasing the crucible from the tongs. Figure 6 shows the tongs holding a platinum crucible. The extreme 5 cm of the tongs including the end pins were

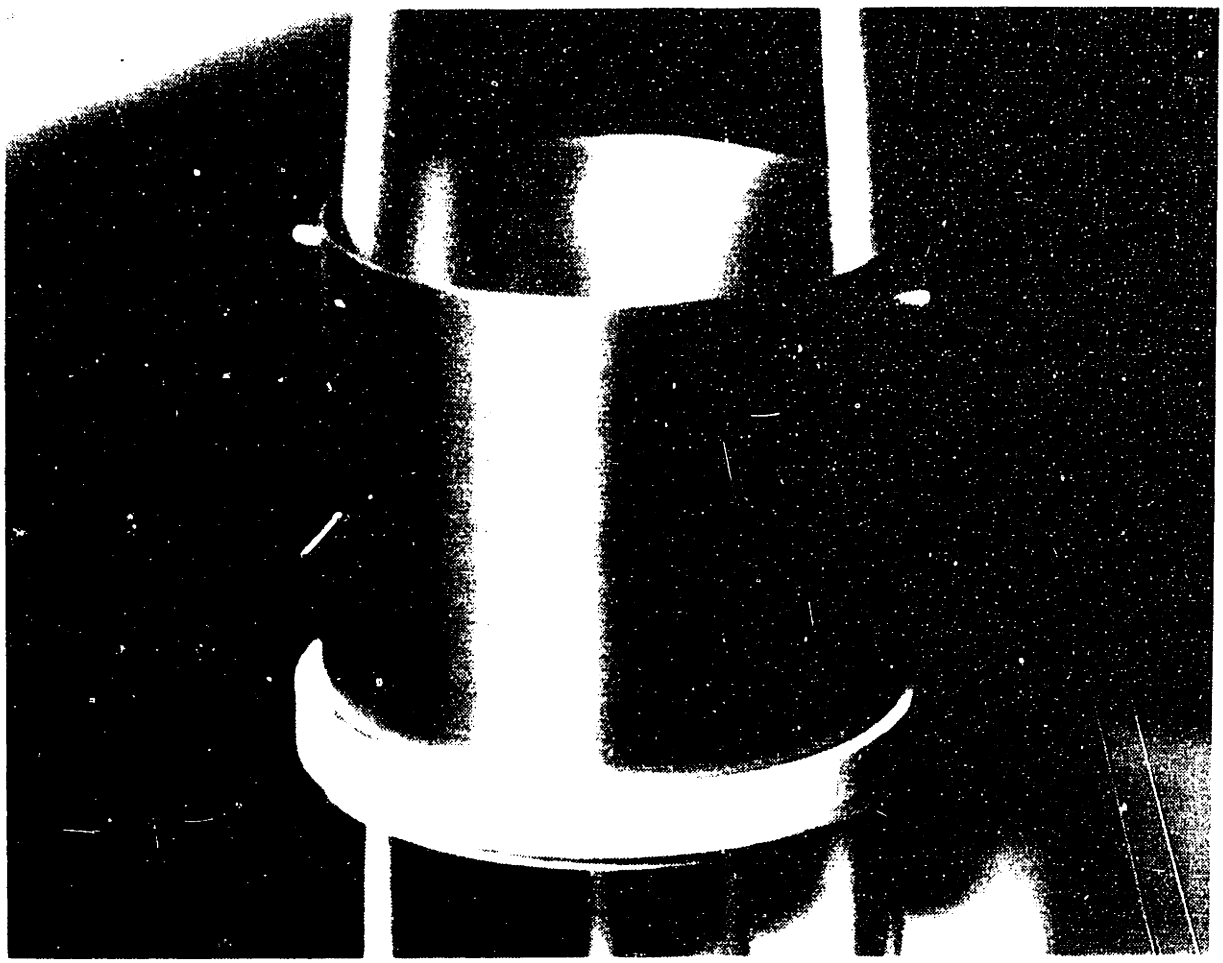

Figure 6. Tongs supporting platinum crucible

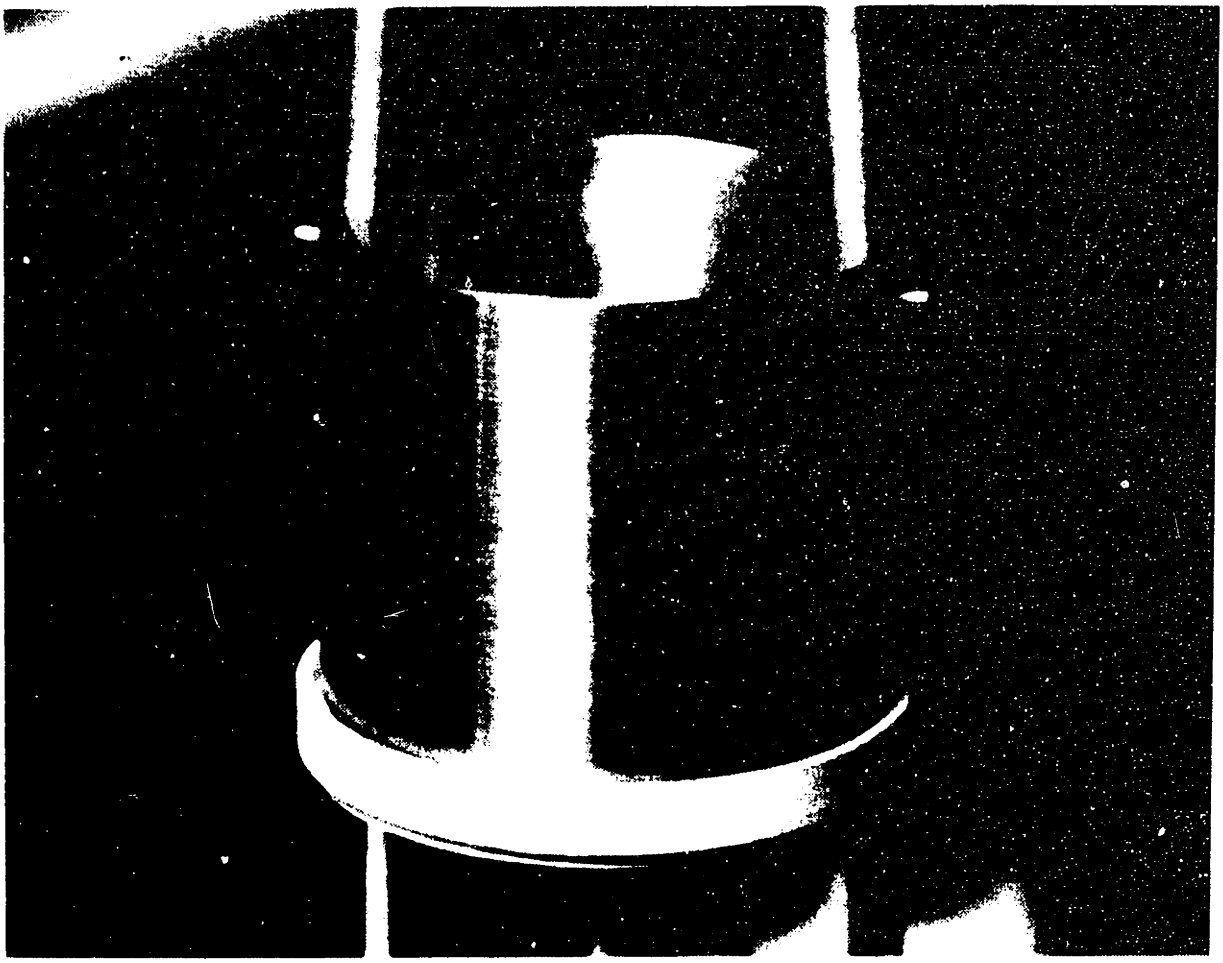

Figure 6. Tongs supporting platinum crucible

INTENTIONAL DUPLICATE EXPOSURE

platinum plated in an attempt to avoid contamination of the liquid solution, should the tongs briefly contact the solution during lowering into the furnace. Use of such tongs enabled the use of crucibles of diameter just slightly less than that of the furnace cavity.

After introduction of a filled crucible into the heat pipe furnace, the solution was stirred with a platinum paddle, 5 cm by 1.5 cm by 2 mm thick. The paddle was welded to the end of a 4.5 cm long platinum rod, attached to the end of a 42 cm long alumina rod, in turn mounted in the Albrecht chuck at the end of the puller extension shaft. The paddle was rotated at roughly 70 RPM for at least 4 hours, with the furnace temperature held roughly 30 ° C above the saturation point of the solution. The objective of this procedure was to re-dissolve any solid precipitate that might have formed during the solution transfer process.

With the filled crucible positioned on the support plate, the solution temperature could be monitored indirectly through the reference thermocouples mounted in the plate. By running the program "TEMP" on the HP-85 desktop computer, the reference thermocouple values were updated every 30 seconds on the computer's CRT. Prior cross-correlation during thermal profiling enabled tracking of the actual solution temperature to within ±0.10 ° C.

After removal of the stirring paddle, the temperature of the solution was lowered to a temperature near its saturation point and allowed time to stabilize. For cooling from a soak temperature of roughly 1000 ° C to a saturation temperature near 970 ° C, stabilization took roughly 45 minutes. The seed, affixed in some fashion to the end of a platinum seed rod in turn affixed to an alumina rod held in the Albrecht chuck, was slowly introduced into the furnace cavity through the circular opening in the center of the split ceramic cover plate. The thermal stresses generated internally in small, unflawed $KTiOPO_4$ seeds upon slow introduction into the furnace may be assumed to be insignificant. Probably more important although also more difficult to calculate was the stress associated with the differential thermal expansion of a threaded platinum rod on which seeds were usually mounted. At least 10 minutes were always allowed to

transfer a mounted seed from a position just above the furnace cover to immersion in the solution. In most cases, such a procedure resulted in no obvious mechanical damage to a seed. On a number of occasions, however, seeds cracked upon introduction into the furnace cavity, falling from their mounting into the liquid below.

3.4 Basic Growth Techniques

As presented in Chapters 6 and 7, a wide variety of growth conditions was applied over the course of the experiments. However, a number of methods for establishing and controlling these conditions remained constant.

A single computer program was developed for the HP-85 to handle the temperature set-point programming and reference thermocouple data acquisition over the course of a growth run. Entitled "GROWTH", it enabled establishment of either a constant linear furnace cooling rate specified in units of degrees Centigrade per day, or a cooling rate varying with the third power of elapsed time, corresponding in principle to a constant rate of solvent deposition at any point on a growing crystal and specified in units of millimeters per day. "GROWTH" updated a CRT readout with the time, set-point, and reference thermocouple readings every 5 minutes, and updated a hardcopy printout with the same information every 60 minutes. Cooling parameter values could be changed by the operator at will throughout a growth run.

Seed rod rotation was controlled by the settings on the control boxes attendent to the puller. Rotation rates were settable between 0 and 100 RPM. For periodic rotation reversal, the values for duration of rotation in each direction were independently settable between 0 and 120 seconds. Delay time for switching directions was 4 seconds in all cases.

A typical growth run spanned a period of about 10 days. A daily practice was the visual inspection of the solution surface and growing crystal through the opening in the furnace cover plate where the alumina seed rod passed through. In general, upon sighting of spurious

nucleation in the form of one or more reflective specks or flakes on the solution surface, a growth run was immediately unloaded. As is well known from aqueous solution crystal growth, continued uncontrolled growth of spurious crystallites often effects growth flaws on the primary crystal. In the present work, it was of course desirable to avoid having such phenomena obscure experimental results, even if it meant ending a growth run after a shorter duration than planned. In almost all cases, at least 7 days of growth were achieved before sighting of nucleation.

3.5 Unloading a Crystal Growth Run

To unload a run, the grown crystal was withdrawn to a position in the furnace cavity roughly 6 cm above the melt surface. The computer program entitled "COOL" was then run, effecting the cooling of the furnace at a rate of roughly 25 ° C/hour until a temperature of roughly 290 ° C was reached, at which point the temperature would be held constant. Since all growth runs ended at temperatures in excess of 900 ° C, this cooling process would take at least 24 hours. The reason for using a cooling program was that grown crystals containing solution occlusion flaws would often crack severely due to thermal shock if removed directly from the furnace at 900 ° C to the outside laboratory ambient, obscuring the experimental results. Direct removal from a 290 ° C furnace to the laboratory ambient appeared to pose no problem.

After cooling of the furnace and removal of the grown crystal, the same tongs used in loading the crucible were used to remove it. The solidified solution remaining in the crucible, usually consisting of small $KTiOPO_4$ crystallites embedded in glass, could be washed away with hot running tap water in a period of about 30 minutes.

3.6 Routine Maintenance

Heat pipe operation was checked at roughly 8-week intervals through performance of the

thermocouple profiling procedure described in Section 2.5. In no case was any significant change noted in the measured thermal field. There was a single incident of a heat pipe rupture during the course of the work. This required abortion of the crystal growth run in progress, disassembly of the furnace, replacement of the heat pipe, and replacement of several other furnace components corroded by the escaping sodium.

The silica heat pipe liners were each replaced after roughly 15 growth runs. By that point, KPO_3 deposition on the inner surface would be built up to where it could flake off and fall into a growth solution.

Alumina rods used for stir paddle and seed holding required replacement after roughly 500 hours of use. Attack by the KPO_3 vapor weakened the rod end nearest the solution surface.

The platinum crucibles would deform due to both routine handling and differential thermal contraction around solidified growth charges on cooling at the end of growth runs. Acrylic plastic rods of semicircular cross section were fabricated for use as dies for crucible reshaping with a rubber or rawhide mallet. Crucibles were generally replaced after 6 months of daily use.

Chapter 4

Viscosity & Density of Growth Solutions

4.1 Introduction

This Chapter presents viscosity and density measurements performed on solutions encountered in the $KTiOPO_4$ crystal growth process under investigation. Specifically, measurements were made of the viscosity and density of four different concentrations of $KTiOPO_4$ dissolved in $K_6P_4O_{13}$ over a temperature range of roughly 940° to 1000°C. The measurements also yielded an estimate of the solution thermal expansion coefficient.

In general, viscosity and density information is useful in elucidating the solution structure and transport properties and, thus, the growth mechanism. In particular, as covered in Chapters 5 and 7, investigation into certain flawing phenomena required such data as prerequisite to accurate flow simulation studies.

4.2 Experimental Technique

The solution property measurements were all performed in one of the heat pipe based furnace systems. The four solution concentrations selected for measurement correspond to saturation concentrations of $KTiOPO_4$ in $K_6P_4O_{13}$ at 988°, 968°, 948°, and 928°C, each within 2°C, respectively. The preparation of a solution for measurement was performed essentially as described in Section 3.2 for growth solution preparation. Starting materials were combined in appropriate ratios, ball-milled for 1 hour, then transferred to a platinum crucible in which they were held at 1050°C for at least 16 hours, yielding a liquid solution of $KTiOPO_4$ in $K_6P_4O_{13}$. A roughly 70 cm^3 volume of solution was transferred to a smaller cylindrical platinum crucible, 5 cm in diameter by 5 cm high. This filled crucible, fashioned with a pair of opposed holes

beneath its rim, was in turn introduced immediately into a pre-heated heat pipe furnace by means of the special platinum-tipped tongs. The reason for using this smaller crucible for the measurements rather than the 8 cm diameter by 7 cm high crucible typically used in the growth experiments was that the smaller crucible enabled use of a smaller, less expensive, platinum bob for the viscosity measurements.

Thermal characterization of a stagnant solution held in the measurement crucible on the support plate in the center of the furnace cavity was performed in the manner described in Section 2.5. Direct profiling with a platinum sheathed thermocouple assembly combined with simplified heat transfer analysis to validate the profiling data yielded estimates of the degree of both spatial uniformity and temporal stability of the solution temperature. In general, compared to the larger solution volume contained in a growth crucible, the solution temperature in the measurement crucible was more spatially uniform and slightly less temporally stable. A conservative estimate indicated spatial temperature uniformity within $\pm 0.5\,^{\circ}C$ throughout the 70 cm^3 liquid volume. Temperature stability over several days at any single location in the solution was better than $\pm 0.3\,^{\circ}C$.

Viscosity measurements were made using a Brookfield Model LVTD rotating cylinder viscometer [56]. The main housing of the viscometer was affixed to the end of the puller shaft by means of a specially-made mounting bracket and an adjustable offset boring head. The rotating bob immersed in the solution was specially constructed from pure platinum according to a design supplied by Brookfield. Basically, the bob was an inverted cylindrical cup, 24 mm I.D. by 30 mm O.D. by 12 mm tall, affixed to a spindle, 3 mm in diameter by 85 mm in length. The upper end of the spindle was attached to a rotating hook on the underside of the viscometer housing via two thin stainless steel links, 61 cm in length overall. The immersion depth of the bob was adjustable to within ± 0.2 mm through control of the translatable shaft. Centering of the bob in the filled crucible was facilitated through motion of the entire furnace by means of the adjustable X-Y platform. Visual inspection through the opening at the top of the furnace

cavity enabled approximate centering. Fine adjustment was accomplished by exploiting the fact that, for a given solution at a given temperature, exact centering of the bob in the crucible corresponded to a relative minimum in the viscometer reading. The viscometer was calibrated at ambient temperature using standard liquids with viscosities in the range of 50 to 100 cP.

Density measurements were made by a two-bob Archimedean technique, employing a bottom-loading electrobalance weighing platinum bobs immersed in solution. The electrobalance was a Scientech Model 202 [57]. Like the viscometer, a specially-made bracket enabled mounting to the puller shaft. The bobs used were spherical in shape, with masses of 38g and 17g, respectively. Each of the bobs was hung from the electrobalance by a 0.381 mm diameter platinum wire, roughly 70 cm in length. The two-bob technique corrects for the force exerted by the solution surface on the entering wire, as described previously [58]. Further, if the contact angle where the wire supporting the bob pierces the solution surface is near 90°, the technique directly yields data that can be used to determine the solution/air surface tension.

4.3 Results

The viscosity data are represented by Figures 7 and 8. Figure 7 shows viscosity versus temperature for the four solutions measured. Figure 8 shows the corresponding natural logarithm of viscosity versus inverse absolute temperature. Over the temperature and concentration ranges measured, the data may be correlated within 1.9% by the following Arrhenius equation:

$$\eta = (-0.0227 + 0.114x)\exp(8990/T) \tag{4.1}$$

where η represents viscosity in centipoise, x the mole fraction of $KTiOPO_4$ in solution with $K_6P_4O_{13}$, and T the absolute temperature in degrees Kelvin.

Care was taken to ensure that the critical Taylor number for non-laminar flow in this geometry [59] was not exceeded. A 30 RPM rotation rate was used in gathering the data shown. Slower rotation rates indicated identical viscosity values, within experimental error, although

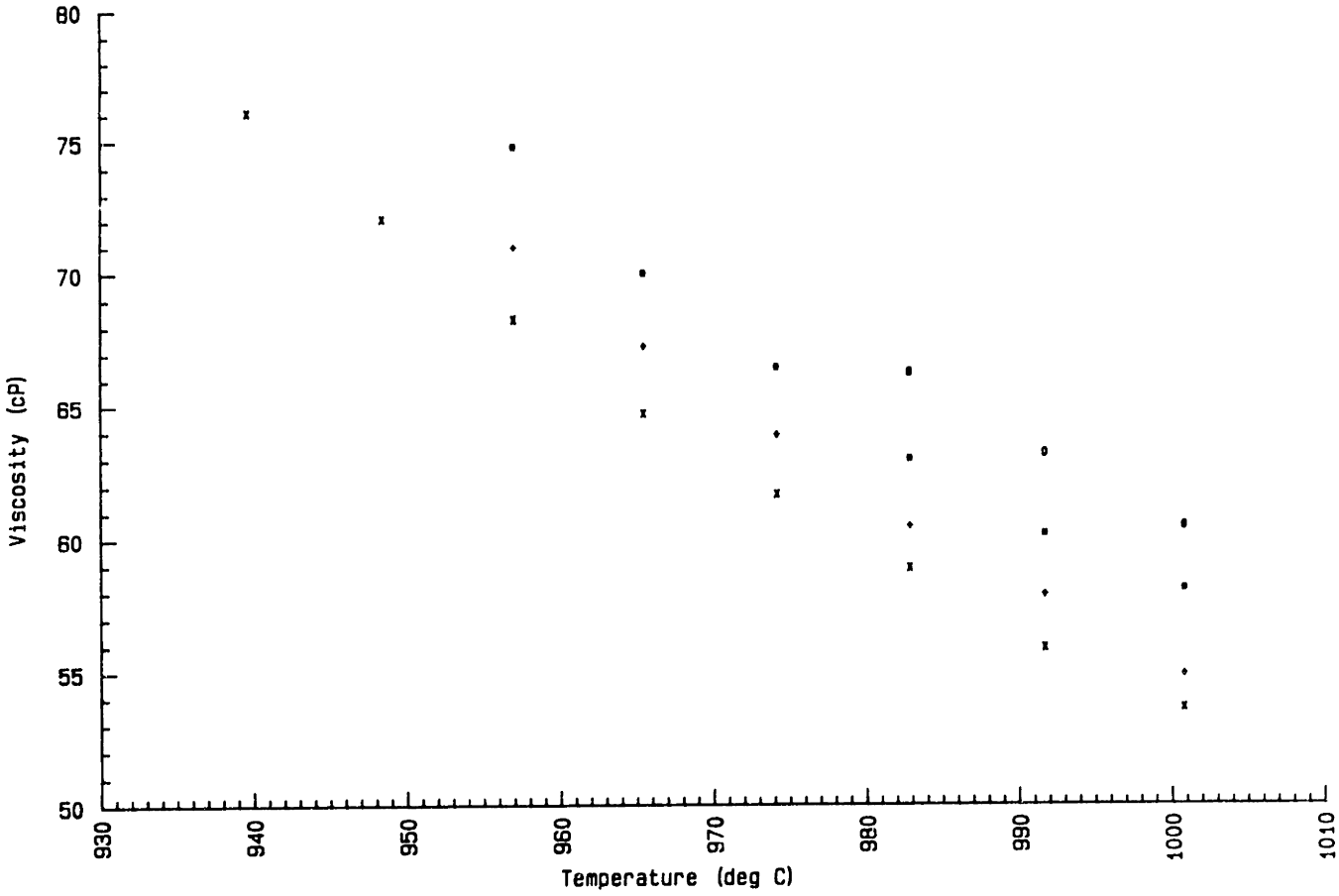

Figure 7. Viscosity of growth solutions versus temperature: (x) 0.515 g $KTiOPO_4$/g $K_6P_4O_{13}$; (+) 0.557 g $KTiOPO_4$/g $K_6P_4O_{13}$; (*) 0.600 g $KTiOPO_4$/g $K_6P_4O_{13}$; (0) 0.642 g $KTiOPO_4$/g $K_6P_4O_{13}$

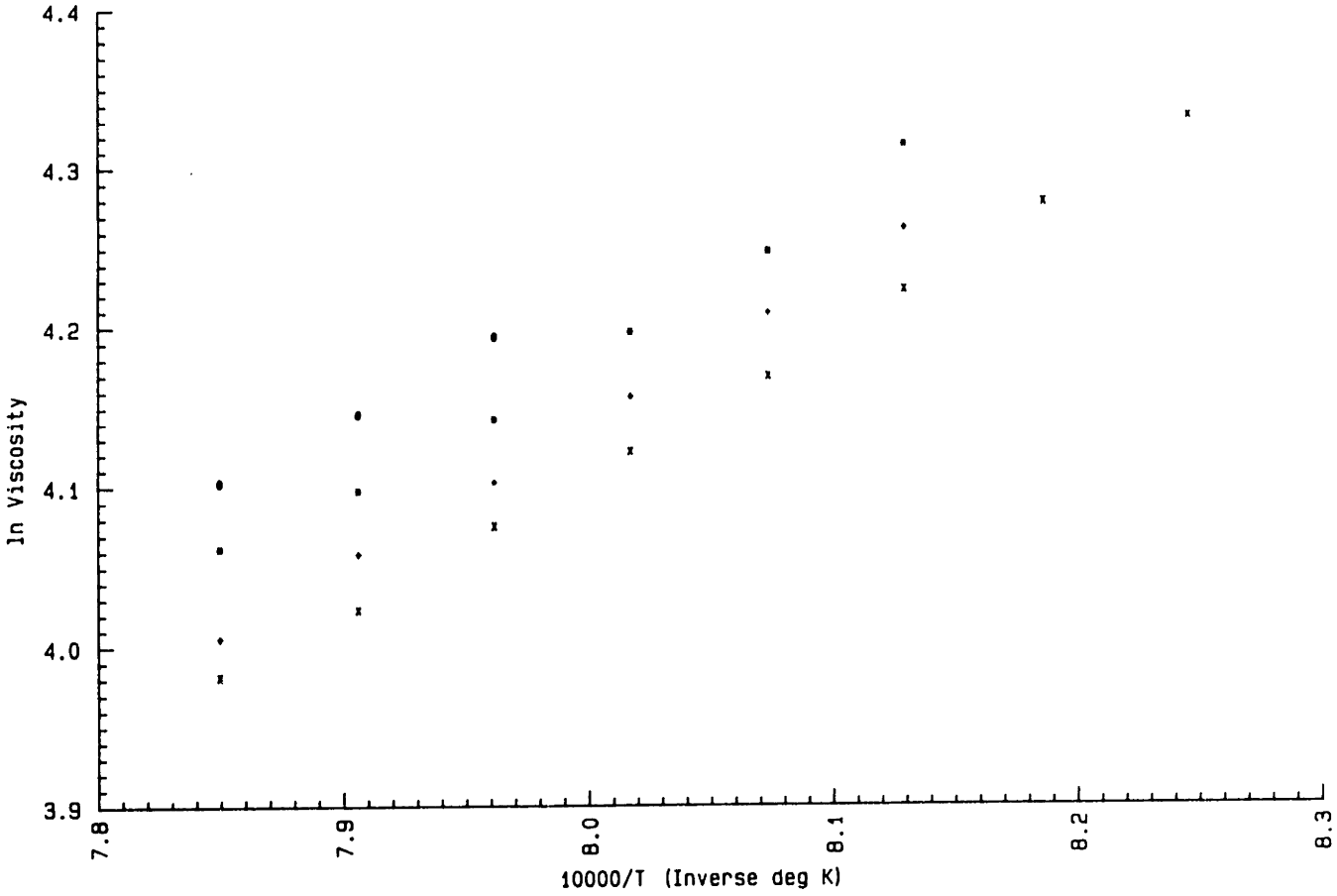

Figure 8. Arrhenius plot of viscosity data (Same key as for Fig. 7)

with coarser measurement resolution. Individual viscosity readings were found to be constant for at least 15 hours. Two of the solutions were cooled into the supersaturated state without onset of spurious nucleation. No discontinuities in the viscosity or its temperature derivative were noted on passing through the saturation point.

The viscosity measurements were reproducible to within ±0.7%, limited largely by the stability and repeatability of the viscometer. The absolute values of the measurements may be in error by as much as ±2.0%, due mainly to inaccuracy associated with the room-temperature calibration procedure. It should be noted that the major source of error in high-temperature viscosity measurement is usually associated with insufficient temperature control [60]. Due to the special furnace system used in the present work, temperature-related inaccuracies were minimal.

Density data were gathered over the same concentration and temperature ranges as the viscosity data. Unfortunately, over these limited ranges, the total variation in density was less than the absolute error associated with its measurement. Thus, all four solutions may be characterized throughout the measured temperature range as having a density of 2.34 ±0.07 g/cm^3. The measurement error was due largely to repeatability problems with the electrobalance. Thus, the concentration dependence of the density could not be determined. Because this repeatability problem was not a factor in measuring thermal variations in density of a given solution, the thermal expansion coefficient of the solutions could be determined. It may be estimated to be 2.4×10^{-4} $^{\circ}C^{-1}$ for all the solutions measured, within 15%. As with the viscosity data, individual density readings were found to be constant for at least 15 hours. Likewise, no discontinuities in the density or its temperature derivative were noted on passing through the saturation point.

As mentioned previously, in many systems, estimates of the liquid/air surface tension are directly forthcoming from application of the two-bob Archimedean technique in measuring liquid

density. In the present case, due to the tendency of the solutions to strongly wet platinum, the contact angle where the platinum support wire pierced the liquid surface was always far from 90°. Assumptions necessary for estimating surface tension using this approach were therefore invalid and no reasonable data could be secured.

Kinematic viscosity, the ratio of viscosity to density, is an important material property parameter in characterizing transport phenomena within a fluid. As an aid to analysis of transport phenomena involving the solutions measured in the present work, Figure 9 combines the viscosity and density data in a plot of kinematic viscosity versus temperature for the four solution concentrations.

4.4 Discussion

The Newtonian flow behavior of the solutions studied is typical of oxide melts. The Arrhenian temperature dependence of the viscosity is also not unexpected. The temperature coefficient of viscosity is approximately 8990°K, corresponding to an activation energy of roughly 75 kJ/mole. This compares reasonably with that measured for sodium phosphate melts [61], one of the few similar systems for which viscosity data exist.

Both viscosity and density data indicate the absence of any structural changes in the solutions as a function of concentration, temperature, or time over the ranges measured. An increase in viscosity with increasing TiO_2 content is observed. This observation may be correlated with a previous study of the infrared spectrum of a glass formed by quenching a typical KTP growth solution consisting of $KTiOPO_4$ dissolved in $K_6P_4O_{13}$ [62]. The IR study revealed the presence of Ti^{4+} coordinated octahedrally by oxygens from chelating bidentate PO_4^{3-} ligands, most probably as the complex $[Ti(PO_4)_3]^{5-}$. It would be reasonable to expect that such a complex would polymerize on addition of TiO_2, leading to an increase in viscosity as observed in the present work.

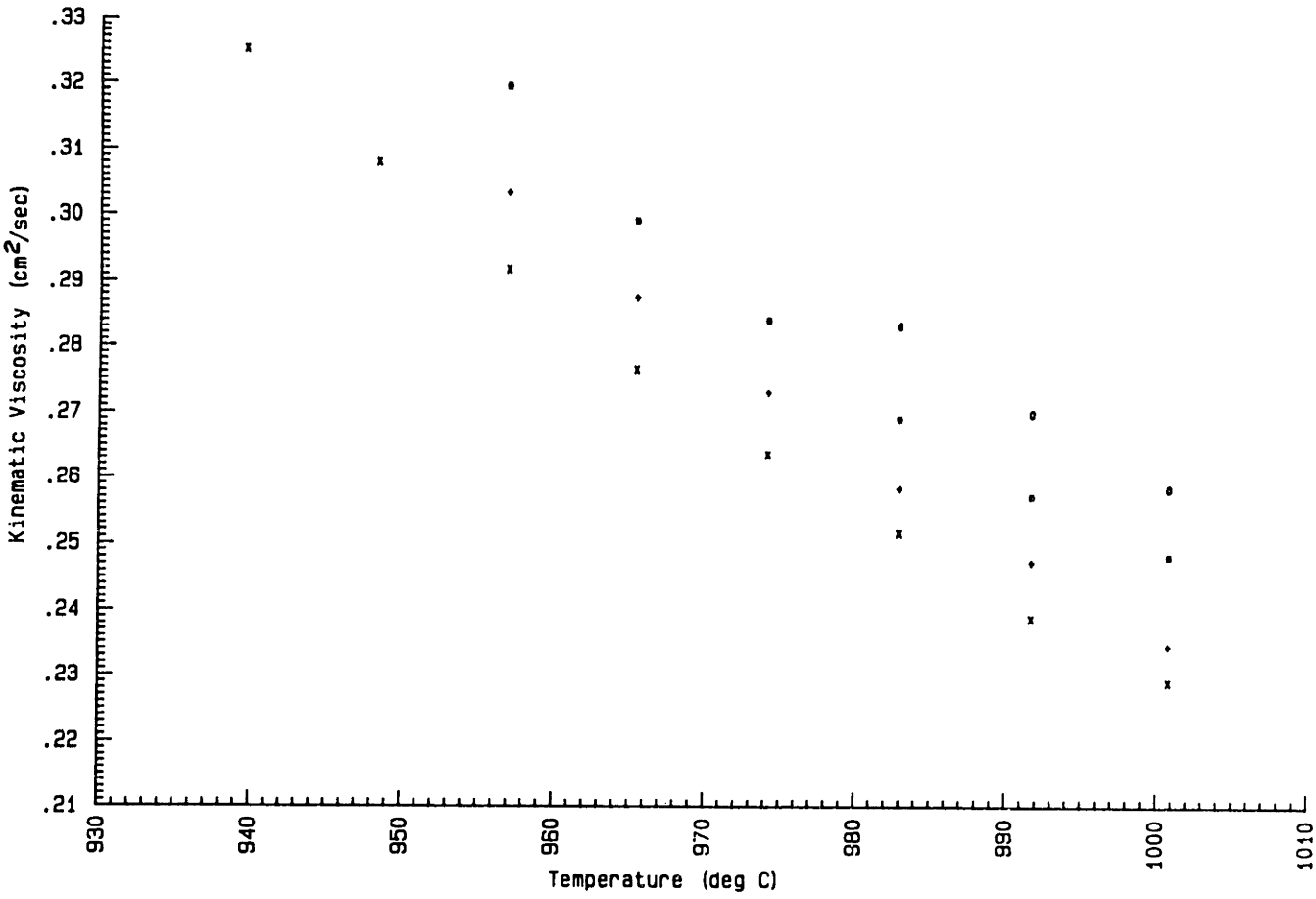

Figure 9. Kinematic viscosity of growth solutions versus temperature (Same key as for Fig. 7)

Regarding crystal growth of $KTiOPO_4$ from $K_6P_4O_{13}$, the generally high value of the kinematic viscosity of these solutions as compared to other solutions commonly encountered in HTS growth operations (see, for example, the discussion in ref. [1]) corresponds well with the observations that the growth process is not controlled by heat transfer and that the system, if not well-stirred, is prone to spurious nucleation.

Chapter 5

Solution Flow Visualization

5.1 Introduction

Chapter 7 presents a report of the occurrence, analysis, and eventual control of solution occlusion flawing phenomena that were encountered in advanced stages of growth of $KTiOPO_4$ crystals in the heat pipe based furnace system. One of the key elements of the work presented there was the ability to model through room temperature simulation experiments the solution flow patterns prevailing during crystal growth. As noted in Section 2.6, the very possibility of such simulation modelling owes to the spatial temperature uniformity obtained throughout the growth solution in using the heat pipe based furnace.

The purpose of the present Chapter is to report some of the details of the flow visualization process itself, irrespective of the particular forced convection patterns it was applied to analyze. Both the relevant analytical background and the experimental techniques applied are discussed.

5.2 Validity of Neglecting Natural Convection

A critical assumption central to the process of solution flow visualization as carried out in the present work was that, for purposes of modelling and analyzing the solution flow patterns prevalent during $KTiOPO_4$ crystallization in the heat pipe based furnace, one could neglect the possibility of natural buoyancy-driven convection and treat the solution flow phenomena as representing a case of purely forced convection brought about by deliberate rotation of the mounted growing crystal. A number of steps were taken to assess the validity of such an assumption.

There are basically two ways through which natural buoyancy-driven convection could

possibly arise in $KTiOPO_4$ crystal growth in the heat pipe furnace system. First, thermal gradients existent in the solution corresponding to the steady-state thermal profile could effect unstable solution density gradients that could lead to recirculating bulk solution flow. Second, the process of crystal growth itself, by necessarily effecting concentration and thermal gradients in the surrounding solution, could effect similar unstable density gradients. Both possibilities must be considered in evaluating the validity of their neglect.

In general, to evaluate analytically the existence and magnitude of buoyancy-driven natural convection due to the existence of a particular thermal field imposed across a fluid, one evaluates the relevant Rayleigh number and then compares the result with experimentation or analysis previously performed and reported on geometrically similar systems. The Rayleigh number is a dimensionless quantitative indication of the tendency in a system toward buoyancy-driven natural convection. For a given geometry, the higher the Rayleigh number, the more likely the existence of such convection. The Rayleigh number is the product of the dimensionless Grashof and Prandtl numbers. Physically, the Grashof number represents the ratio of buoyant forces to viscous forces existent in a system; the Prandtl number is a fluid property parameter representing the relative significance of convective versus conductive modes of heat transfer.

The Grashof and Prandtl numbers are represented in the present situation by the following expressions:

$$Gr = \frac{g\beta L^3 \Delta T \rho^2}{\eta^2} \tag{5.1}$$

$$Pr = \frac{c\eta}{\kappa} \tag{5.2}$$

where g is the gravitational acceleration, β the thermal expansion of the fluid, L the height of the fluid column, ΔT the magnitude of the vertical temperature inversion across the fluid column, ρ the density of the fluid, η the viscosity of the fluid, c the constant-pressure heat

capacity of the fluid, and κ the thermal conductivity of the fluid. For purposes of analysis, the conditions selected were a solution concentration of 0.6 g $KTiOPO_4$/g $K_6P_4O_{13}$, an average solution temperature of 970 ° C, and the conservative case of no forced convection in the solution. The gravitational acceleration is 980 cm/sec^2. The depth of the solution in the crucible, L, was roughly 5.0 cm. Following the analysis presented in Section 2.5, ΔT was taken as 1.4 ° C. β, ρ, and η for the selected conditions were taken from the measurements presented in Chapter 4 as 2.4 x 10^{-4} ° C^{-1}, 2.34 g/cm^3, and 0.7 P, respectively. κ was estimated as in Section 2.6 to be 2 W/m ° K. c was taken conservatively to be 2 J/g ° C. The Grashof number was thereby calculated to be roughly 600, the Prandtl number to be roughly 80, and the resultant Rayleigh number to be 4.8 x 10^4.

In the present case, there were two difficulties associated with comparison of these values to previously reported experimentation and analysis. First, the relevant geometry has not been extensively characterized either analytically or experimentally in the related literature. Second, because the Prandtl number in the present case of interest is much higher than for most of the relevant analyses that have been done, it is likely that conclusions suggested by comparison with these analyses could be in error. In particular, as discussed by Rosenberger and Muller [63], one could imagine a situation where, due in large part to the contribution of the high Prandtl number, the calculated Rayleigh number is found to correspond to a super-critical value as determined in a previous case involving identical geometry but a fluid of lower Prandtl number. If, despite the apparently high Rayleigh number, there is insufficient power as measured by the Grashof number to overcome the viscous drag forces associated with maintaining liquid flow, natural convection might not in fact occur. Thus, in utilizing results derived through experiments or calculations involving fluids of lower Prandtl number, the analysis must be viewed for present purposes as conservative. That is, a critical Rayleigh number corresponding to the onset of natural convection in the case of a lower Prandtl number may well not represent natural convection in the high Prandtl number case of interest.

With these limitations in mind, probably the most relevant previous work was that presented by Brice [64]. Reproduced as Figure 10, it is a plot of critical Rayleigh number for the onset of natural buoyancy-driven convection as a function of liquid aspect ratio for the case of a liquid contained in a cylindrical crucible. In general, the liquid Prandtl numbers represented by the plot fall in the range of 0.1 to 1.

As shown on the figure, for the relevant aspect ratio of 1.25, the Rayleigh number of 4.8 x 10^4 calculated for the present case falls almost exactly on the line representing the critical Rayleigh number for the onset of natural buoyancy-driven convection. However, as noted by Brice, in a situation like the present one where the thermal diffusivity of the crucible material is much higher than that of the liquid, the critical Rayleigh numbers are actually a factor of about 1.6 higher than those represented by the plot. Considering in addition both that the fluids represented by the plot are of lower Prandtl number than the fluid of interest and that the effect of imposed forced convection on lowering the magnitude of the vertical temperature inversion is being conservatively ignored, it appears safe to conclude that, based on this analysis, the assumed neglect of bulk natural convection in the growth crucible is justified.

This conclusion was corroborated experimentally through visual inspection of the solution and also examination of the temporal variation of the output of the profiling thermocouple assembly discussed in Section 2.6. In viewing an unstirred solution through the furnace cover opening, there was no visual evidence of bulk fluid motion. More important, there were observed to be no periodic temperature fluctuations at a given location in the unstirred liquid such as would be expected in the case of recirculating bulk convection.

Turning to the issue of the crystallization process itself effecting natural convection in the region of the growth interface, the validity of neglecting such phenomena was assessed through a simplified but conservative analysis based on the work of Chen et. al. [65]. The situation selected for analysis was the case of a growing $KTiOPO_4$ crystal several centimeters on an edge

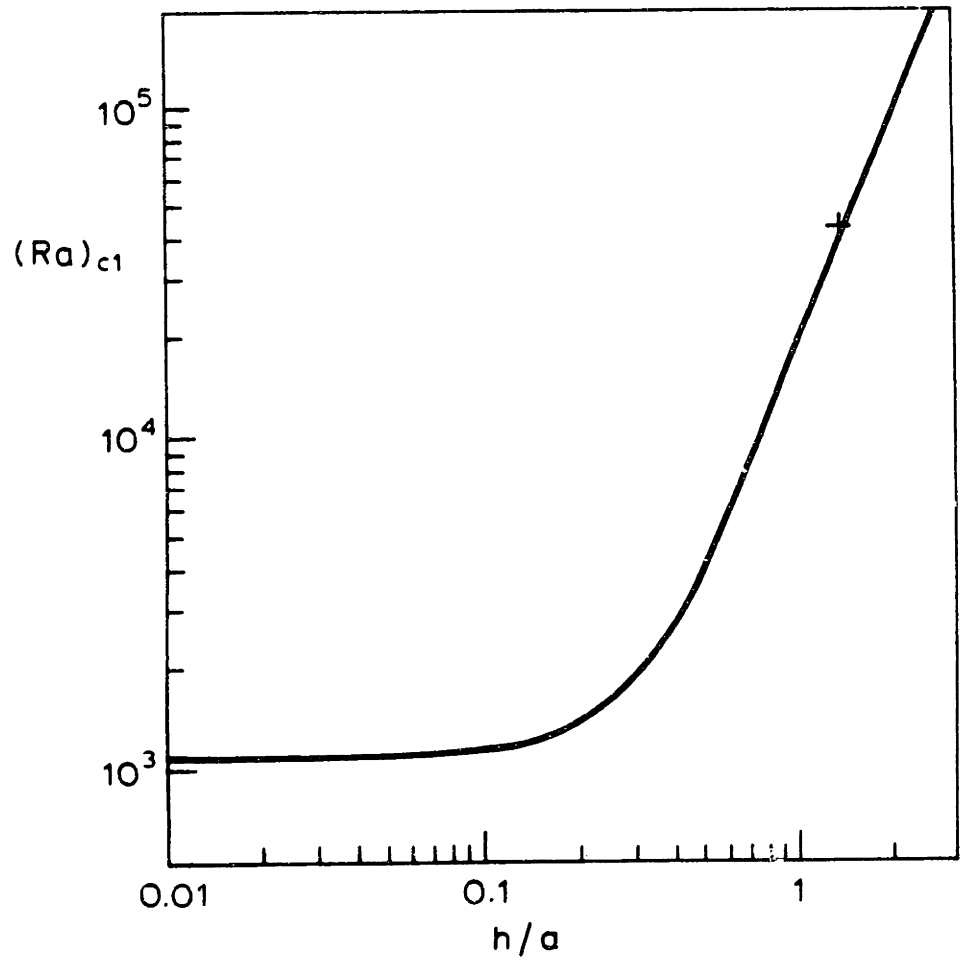

Figure 10. Critical Rayleigh number versus liquid aspect ratio for natural convection in cylindrical crucible [64]. (+ represents present case)

being rotated in the center of the solution volume about its own central vertical axis at a frequency of 60 RPM. The temperature of the solution was taken to be 950 ° C.

First, as reported by Chen et. al., the influence of natural buoyancy-driven convection effected by the crystallization process itself is by far most significant on the facet whose normal points either along or opposite to the gravitational vector, depending on the sign of the liquid density difference effected by crystallization. Therefore, for purposes of the present analysis, only one facet needed to be considered in investigating the relative influence of natural convection.

Second, for crystallization from solution in cases like the present where, as discussed in Section 2.3, the mass transfer process dominates the heat transfer process in terms of its kinetic resistance to growth, the buoyant force due to mass transfer near the growth interface is generally several orders of magnitude greater than the force due to heat transfer. As such, it was felt reasonable to ignore any possible effects stemming from the evolution at the growth interface of the heat of crystallization and to focus solely on the solutal effects of crystallization and their possible influence on natural convection.

Third, Chen et. al. presented the formulation of a Grashof number that could be applied in the present situation as an index of the buoyant forces existent near a growing horizontally-oriented interface due to the solutal effects of crystallization. It is given by the following expression:

$$Gr = \frac{g\rho(\frac{\partial \rho}{\partial C})(C_0 - C_{SAT})}{\eta^2} \left(\frac{xy}{2x + 2y}\right)^3 \tag{5.3}$$

where g is the gravitational acceleration, ρ the average density of the fluid, η the average viscosity of the fluid, the product of $(\partial\rho/\partial C)$ and $(C_0 - C_{SAT})$ the unstable density difference normal to the growing surface corresponding to the concentration gradient, and x and y the linear dimensions of that surface.

As in similar cases of evaluating the relative influence of natural and forced convection, this Grashof number could presumably be compared with a Reynolds number indicating the magnitude of the forced convection in the vicinity of the growing crystal. For values of $Gr/\mathrm{Re}^2 < 1$, the flow field can be considered to be dominated by forced convection with natural convection effects negligible. The Reynolds number was expressed in the present case as

$$\mathrm{Re} = \frac{D^2 \omega \rho}{2\eta} \tag{5.4}$$

where D is an average linear dimension of the crystal, ω is the imposed rotation frequency of the crystal, and ρ and η are as above.

The gravitational acceleration is 980 cm/sec^2. D was taken as 2 cm. x and y were taken as 2 cm and 1 cm, respectively. ω was taken as 60 RPM. ρ and η were taken as before as 2.34 g/cm^3 and 0.7 P, respectively. The product of $(\partial\rho/\partial C)$ and $(C_0 - C_{SAT})$ was estimated conservatively as follows. As presented in Chapter 4, in measuring the density difference between growth solutions with saturation temperatures roughly 60 °C apart, no difference was detectable within a resolution of 0.07 g/cm^3. Thus, as a worst case, such solutions could differ in density by at most 0.14 g/cm^3. For the present case, a conservatively high effective temperature difference corresponding to the imposed bulk supersaturation was taken as 5 °C. An upper limit on the unstable density difference due to the solutal effects of growth was thus taken as the product of (5/60) and 0.14 g/cm^3, or 1.2 x 10^{-2} g/cm^3.

The Grashof number was thereby conservatively calculated to be 2, the Reynolds number to be 7, and the resulting ratio of Gr/Re^2 to be 4 x 10^{-2}. It was thus concluded that any natural buoyancy-driven convection effects brought about by the crystallization process itself could be safely ignored for purposes of flow visualization in cases where even moderate forced convection effects corresponding to imposed crystal rotation frequencies of tens of RPMs were involved.

5.3 Experimental Technique

Given the validity of neglecting natural buoyancy-driven convection effects, the techniques and apparatus involved in modelling through room temperature simulation the solution flow patterns prevailing during crystal growth were relatively simple and straightforward. Water was used as the model fluid. Lucite models were fabricated having various sizes and shapes typical of growing $KTiOPO_4$ crystals. These were provided with threaded mounting holes for attachment to aluminum rods. The rods had the same diameter and shapes as the platinum seed-holding rods and were each provided with a coupling enabling connection to a reversing rotation motor similar to the ones incorporated in the puller units. A borosilicate glass crucible was fabricated with dimensions identical to those of the platinum growth crucibles.

There were two methods employed for the actual flow visualization. The first involved the injection of dye into the visualization crucible during imposed motion of a model crystal. By using a hypodermic syringe with a long needle that could be bent into a variety of desired configurations, dye could be injected in various locations in the fluid with minimal intrusion on the forced convection pattern. The second method involved the suspension in the water of micron-sized aluminum particles. These would remain in suspension effectively indefinitely, following the motion of the fluid. The moving aluminum particles were selectively illuminated by a beam from an argon gas laser formed into a thin sheet through the use of cylindrical lenses. Through variation of the crucible position and the lens orientation, the plane of illumination could be moved throughout the fluid volume. Figure 11 shows the flow simulation apparatus with the laser sheet beam illuminating suspended aluminum particles in a selected plane of fluid.

In analyzing a given forced convection pattern, the two visualization methods were complementary. Dye injection generally served to indicate the flow pattern throughout the bulk of the fluid; sheet beam illumination of suspended aluminum particles was particularly useful in elucidating the details of a flow pattern near the moving surfaces of a crystal model.

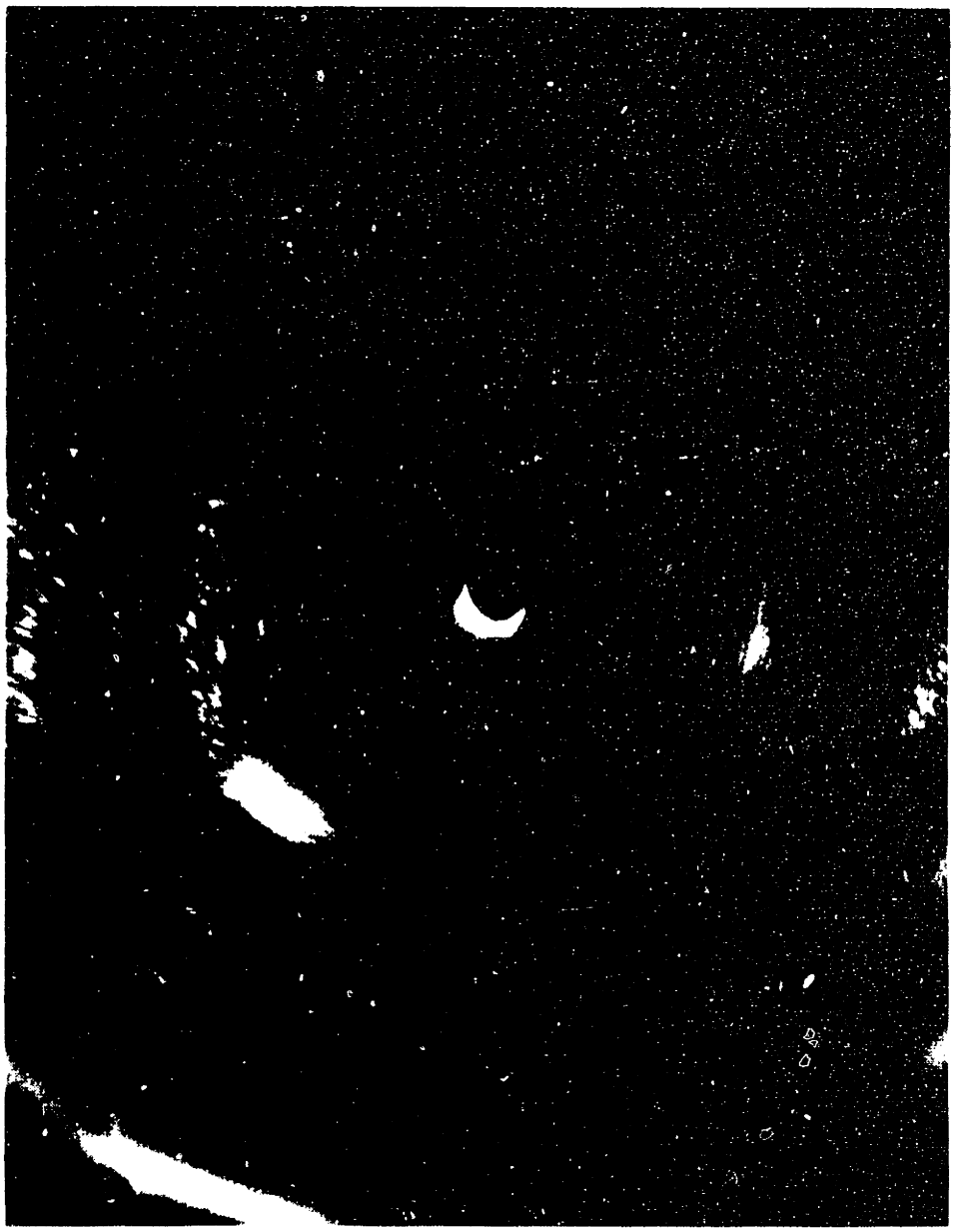

Figure 11. Flow visualization by laser sheet beam illumination of suspended aluminum particles

INTENTIONAL DUPLICATE EXPOSURE

It was originally intended to record photographically the flow patterns observed in the simulation experiments. It was soon realized that the effort and expense of such an approach far outweighed its potential benefits. As such, visual records of flow patterns, when needed, were provided through collaboration with graphic artists.

It should also be noted that, in a number of cases, numerical flow simulation using finite-difference flow tracking software [66] was performed in collaboration with the present work [67].

5.4 Model Scaling for Dynamic Similarity

The basis of flow simulation modelling is the establishment of equivalence between the relevant dimensionless groups in the model system and the actual system of interest. In the present case, given that the flow patterns involved represented cases of purely forced convection, there were two such dimensionless groups to take into account. These were the Ekman number and a dimensionless characteristic time.

The Ekman number is represented by the following expression:

$$E = \frac{\nu}{\omega r^2} \tag{5.5}$$

where ν represents the kinematic viscosity, ω the rotation frequency, and r a radius associated with the rotating crystal. According to the principles of dynamic similarity, for a case of rotational forced convection, two geometrically similar systems having equivalent Ekman numbers will at steady state posess geometrically similar flow velocity vector fields. In the present case, the relevant linear dimensions of the actual and model systems were identical. As such, equivalence of the Ekman numbers required that the following equation be satisfied:

$$\frac{\omega_{MODEL}}{\nu_{MODEL}} = \frac{\omega_{ACTUAL}}{\nu_{ACTUAL}}. \tag{5.6}$$

The kinematic viscosity of water is approximately 0.01 cm^2/sec. As presented in Chapter 4, the

kinematic viscosity of $KTiOPO_4$-$K_6P_4O_{13}$ growth solution was measured to be roughly 0.30 cm^2/sec. Appropriate scaling therefore required that the respective rotation frequencies of the actual and model cases be in the ratio of roughly 30 to 1. Thus, for example, to simulate a crystal growth flow pattern brought about through a rotation frequency of 60 RPM, the room temperature model system was operated with a rotation frequency of 2 RPM.

The dimensionless characteristic time variable was involved in scaling the flow transients associated with start-up, stoppage, and reversal of crystal rotation. This variable is represented by the following expression:

$$t^* = \frac{t}{\tau} = \frac{t\nu}{l^2} \tag{5.7}$$

where t^* is the dimensionless time variable, t is the actual time increment associated with the particular transient of interest, and τ is some characteristic system time constant in turn equal to the ratio of the square of some characteristic length, l, to the kinematic viscosity of the fluid, ν. Analogous to the case of the Ekman number scaling, because the linear dimensions of the actual and model systems were identical, appropriate modelling of transients required that the following equation be satisfied:

$$(t_{MODEL})(\nu_{MODEL}) = (t_{ACTUAL})(\nu_{ACTUAL}). \tag{5.8}$$

Here, therefore, the ratio of the relevant time increments for the model and actual cases was inversely proportional to the ratio of the kinematic viscosities of the corresponding fluids. Thus, for example, the change effected in the fluid velocity vector field in the actual crystal growth system by a rotation stoppage of 2 seconds was modelled in the room temperature simulation system by a rotation stoppage of 60 seconds.

Chapter 6

Seeding Process

6.1 Introduction

The first step in any controllable and reproducible process of crystal growth from solution is a controllable and reproducible seeding operation. Unfortunately, the development of a seeding operation is a largely empirical and often time-consuming task. Over the course of the present project, significant effort was devoted to developing and optimizing a viable seeding operation for the growth of $KTiOPO_4$ from its solution in $K_6P_4O_{13}$ using the heat pipe based furnace system. This Chapter reports the content and results of that effort. Included are discussions of seed attachment and the effects of immersion, rotation, and supersaturation on initial seeded growth.

6.2 Seed Attachment

Although a number of methods were considered for attaching seeds to the end of the alumina seed rod, only two basic approaches were applied experimentally. The initial approach involved securing a small piece of single-crystalline $KTiOPO_4$ in the end of a hollow platinum tube in turn affixed to the lower end of the alumina rod. A tube measured roughly 7 cm in length with a 5.8 mm inner diameter and a 0.3 mm wall thickness and was secured to the alumina rod with a locking wire threaded through a cross-bored hole. The seed was held in the lower end of the platinum tube by pinching the malleable platinum tube walls tight up against the seed using needlenose pliers.

Although seeds held in this manner were surprisingly secure, there were felt to be a number of problems with the approach. Unavoidable folds and scratches in a pinched platinum tube

tended to serve as preferred sites for spurious nucleation. As a crystal grew up and around the lip of a seed holding tube, cracking tended to result, apparently from strain induced by growth around the uneven surface. Most important was the fact that reproducibility in crystallographic seed orientation was impossible to achieve within better than about 10°. Also, the sizes and shapes of potential seeds were severely restricted.

The preferred seeding approach involved drilling and threading a hole in a small piece of single-crystalline $KTiOPO_4$ and screwing it onto the end of a threaded solid platinum rod in turn affixed to the lower end of the alumina rod. A hole was drilled in a $KTiOPO_4$ seed with a 2.3 mm diameter diamond core drill. Threading a drilled hole was performed by means of an ultrasonic drill operating at 20,000 Hz with a 0.025 mm vibration amplitude. A solid tungsten carbide tap was used along with a cutting slurry of 8 μm silicon carbide in water. The final thread size was 4-40 UNC.

Some seeds were drilled and threaded through, while in other seeds a blind hole was made. The main difference between the two approaches was that a better thread could be cut in a hole drilled through. The thread quality in seeds with blind holes was generally such that at most one full turn could be achieved in screwing a seed onto a threaded platinum rod. As a result, if slight dissolution occurred upon introducing into the growth solution a seed mounted with a blind hole, the probability of the seed falling from its mounting to the bottom of the crucible was about one in two. In the case of a seed with a mounting hole tapped through, the mounting was much more secure, and there appeared to be no problem in having deposited crystalline material "heal" over the opening at the bottom of the mounting hole. In either case, there was no evidence of any problem associated with the advancement of a growing crystal over and around the platinum seed rod. In fabricating a grown crystal, the seed rod and the material immediately surrounding it needed to be cut away from the bulk of the crystalline material.

Both fabricated parallelpiped and naturally-facetted seeds were used, the latter the product

of random nucleation from slow-cooling of $KTiOPO_4$-$K_6P_4O_{13}$ solutions using other furnaces. A variety of orientations was examined for placement of the mounting hole. There appeared to be no relationship between seed orientation and the quality of initial growth on a seed.

Figure 12 shows the typical habit of spontaneously nucleated $KTiOPO_4$ crystals. In the case of using naturally-facetted seeds, due to their typical habit, geometric constraints dictated that, in general, as can be seen from the figure, drilling the mounting hole parallel to the $\vec{a}$ direction afforded the use of the smallest seeds. Since, as discussed in Section 6.4, initial growth off a seed was always accompanied by a flaw corresponding to the outline of the original seed, it was desirable to minimize the seed size. As such, in most experiments involving naturally-facetted seeds, the seeds were drilled and threaded in the $\vec{a}$ direction.

Figure 13 shows a fabricated parallelpiped seed, mounted on a platinum rod. Platinum rods were coupled to the alumina rod with a locking pin through a cross-bored hole.

6.3 Effect of Immersion & Rotation on Initial Growth

As noted in the last Section, in using a pinched platinum tube for seed holding, problems were encountered when a crystal grew up and around the scratched and uneven lip of the tube. The resulting growth tended to be cracked, strained, and filled with regions of occluded solution. In an attempt to avoid such problems without changing the seed attachment method, growth was attempted using a seed held in a position where it was just piercing the surface of the liquid solution. Such an experiment was repeated using a drilled and threaded seed mounted on a solid platinum rod.

In both cases, due presumably to surface tension effects, the liquid solution tended to "creep" up the crystal seed onto the platinum rod, precipitating there as a random polycrystalline aggregate. This process continued until the end of the growth run, by which time more $KTiOPO_4$ had precipitated in polycrystalline form on the seed holder than had grown beneath

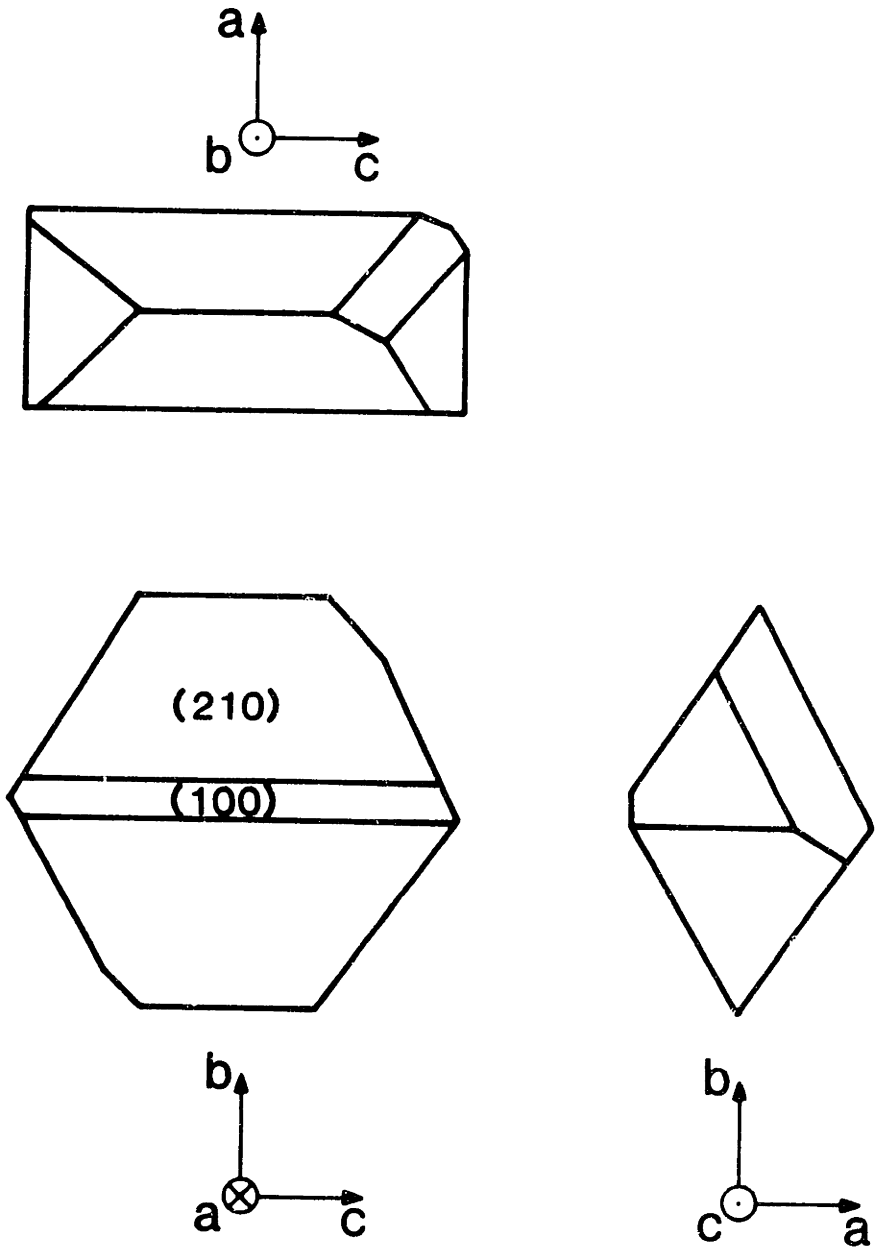

Figure 12. Typical habit of $KTiOPO_4$ crystals

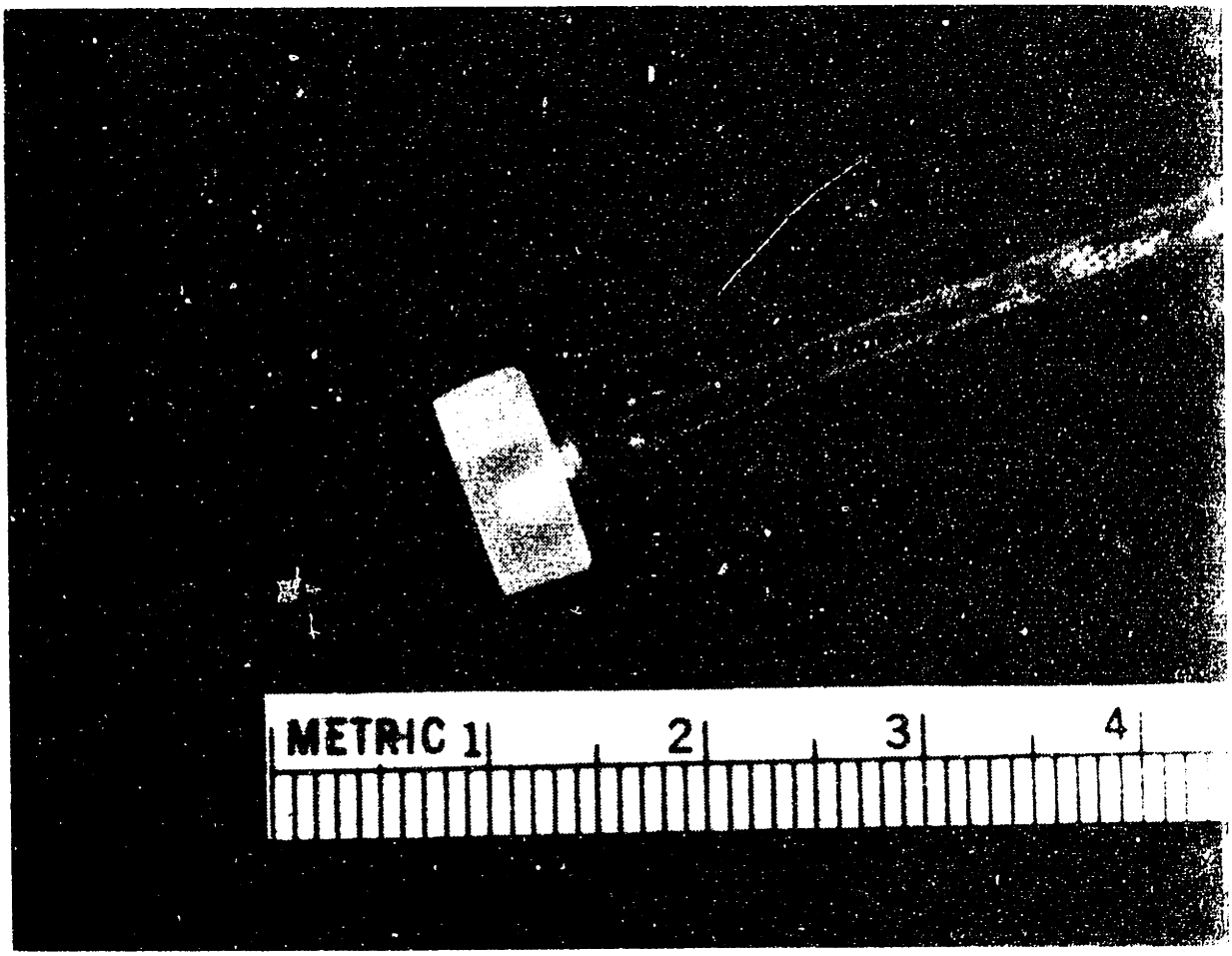
METRIC 1
2
3
4

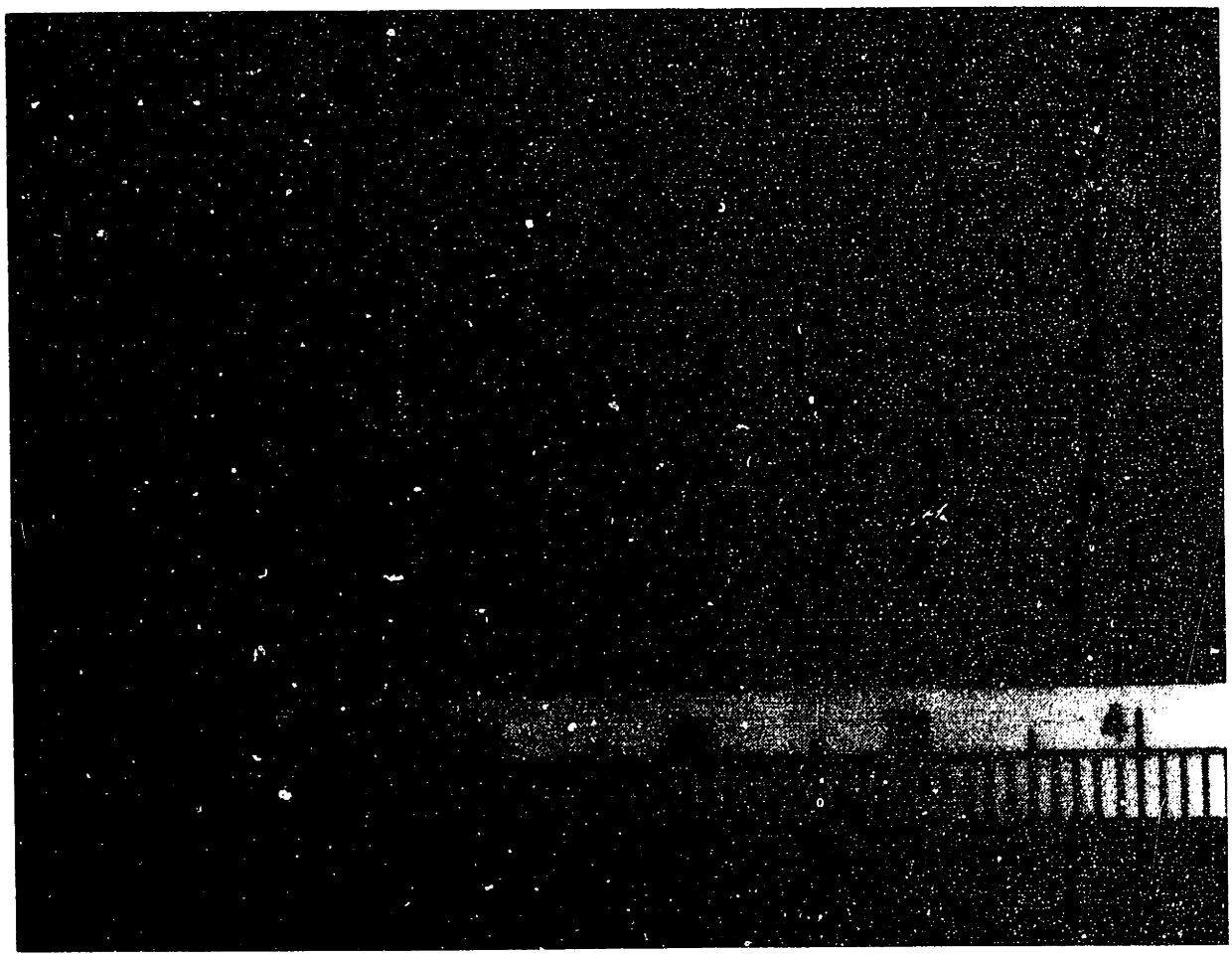

Figure 13. Fabricated seed, screw-mounted on platinum rod

the liquid surface as a single crystal. Aside from these two experiments, all other growth runs were initiated with the seed immersed roughly midway between the solution surface and the bottom of the crucible.

Solution flow conditions around immersed seeds were varied widely over the course of the experiments through application of different rotation rates and different time periods for intermittent reversal of seed rotation. Although, as discussed in Chapter 7, these parameters were identified as critical to controlling and avoiding solution occlusion phenomena in advanced stages of growth, they appeared to be of negligible significance in affecting initial growth on a seed.

6.4 Effect of Supersaturation on Initial Growth

The initial state of undersaturation or supersaturation in the growth solution at the time of seed immersion appeared to be the most important parameter influencing the quality of initial growth on a seed. In general, it was found empirically that if slight initial dissolution of original seed surfaces could be achieved through achievement of a state of undersaturation in the solution at the time of seed immersion, then the growth that followed upon attainment and maintenance of supersaturation would be of far superior quality to the growth that would occur if there were no initial dissolution. Following this observation, the major difficulty to be addressed was the achievement of sufficient control over the process necessary to enable slight dissolution without having a seed dissolve to the point of falling from its mounting. Apart from its initial positive or negative state at the time of seed immersion, the supersaturation program as controlled by the furnace cooling program appeared to have no effect on the early stages of growth.

The issues involved are best illustrated by reference to the $KTiOPO_4$-$K_6P_4O_{13}$ solubility curve, presented as Figure 14. The data represented by the curve were gathered over a large

number of growth experiments and can be considered accurate within ±1%. The key region of the solubility curve for purposes of the present work lies between 965 ° and 970 ° C. This is the region where almost all the growth experiments were seeded. The most commonly used initial growth solution concentration of 0.6 g $KTiOPO_4$/g $K_6P_4O_{13}$ is saturated with respect to $KTiOPO_4$ at 968±0.5 ° C. The slope of the curve at this point is roughly 2.13 x 10^{-3} g $KTiOPO_4$/g $K_6P_4O_{13}$/ ° C.

With finite error limits associated with solution concentration preparation, furnace temperature repeatability, and, especially, temporal furnace temperature stability, there was a corresponding error limit associated with the control resolution on the initial level of supersaturation at the time of seed immersion. The value of this error limit can be estimated to be about ±9.64 x 10^{-4} g $KTiOPO_4$/g $K_6P_4O_{13}$, corresponding to an effective temperature control limit of about ±0.45 ° C. Due to the existence of this control limitation, in an operational sense, the "saturation point" for a given nominal solution concentration value could be considered to have a finite width of roughly 0.90 ° C. Therefore, for example, in order to ensure that an intended initial state of supersaturation was achieved, there was a finite minimum to the nominal supersaturation value, a minimum of 9.6 x 10^{-4} g $KTiOPO_4$/g $K_6P_4O_{13}$. In terms of dimensionless relative supersaturation, this corresponds to a nominal minimum of $\sigma = 1.6 \times 10^{-3}$. Similarly, in the case of undersaturation, the minimum nominal value was -9.6 x 10^{-4} g $KTiOPO_4$/g $K_6P_4O_{13}$ or $\sigma = -1.6 \times 10^{-3}$. In the experiments to be described, these minima were in all cases the values associated respectively with the initially supersaturated and undersaturated states.

The first experiments on the effect of supersaturation on initial seeded growth involved the minimum controllable positive supersaturation level and therefore no initial seed dissolution. The original attraction of employing a state of positive supersaturation at the time of seed immersion followed the belief that the effected slight initial growth and avoidance of dissolution would promote the security of the mounted seed. This belief was generally confirmed by

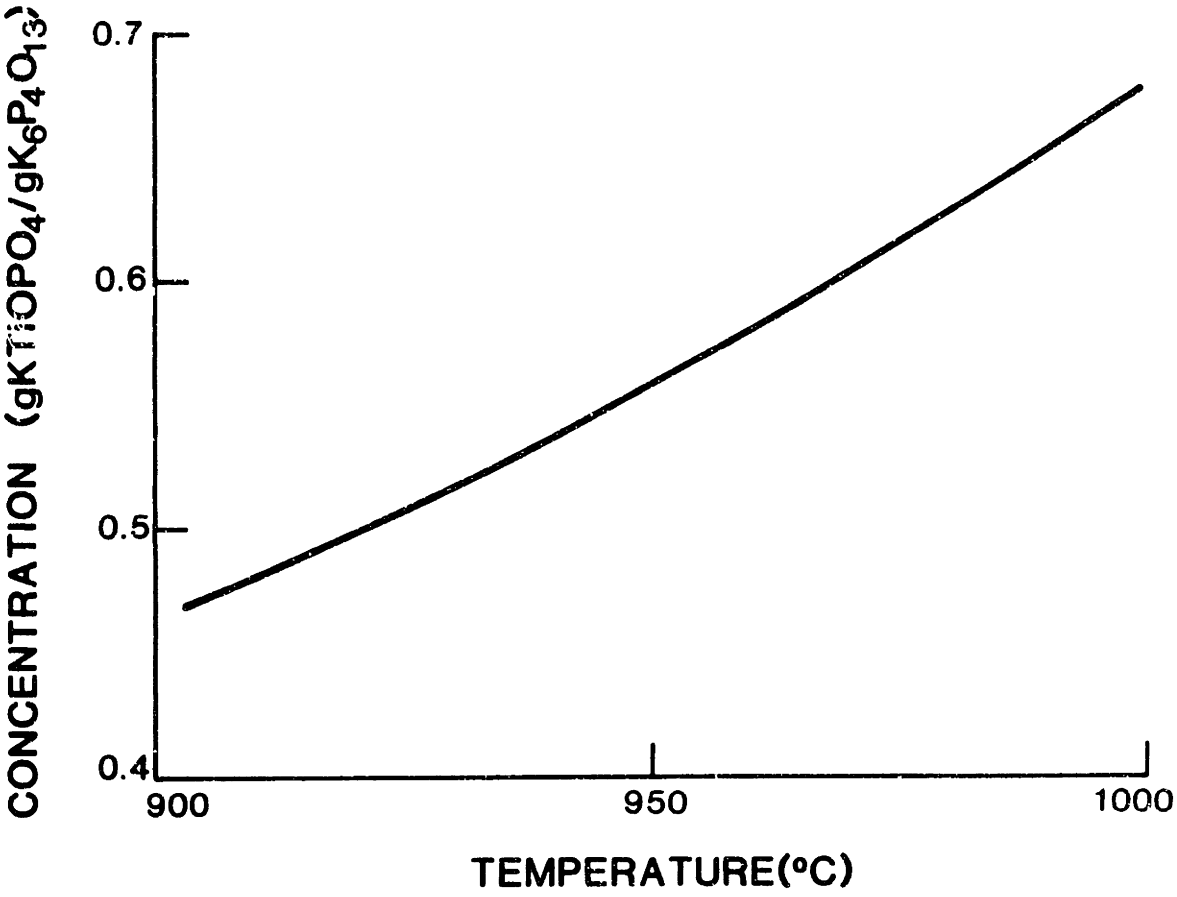

Figure 14. Solubility versus temperature of $KTiOPO_4$ in $K_6P_4O_{13}$

experiment. In all cases of inserting a mounted seed into a supersaturated solution, the seed held fast to its mounting. This was true for seeds held in pinched platinum tubes and for seeds drilled, threaded, and secured onto platinum rods with both blind and through mounting holes.

A number of different furnace cooling programs were employed following i nmersion of seeds into supersaturated solutions. In general, although quantitative in-line cross-correlation between bulk supersaturation and furnace cooling rate is difficult, for a given crystal size the bulk supersaturation increases roughly linearly with furnace cooling rate. Initial furnace cooling rates following seed immersion into supersaturated solutions ranged from as high as 10 °C/day to as low as 0.5 °C/day. The latter value corresponds to an initial cooling rate established by the crystal area dependent cooling program described in Section 3.4.

Over this range of cooling rates, the nature of the cooling program imposed following immersion of a seed into an initially minimally supersaturated solution appeared to have no effect on the initial growth off the seed. In general, such growth was marked by grossly non-uniform advance of habit-forming faces and, correspondingly, extensive regions of solution occlusion. A notable exception was the case of faces on naturally-facetted seeds oriented perpendicular to the $\vec{c}$ direction. Initial growth on these faces following seed immersion into supersaturated solution was in certain cases visually uniform and flaw-free.

In all cases of flawed growth on seeds immersed in initially supersaturated solution, as growth progressed, the discontinuous growth facets would gradually coalesce into a habit-forming surface consisting of a set of crystallographically unique planes upon which visually uniform and flaw-free growth could occur. In the case of starting with a roughly 4 x 4 x 3 mm^3 naturally-facetted seed screwed onto a platinum rod and immersed in an initially supersaturated growth solution subsequently cooled at 5 °C/day, such coalescence of the habit-forming faces following their initial non-uniform advance would be completed by the time the crystal reached a size of roughly 4 x 4 x 3 cm^3. In the case of original seeds containing surfaces not

corresponding to natural facets, the corresponding size required for the completion of such coalescence was greater.

Unfortunately, given the limited volume of the growth crucible, this phenomenon of the "healing" of the effects of initial growth non-uniformities did not occur quickly enough to allow growth following seed immersion into initially supersaturated solution to be considered technically feasible for the production of large volumes of flaw-free crystalline material. Given an apparently necessarily flawed volume of at least roughly 4 x 4 x 3 cm^3 in its center, a crystal could at best add on less than 1 cm of visually flaw-free growth in all directions before running out of space in the growth crucible.

The mechanism responsible for the observed flawed, non-uniform growth on a seed immersed in an initially supersaturated solution was not explained in the course of the present work. It is known that $KTiOPO_4$ crystals held in air at a temperature of 1000 ° C for 24 hours will undergo a surface degradation effect whereby a thin film of TiO_2 and KPO_3 forms on the surface [24]. It was thus hypothesized that a similar degradation effect could be occurring upon introduction of a $KTiOPO_4$ seed into the heated furnace cavity prior to its immersion in the solution and that such degradation could result in a surface structure somehow unsuitable for flaw-free growth. To investigate the hypothesis, an X-ray photoelectron spectroscopic study of the effect of brief exposure to the heated furnace cavity on $KTiOPO_4$ crystal seeds was initiated. At the time of the present report, the results of this study were as yet inconclusive [68].

Further experiments on the effect of supersaturation on initial seeded growth involved the minimum controllable level of undersaturation at the time of seed immersion and therfore initial dissolution of original seed surfaces. It was clear from the first such experiment that, if the dissolution could be controlled to the extent that the seed did not dissolve enough to fall from its mounting, the growth immediately following attainment and maintenance of supersaturation could be visually uniform and flaw-free. A number of cooling programs were applied following

initial controlled dissolution, the most common being a constant cooling rate of 5 ° C/day. In all cases, the transition from dissolution to growth was marked by a thin "veil" of solution occlusion corresponding roughly to the outline of the original seed. The growth immediately beyond the veil was visually flaw-free in all directions. Figure 15 illustrates such a seeding veil within a grown crystal corresponding to the transition from initial dissolution to growth. Because of the apparent necessity of formation of such a seeding veil, it should be noted that, in using such a seeding technique, the potential volume of usable flaw-free crystalline material from growth in a crucible of a given size is maximized by using the smallest possible seed.

Given the desirability of achieving initial seed surface dissolution, a number of steps were commonly taken to minimize the possibility of having a seed dissolve to the point of falling from its mounting. First, as mentioned in Section 6.2, it was determined that if mounting holes in seeds were drilled and threaded through the entire seed volume rather than blind, the resulting improvement in thread integrity effected a mounting more able to withstand slight dissolution. Second, after seed immersion into undersaturated solution, seed rotation was not begun until the reference thermocouple readings indicated a solution temperature below the initial saturation temperature. Such an approach presumably served to impede and therefore control the dissolution process by increasing the associated mass transfer resistance. By the end of the present project, this seeding process involving initial surface dissolution was controllable and reproducible to the extent that 6 of the last 7 growth run attempts were seeded effectively without either losing the seed or promoting seeding-related flaws beyond the extent of the original seed surfaces.

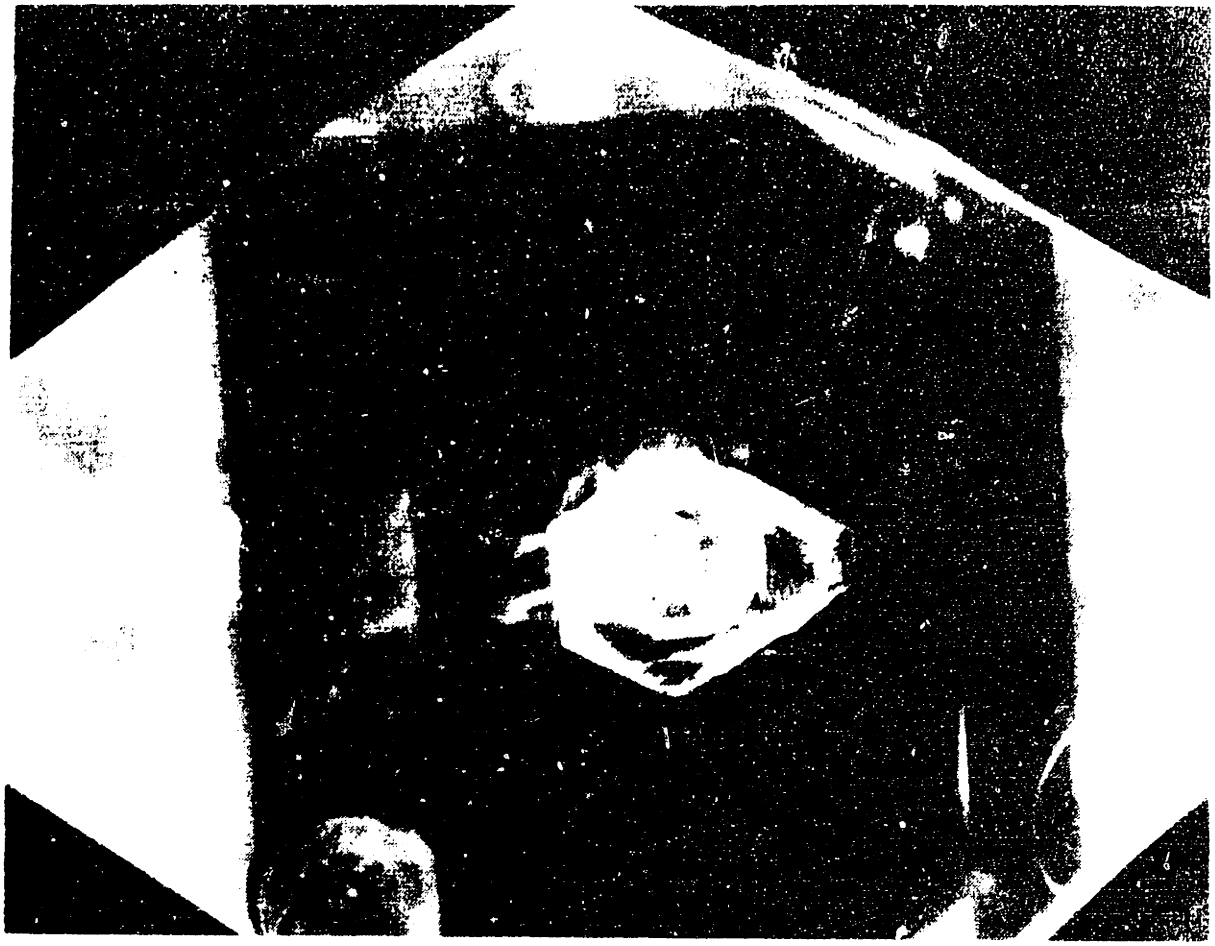

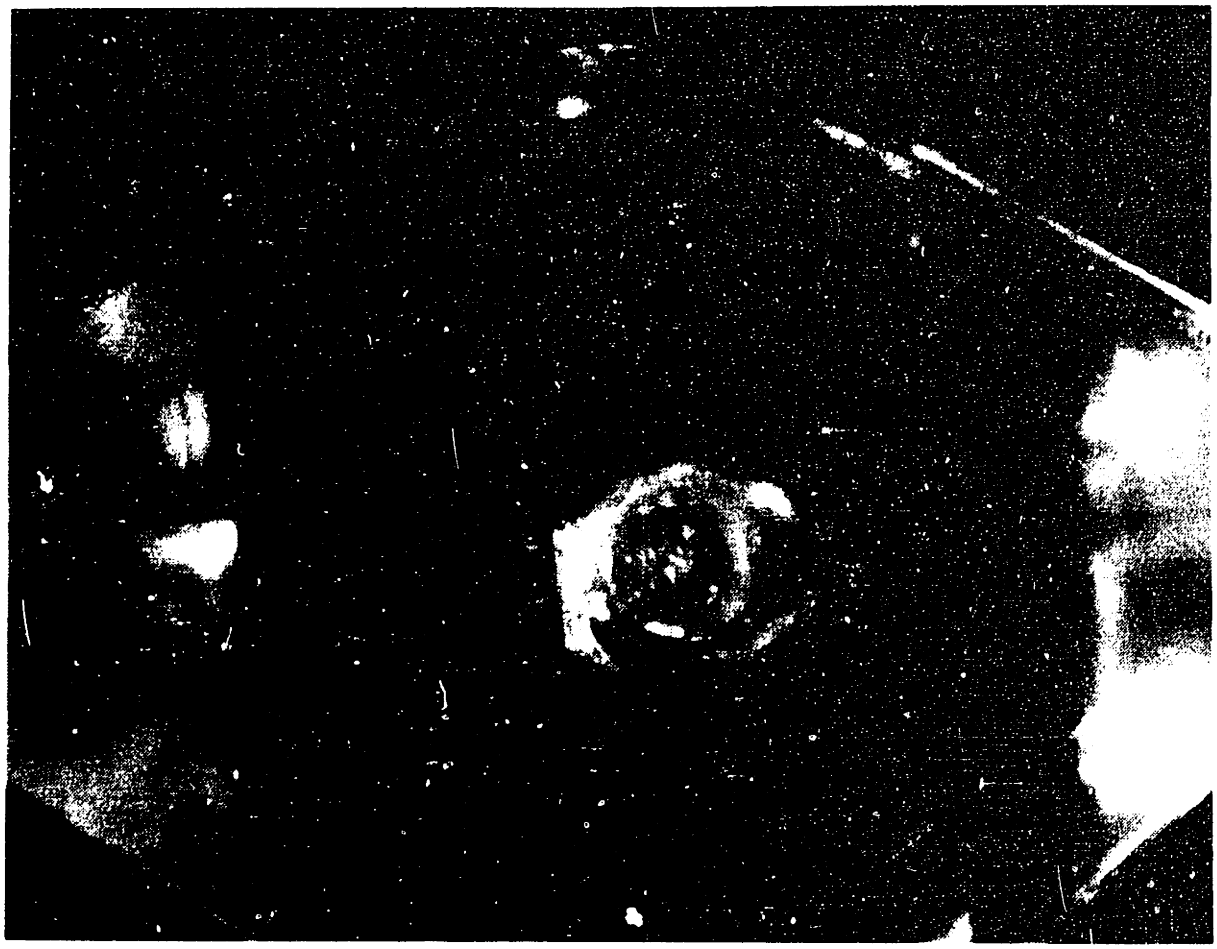

Figure 15. Seeding veil in grown crystal of $KTiOPO_4$

Chapter 7

Advanced Stages of Growth

7.1 Introduction

In carrying out the present project, the first major issue addressed, presented in Chapter 2, was the development of a furnace system that allowed $KTiOPO_4$ crystallization from its solution in $K_6P_4O_{13}$ to proceed free from the occurrence of uncontrollable spurious nucleation. The second major issue, presented in Chapter 6, was the development of an effective and reproducible seeding operation by which a $KTiOPO_4$ growth process could be controllably initiated while minimizing the associated flawing. The third and final major issue, that of sustaining the growth of high-quality $KTiOPO_4$ crystalline material from beyond the seeding stage to the ultimate size limit imposed by the dimensions of the crucible, is the subject of the present Chapter.

The primary problem encountered in this endeavor involved a macroscopic flawing effect whereby chronic instability of growing interfaces would lead to bands of occluded solution in grown crystals. As is discussed, the treatment of this problem involved the solution flow visualization techniques presented in Chapter 5 in concert with a body of theory still in its infancy concerning the relationships between bulk fluid flow and interfacial stability of crystals growing from solution.

7.2 Interfacial Instability in Crystal Growth from Solution

The trapping and inclusion of volumes of growth liquid is a common mode of defect formation in crystals growing from solution. Previous work on high-temperature solution growth of $KTiOPO_4$ identified solution inclusion as a common flawing effect [13,24]. From the first attempts in the present project to grow crystals to sizes much beyond the initial stages of

seeded growth, it was clear that solution inclusion flawing was an important issue to be addressed.

Although solution inclusion flaws have for centuries been a recognized feature of many crystals, only in the past several decades has a reasonable mechanistic description of their formation begun to be assembled. The interfacial instability giving rise to solution inclusion is generally a subtle function of a large number of independent variables. Further, the measurement and control of these variables necessary for effective experimentation is in practice often a monumental undertaking. As such, as generally recognized by those commenting on the subject [31], quantitative description or prediction of solution inclusion phenomena in actual crystal growth processes is not currently possible. Nonetheless, a partially verified qualitative model of interfacial instability in crystal growth from solution does exist and it is here that one must turn in approaching practical problems involving solution inclusion flawing.

The qualitative model for currently understanding interfacial instability and liquid inclusion in crystal growth from solution has as its basis two separate but related phenomena. The first is the layer by layer mode of interface attachment operative on the atomically smooth surfaces of crystals growing from solution. The second is the variation in supersaturation over the growing crystal surfaces brought about through the interplay of the fluid convection over and around the advancing surfaces with the interface attachment process itself.

As discussed in Section 2.3, there are essentially two mechanisms for layer by layer interface attachment: repeated formation and enlargement of "pillbox" nuclei of growth units, and growth unit attachment to edges of self-sustaining spirals generated by the intersection of screw dislocations with the surface. Through either mechanism, trains of steps emanate laterally over and across a growth surface from their point of origin. The advance of a growth step is sustained through the arrival of growth units at the step edge either directly from the liquid solution phase or via surface diffusion from other sites of adsorption from the liquid.

Normally, in the case of uniform and stable growth, the propogation of growth steps across a surface occurs more rapidly than their generation, thereby accounting for the maintenance of a crystal's macroscopically facetted habit. In certain situations, however, due apparently to any of a number of factors, the propogation of growth steps can become impeded. If the rate of step generation remains constant or nearly so, the result is a "pileup" of growth steps in the vicinity of the growth impediment. Such a pileup, by in turn influencing the condition that led to the original impediment, can effect an unstable situation whereby overlying steps at the top of the pileup advance more rapidly than steps at the bottom. The result is trapping and inclusion of solution.

The most common factor contributing to the slow-down of propogating growth steps and subsequent trapping and inclusion of solution is the variation of supersaturation across a growing surface, as depicted in Figure 16. Here, steps entering a region of decreasing interfacial supersaturation slow down due to decrease in availability of additional growth units to sustain propogation. Additional steps approach from the rear, their progress sustained by the locally higher level of interfacial supersaturation. If the pileup that results effects in turn a condition whereby the upper layers in the pileup have greater access to growth units, that is, they experience a higher level of interfacial supersaturation, than the lower layers, an overhang will develop, the propogation of which amounts to solution trapping and inclusion.

A number of phenomena are involved in the interfacial supersaturation profile around a crystal growing from solution. For the common case of forced convection established through imposed motion of the crystal, the corners and edges of the facetted body generally experience the most efficient mass transfer with the bulk of the growth liquid, and thus, the highest interfacial supersaturation levels. By comparison, regions near the centers of growing faces generally experience the lowest interfacial supersaturation levels. Another important phenomenon is that of boundary layer separation leading to the formation of stable, closed eddies of growth solution positioned over certain regions of a growth surface. By feeding the propogation of growth steps

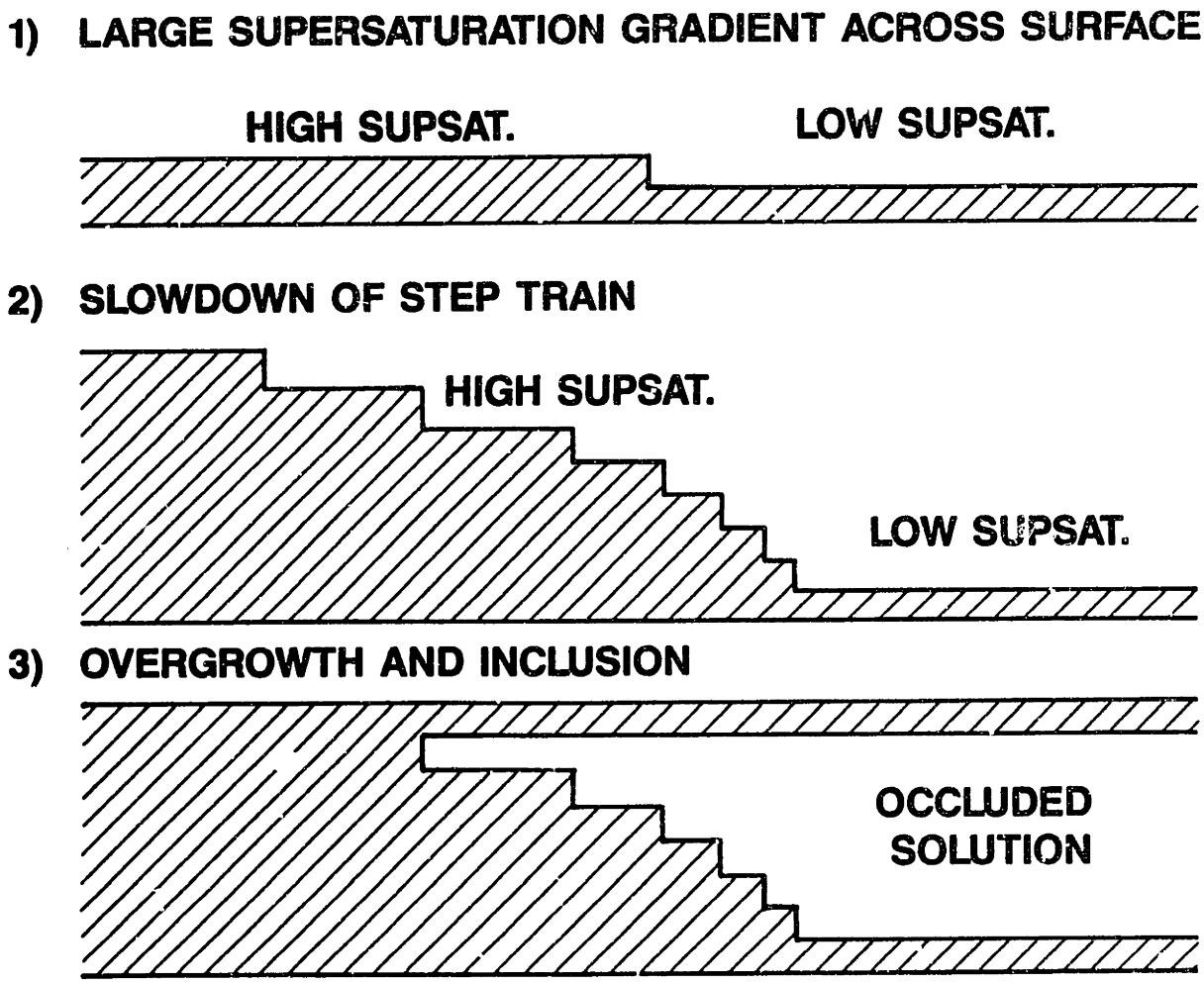

Figure 16. Step pileup leading to liquid inclusion (schematic)

through a region, a closed recirculating eddy positioned over that region can become depleted in solute. The result can be a sharp interfacial supersaturation gradient at the edge of the region under the eddy [69-70].

The tendency toward solution inclusion due to an interfacial supersaturation gradient effect increases both with increasing bulk supersaturation level and increasing crystal size. The range of possible supersaturation variation across a growing surface must be supposed to increase with increasing bulk supersaturation level and crystal surface area. An important additional effect is contributed by a change in growth mechanism. At low levels of bulk supersaturation, the most common interface attachment mechanism on atomically smooth surfaces is growth on spiral steps generated by screw dislocations. Statistically, the growth centers corresponding to screw dislocations tend to be located in the central regions of growing faces [31]. Step propogation is thus generally in a direction outward from the center to the edges of the faces, normally a stable situation in which the growth steps propogate into regions of higher interfacial supersaturation. As the level of bulk supersaturation increases, however, so does the tendency toward a surface nucleation growth mechanism. Surface nuclei naturally tend to form on regions of the growth surface where interfacial supersaturation is highest, commonly near face edges. The growth steps generated by such surface nucleation events thus necessarily propogate into regions of lower interfacial supersaturation.

It should be underscored that step propogation into a region of decreasing interfacial supersaturation does not necessarily lead immediately to solution inclusion. The points to be noted are simply (i), step propogation into a region of increasing interfacial supersaturation is necessarily stable and (ii), if the magnitude of an unfavorable supersaturation gradient reaches a critical level, step pileup, overgrowth, and inclusion can possibly result.

Given this current qualitative model for interfacial instability and liquid inclusion in crystal growth from solution, practical approaches to ameliorating inclusion problems in growing cry-

stals to a desired size consist of either reducing the prevailing level of bulk supersaturation or attempting to establish solution convection patterns less likely to effect undesirable gradients in interfacial supersaturation.

7.3 Experiments on Inclusion Flawing

A complete characterization of the interfacial stability phenomena involved in the growth of $KTiOPO_4$ in the heat pipe furnace system on even a qualitative level would require an extensive amount of additional experimentation and analysis beyond what was undertaken in the present project. The goal of the experiments performed and reported here was simply to determine a set of process conditions in the system that would enable the growth of large $KTiOPO_4$ crystals free from solution inclusions. To accomplish this, qualitative understanding of interfacial instability in crystal growth from solution as just presented was brought to bear in concert with the solution flow visualization techniques described in Chapter 5. With an eye toward viability in an eventual production process, it was necessary in addition that the establishment of such conditions take into account the desirability of maximizing both the crystal growth rate and the achieveable size of a grown crystal.

For all of the experiments discussed in this Section, the seeding process involved the initial slight dissolution of the original seed surfaces and thus, as covered in Section 6.4, initially flaw-free growth immediately beyond the inclusion veil outlining the seed. All seeds were drilled and threaded parallel to the crystallographic $\vec{a}$ direction and were screwed onto the ends of solid platinum seed rods, as described in Section 6.2.

As discussed in the last Section, for crystals of a given desired size, the basic practical approaches to avoiding solution inclusion flawing consist of either lowering the prevailing level of bulk supersaturation or effecting a convection pattern that more evenly exposes all areas of the growing crystal surfaces to well-mixed growth liquid. For the present work, it was chosen to

focus strictly on the latter approach of improving convection and therefore the same bulk supersaturation program, as established by the furnace cooling program, was applied in all the experiments on solution inclusion. The furnace cooling program selected was a constant linear ramp of 5 °C/day. As covered in Section 6.4, such an effected level of bulk supersaturation appeared to be low enough to enable good initial growth off a seed, regardless of the convection pattern. At the same time, it was felt that such a supersaturation program would yield an overall growth rate high enough to be viable for a production process. It should be noted that, due to the continuous increase in crystal surface area over the course of a growth run, such a linear cooling rate could be expected to effect a bulk supersaturation level tha' actually decreased with roughly the two-thirds power of time. Thus, built into the selection of the furnace cooling program was a natural provision for decreasing supersaturation with increasing crystal size.

The following discussion presents experiments performed on four different crystal orientation configurations. As indicated schematically in Figure 17, the configurations differed in the angle of a bend in the seed holding rod, roughly 12 mm from the threaded end where the seed was attached. For all four configurations, the rod was immersed to a depth in the solution whereby the seed was positioned midway between the liquid surface and the crucible bottom. The experiments on these different orientation configurations and in fact even the selection of the configurations themselves involved an iterative process consisting of a combination of both flow visualization experiments performed as described in Chapter 5 and actual crystal growth experiments performed using the heat pipe based furnace system.

7.3.1 0° Crystal Orientation

The first crystal orientation configuration investigated involved mounting the seed on the end of an unbent seed rod, rotating about its own central $\vec{a}$ axis. This corresponds to the 0° orientation shown in Figure 17. The initial attraction of this configuration was its allowance for the largest possible crystal to fit in a crucible of given size. Thus, if flaw-free crystals could be

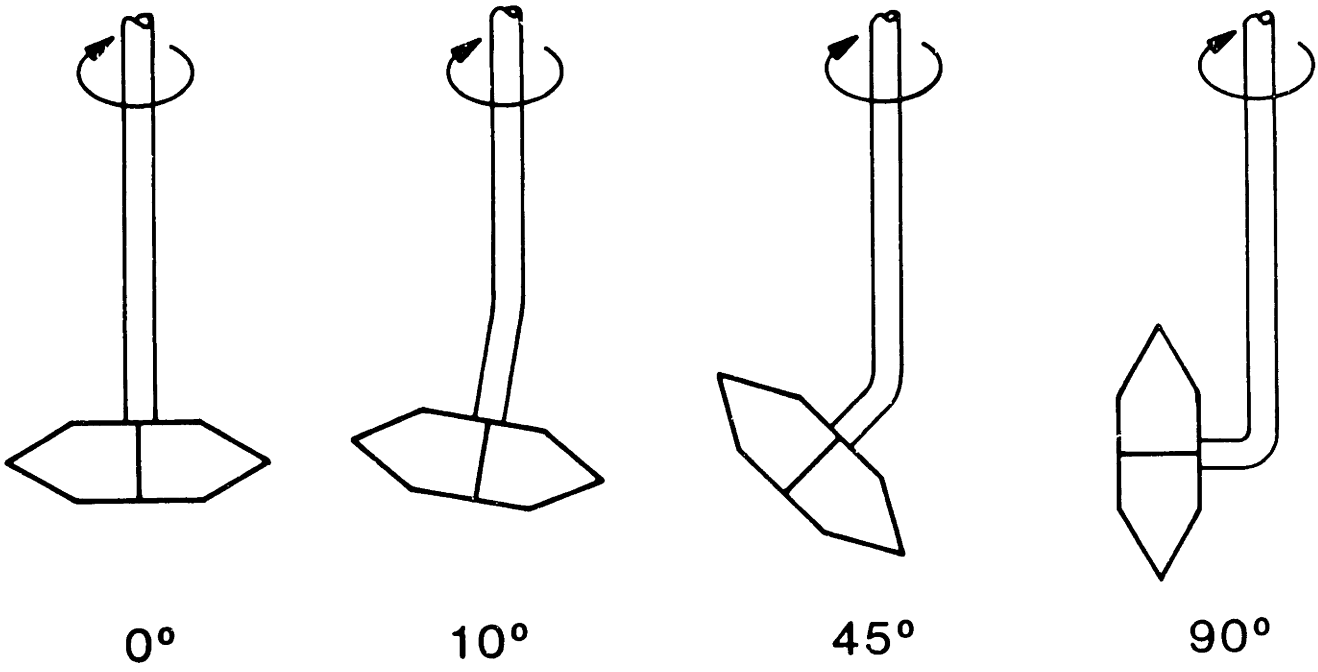

Figure 17. Crystal orientation configurations studied (schematic)

grown using this configuration, it would be ideal from the standpoint of $KTiOPO_4$ production efficiency.

Five crystal growth experiments were performed in the heat pipe furnace system employing this 0° configuration. Crystal rotation rates ranged from 10 to 70 RPM. Experiments were performed both with and without rotation reversal. For most experiments, rotation direction was reversed every 14 seconds, including a 4 second pause.

For all the experiments, the solvent inclusion flawing effects were essentially the same. Figure 18 shows two views of a crystal grown using the 0° orientation configuration. As shown, a thin region of solution inclusion flaws formed in the plane of rotation midway along the $\vec{a}$ dimension of the crystal. The flaws began to form after some time into the growth process, beyond the initial seeding stage. They appeared to first form in the centers of the side-facing {011} facets, the facets whose normals lie in the plane of crystal rotation. The flawing became more pronounced as growth progressed. Crystalline material both above and below the central planar flawed region appeared generally visually clear and flaw-free. In the several experiments performed without rotation reversal, the flawed region appeared to be thicker in the $\vec{a}$ dimension.

Flow visualization experiments were performed to analyze the corresponding forced convection patterns. Scaled rotation rates corresponding to actual crystal rotation rates of from 10 to several hundred RPM were investigated, as were the effects of crystal size and of rotation stoppage and reversal. The basic steady-state flow pattern found to correspond to the entire range of crystal sizes and rotation rates employed is shown schematically in Figure 19. The important feature to notice about the pattern is the flow relative to the side-facing {011} facets. As shown, the steamlines passing over the side-facing facets both down from the top and up from the bottom of the crystal separate from the vicinity of the facet surfaces very near the facet edges, moving with radial velocity components directed away from the facet surfaces. The

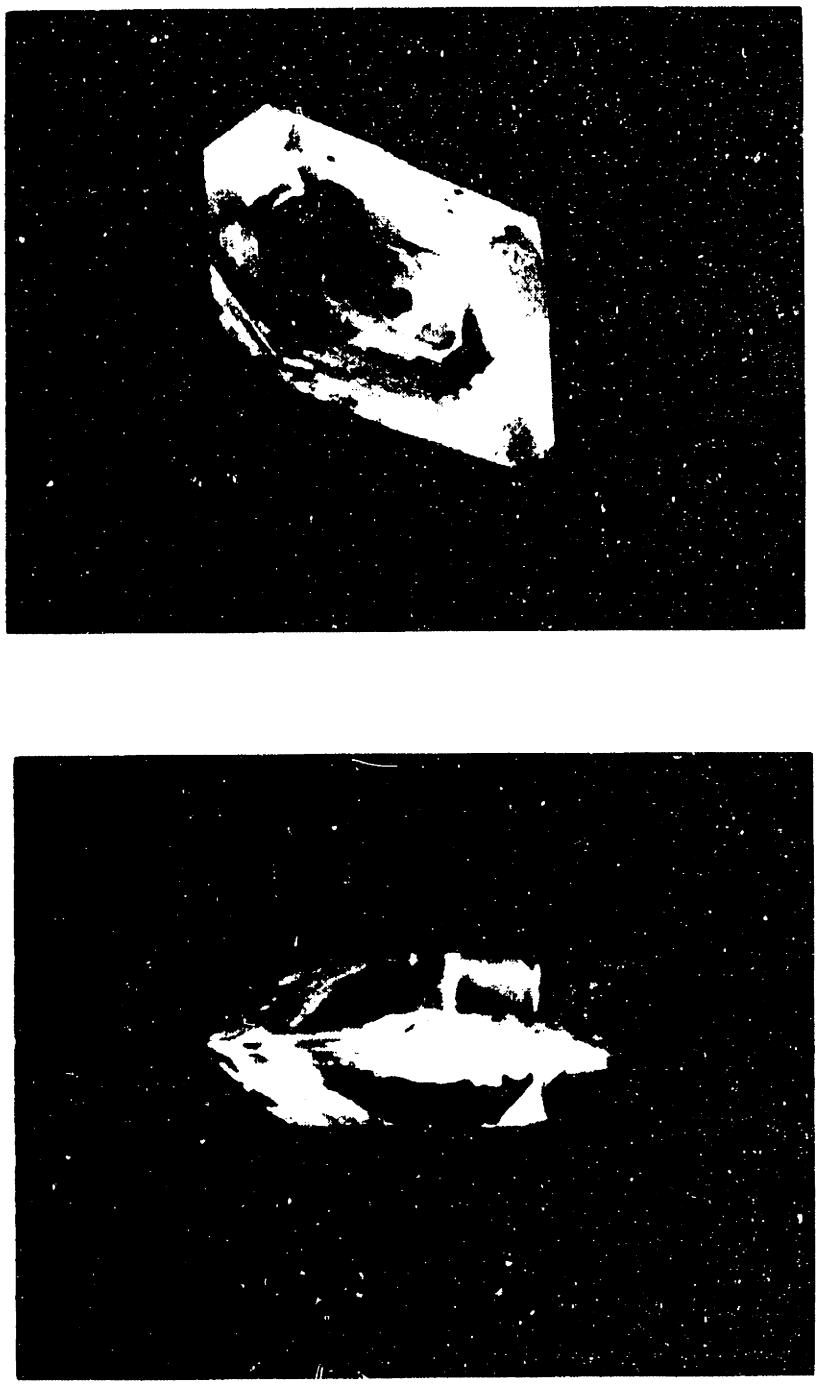

Figure 18. Typical crystal grown using 0 orientation (Top view down $\vec{a}$ axis, bottom view down $\vec{c}$ axis)

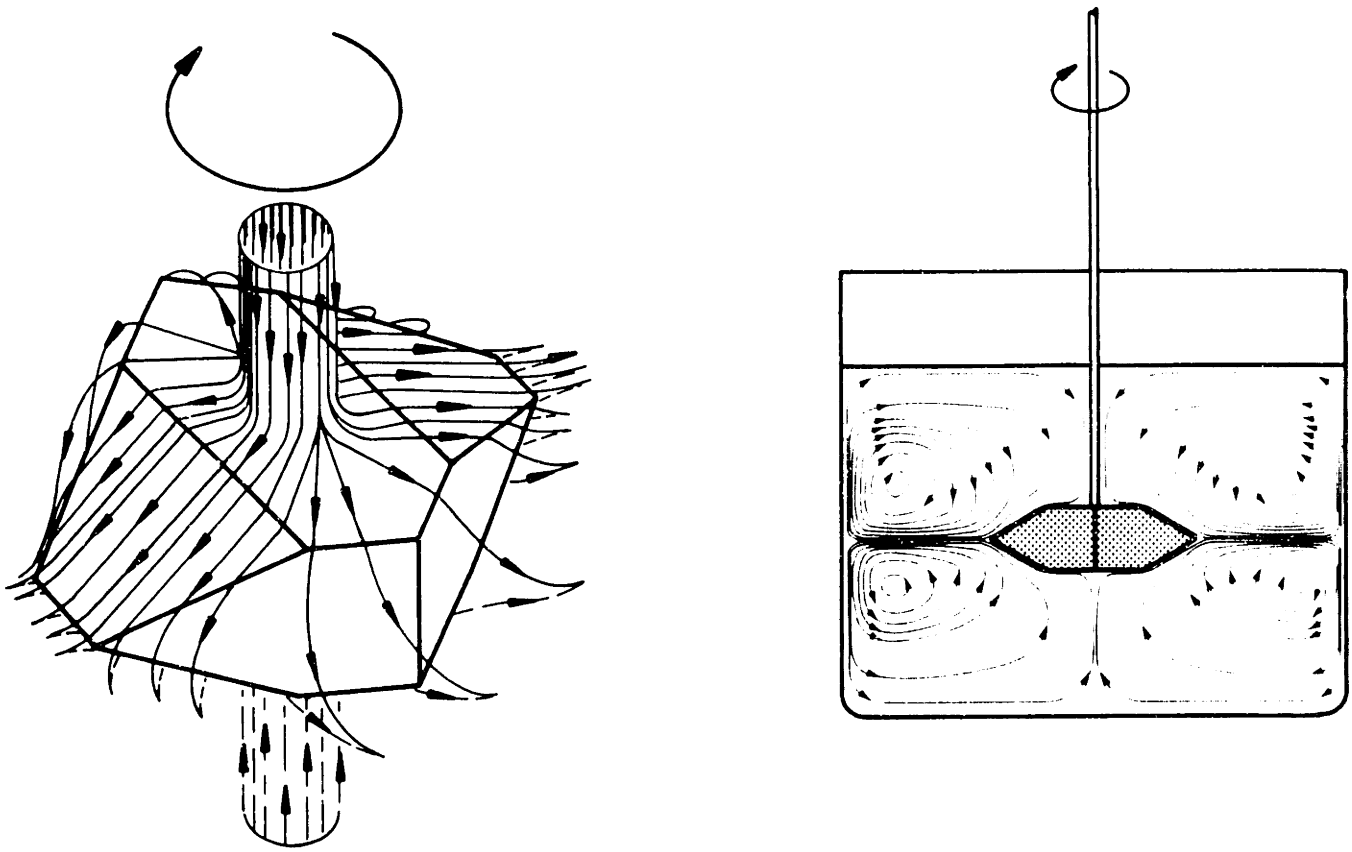

Figure 19. Flow streamlines for 0° crystal orientation

downward-directed and upward-directed streamlines meet in a central horizontal plane of flow symmetry at a radial distance from the side-facing facets corresponding to a significant fraction of the major dimension of the crystal itself.

The primary consequence of this flow separation over the side-facing facets is the existence on each side of the rotating crystal of a region of unstirred fluid bounded by the separating streamlines on two surfaces and the side-facing facet surfaces on the other. These regions of unstirred fluid rotate along with the crystal, interacting minimally with the bulk of the moving fluid. At the rotation rates applied, rotation stoppage and reversal was observed to not effect the shedding and replenishment of the unstirred regions.

Turning this analysis toward consideration of the crystal growth experiments, qualitative interfacial stability theory would suggest that, if the prevailing level of bulk supersaturation were sufficiently high, growth on the side-facing facets would occur via a surface nucleation interface attachment mechanism. Due to the proximity of the facet edges to the relatively fast-moving solution streamlines, the surface nuclei would be expected to form near these edges. Growth step motion would therefore be in directions inward from the edges over the side-facing facet surfaces. Due to the existence of the regions of stagnant solution over these surfaces, growth step motion would thus be in directions of decreasing interfacial supersaturation, a potentially unstable condition. After depletion of solute in the unstirred regions, the supply of growth units to these propogating steps would presumably have to involve either bulk diffusion through the unstirred regions or surface diffusion from points near the relatively well-supplied facet edges. Therefore, if interfacial instability were to occur giving rise to solution inclusion flawing, it would be expected on the basis of this model to occur in the vicinity of the centers of the side-facing facets, the locations farthest from sources of growth units, an expectation corresponding with the solution inclusion flawing effects actually observed in the crystal growth experiments.

Lacking the ability to pursue meaningful quantitative analysis based on the model of interfacial instability, and given the goal of establishing a forced convection pattern that would enable growth of $KTiOPO_4$ free from solution inclusion flaws, it was felt reasonable to assume that the observed flawing effects were a consequence of the observed flow stagnation effects in the manner described and to proceed on that basis to the investigation of other crystal orientation configurations.

7.3.2 10° Crystal Orientation

The second crystal orientation configuration investigated involved mounting the seed on the end of a seed rod featuring a 10° bend roughly 12 mm from its threaded end. This 10° orientation is illustrated in Figure 17.

Flow visualization experiments were performed for this orientation configuration over the same ranges in crystal size, rotation rate, and rotation reversal periodictiy as were investigated for the 0° orientation. In all cases, the flow fields observed were qualitatively similar to those observed in using the 0° orientation, the presumably important feature being the existence of stable regions of stagnant solution over the {011} facets.

A single crystal growth experiment was performed using this 10° orientation configuration. It featured a 50 RPM rotation rate with rotation reversal every 14 seconds, including a 4 second pause. The resulting pattern of solution inclusion flawing was similar to that observed for the 0° orientation, the sole difference being that, corresponding to the 10° angle between the crystallographic $\vec{b} \cdot \vec{c}$ plane and the imposed plane of crystal rotation, the plane of solution inclusion flawing was oriented at a 10° angle relative to the $\vec{b} \cdot \vec{c}$ plane in the crystal.

Considerations of interfacial instability parallel to those outlined above for the case of the 0° crystal orientation suggested that the onset of solution inclusion flawing effects should be expected to occur in locations on the {011} surfaces farthest from potential sources of growth

units to sustain step propogation. Given the orientation of the crystal, these locations correspond to the intersection of the {011} surfaces with a plane parallel to the imposed plane of rotation passing through the center of the crystal. The generated flawing pattern in the grown crystal conformed to this expectation.

7.3.2 45° Crystal Orientation

The third crystal orientation configuration investigated involved a 45° bend in the seed rod, as shown in Figure 17. Flow visualization experiments were performed for this orientation configuration over the same ranges in crystal size, rotation rate, and rotation reversal periodicity as were investigated for the 0° and 10° orientations. Two distinct flow regimes were observed, dependent on the size of the crystal but relatively independent of the rotation rate. For small sizes of the crystal, the crystal traversed through the fluid at some distance from the axis of rotation. The steady-state flow field for rotation in one direction featured fluid streamlines passing over the crystal surfaces on all but the trailing facets where a wake effect dominated, involving closed recirculating eddies of trailing solution. Rotation reversal was observed to be effective in breaking up this wake effect.

For large sizes of the crystal, the region of the crystal nearest the crucible bottom was effectively rotating in place, no longer traversing through the fluid. The steady-state flow field for this situation was observed to feature a region of stagnant liquid off the bottom of the crystal, rotating along with the motion of the crystal. Rotation stoppage and reversal was observed to be ineffective in breaking up this flow stagnation.

A single crystal growth experiment was performed using the 45° crystal orientation configuration, featuring a rotation rate of 50 RPM with reversal every 14 seconds, including a 4 second pause. Initial growth off the seed was visually flaw-free and continued as such to a greater extent than was observed in the crystals grown using 0° and 10° orientations. Solution

inclusion flawing appeared to be initiated on the approximately bottom-facing facets of the crystal in a plane roughly parallel to the imposed plane of rotation. The flawing became more extensive as growth progressed.

Based on the model of interfacial instability and the results of the growth experiments involving the first two crystal orientations, the correspondence between the observed flow patterns and flawing effects could be explained as follows. At the early stages of growth, the only elements of flow stagnation were due to a wake effect and were periodically broken up by rotation reversal. The result was sufficient exposure of all the growing surfaces to sources of growth units from the bulk of the solution and correspondingly flaw-free growth in all directions. As the crystal increased in size, a second stagnation effect not subject to break-up developed off the bottom-facing facets of the crystal. By a mechanism presumably similar to that responsible for the solution inclusion flawing in the first two cases studied, flawing was initiated in the central regions of the surfaces of these bottom-facing facets and worsened with further growth.

7.3.4 90° Crystal Orientation

The final orientation configuration investigated involved a 90° bend in the seed rod, as shown schematically on the far right of Figure 17. In this case, the initial crystal growth experiments were performed in advance of flow visualization. Following the results of the investigations on the other three crystal orientations, it was reasoned that the only flow stagnation phenomena accompanying such a 90° crystal orientation would result from wake effects and therefore be subject to break-up thrcugh periodic rotation reversal. The sort of stable flow stagnation effects assumed to be responsible for the solution inclusion flawing in the crystals grown using the other three orientation configurations would thus be avoided and the initial prospects for flaw-free growth were attractive.

Four crystal growth runs were attempted using this 90° orientation configuration. In all of

these growth experiments, the rotation rate used was 50 RPM with periodic reversal every 14 seconds, including a 4 second pause. With one exception, the crystals grown were free from solution inclusion flaws beyond the initial seeding veil. In the exceptional case, a temperature controller malfunction resulted in a temporary spike in the furnace temperature, causing a slight additional veil in the grown crystal. The largest crystal grown measured 1.7 cm in the $\vec{a}$ direction by 4.0 cm in the $\vec{b}$ direction by 3.3 cm in the $\vec{c}$ direction and, given the orientation geometry, essentially occupied all the available space in the growth crucible.

Flow visualization experiments were performed to confirm the predicted flow patterns. As anticipated, the major feature was the wake effect on the trailing facets of the traversing crystal. Rotation reversal was observed to successfully break up the related flow stagnation.

7.4 Discussion

There are two major points to be noted following the results of the experiments on solution inclusion flawing in $KTiOPO_4$ crystal growth in the heat pipe furnace system. First, the qualitative model of interfacial instability and liquid inclusion in crystal growth from solution was put to good use in the present work. Although quantitative prediction was not possible, the model enabled the correlation of the flawing effects observed in the crystal growth experiments with the flow patterns observed through room-temperature simulation. Such correlation proved to be critical to establishment of a crystal orientation configuration enabling flaw-free growth. To the author's knowledge, such practical application of qualitative interfacial instability theory is uncommon in investigations into solution crystal growth.

Second, with the discovery of a crystal orientation configuration enabling flaw-free growth of $KTiOPO_4$ crystals to sizes limited only by the dimensions of the furnace cavity, the project goal stated in Chapter 1 of developing improved technological capacity for production of $KTiOPO_4$ was directly and dramatically achieved. Figure 20 shows two $KTiOPO_4$ crystals grown in the

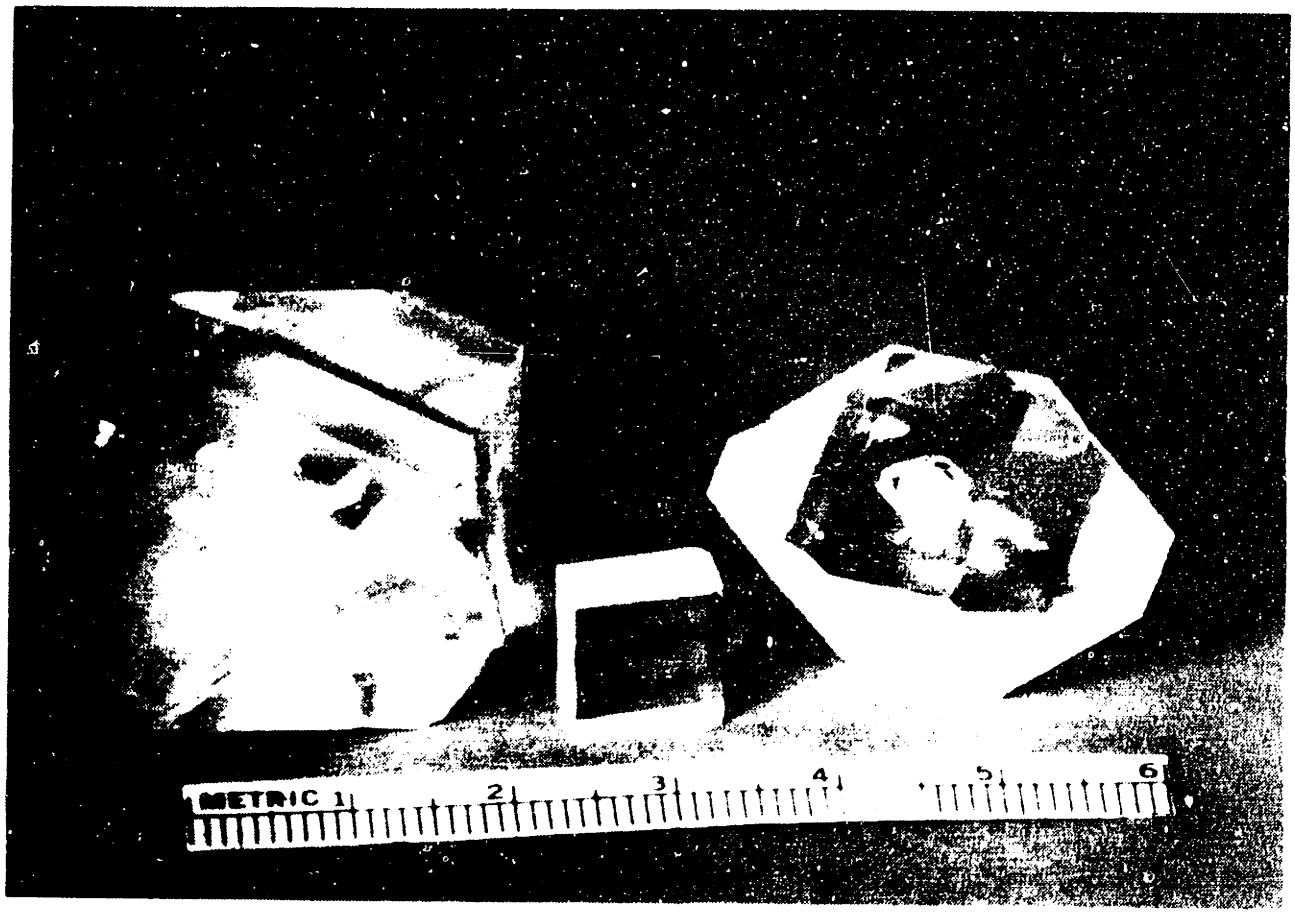

Figure 20. Inclusion-free crystals and fabricated plate grown using 90 ° orientation

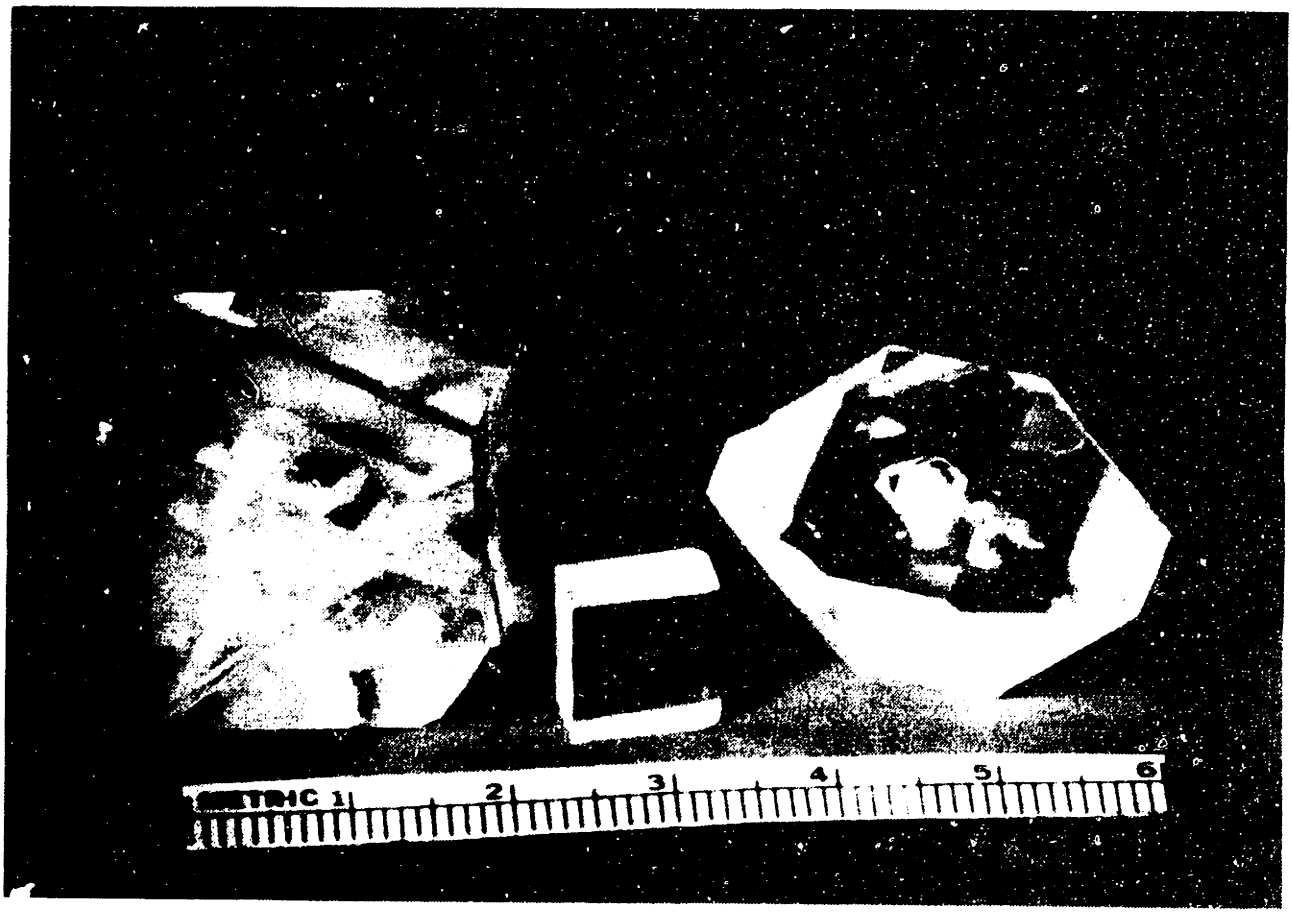

Figure 20. Inclusion-free crystals and fabricated plate grown using 90° orientation

heat pipe furnace system along with a plate cut from a third crystal, oriented and polished along the proper direction for efficient second harmonic generation. As far as the author is aware, these represent the largest visually flaw-free crystals of $KTiOPO_4$ growable on a routine basis from high-temperature solution. The time required for the process is roughly 10 days.

Chapter 8

Characterization of Material Grown

8.1 Introduction

As should be clear from the discussions presented so far, unlike many projects directed toward the development and improvement of a crystal growth process, intimate involvement with sophisticated materials characterization techniques was not a requisite component of the present work. Given the nature of the major problems addressed, specifically, spurious nucleation and solution occlusion flawing, in general, visual inspection and standard optical microscopy provided sufficient feedback to guide further experimentation and analysis throughout the course of the project.

Nevertheless, it was felt desirable both to verify that the crystalline $KTiOPO_4$ produced through the techniques described herein was not inferior to that produced by other growth techniques and also to attempt to motivate second-generation crystal growth work aimed at further control over the properties of the material. For these reasons, a series of standard characterization experiments was performed on crystals grown in the heat pipe based furnace system. This Chapter presents the results of these experiments.

8.2 Purity

A number of experiments were aimed at determining the chemical purity of the grown crystals. The primary applications of $KTiOPO_4$ are in optical devices operating in the visible and near-infrared range of the spectrum. As such, the critical impurities to be avoided are, in general, transition metal species which cause optical absorption in this range.

Several samples were analyzed for impurities through semi-quantitative spark source mass

spectroscopy [71]. The main advantages of this technique are first, it allows for relatively efficient testing for a wide range of species, and second, it rarely yields false negative results. Thus, it can be applied to quickly eliminate from consideration the majority of elements that are clearly not present in significant amounts. For purposes of the present analysis, concentrations below 5 ppm were considered insignificant.

Following the identification by spark source mass spectroscopy of impurity elements possibly present in concentrations greater than 5 ppm, an additional series of samples was analyzed by inductively coupled plasma (ICP) spectroscopy. Although involving more elaborate techniques, ICP in general offers greater precision in establishing impurity concentration levels than does spark source mass spectroscopy. ICP could thus be applied to rule out any false positives resulting from the earlier analysis and to more accurately quantify the concentration levels of impurities that were significant.

Table 2 presents the major impurities detected. The sodium contamination presumably corresponds to the sodium found in the K_2HPO_4 starting material, as discussed in Section 3.2. The platinum presumably originated from slight crucible corrosion.

In addition to the spark source mass spectroscopy and ICP analyses, optical transmission spectroscopy was performed on polished crystalline samples of $KTiOPO_4$. The equipment used was a Perkin-Elmer Model 283 spectrophotometer for the infrared region and a Perkin-Elmer Model 330 spectrophotometer for the visible and ultraviolet region. The samples were parallelpipeds oriented along the principal crystallographic axes measuring 2.5 x 2.5 x 2.5 mm^3 and polished to within one-eighth of a wave at 580 nm with a standard scratch/dig specification of 5/10.

Figure 21 shows the resulting combined IR and UV/visible transmission curves. The UV cutoff is at roughly 350 nm, typical of $KTiOPO_4$ samples grown by other techniques [13,20]. The

ELEMENT	CONCENTRATION (ppm)
Ca	5.0
Na	41.0
Pt	6.3
Zr	10.0

Table 2. Impurities detected in $KTiOPO_4$ grown in system

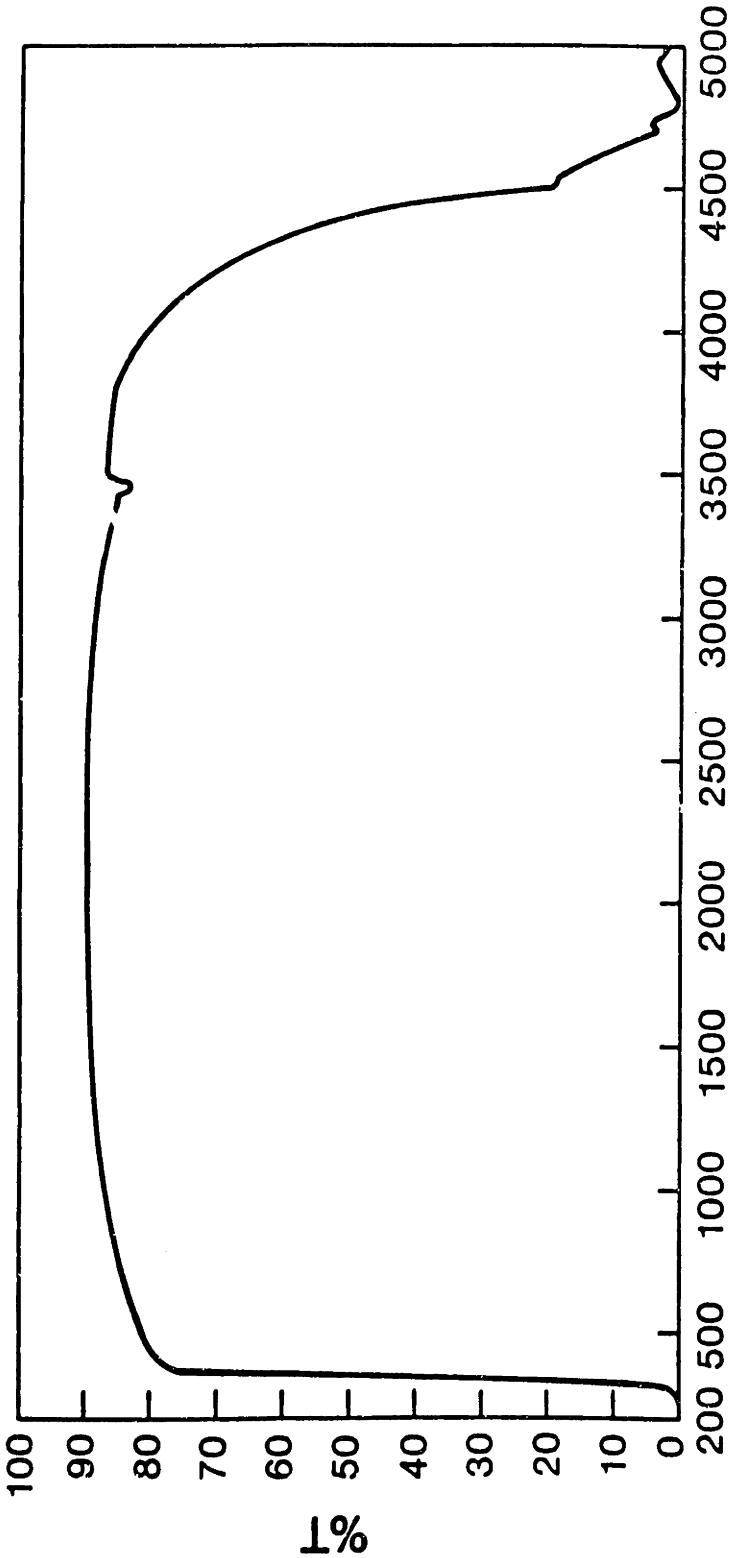

Figure 21. Optical transmission of $KTiOPO_4$ grown in system

dip in the transmission curve near 3500 nm is due to an overtone from a lower frequency phosphate or titanate resonance. A slight absorption at 2800 nm, too small to be seen in the Figure, is indicative of the presence of OH^- species in the crystal. The probable origin of the OH^- involves the incomplete reaction of the potassium hydrogen phosphate starting materials, as discussed in Section 3.2. It should be noted that, although a quantitative comparitive measurement was not made, typical of $KTiOPO_4$ grown from HTS, the OH^- concentration was much less than that commonly found in $KTiOPO_4$ grown hydrothermally [20].

8.3 Second Harmonic Generation and Electro-Optic Measurements

As mentioned in Section 1.2, currently, the primary specific application for $KTiOPO_4$ single crystals is in second-harmonic generation of laser radiation, particularly that from Nd:YAG. Near the end of the present project, due to interest generated by the crystal growth work reported in earlier Chapters, facilities and resources became available for more elaborate material characterization measurements specially relevant to this application. Although these characterization experiments were not performed by the author, a brief highlighting of their results is included here for the sake of completeness.

A Q-switched Nd:YAG laser was employed in the measurements. It featured a beam energy of 46 mJ, a pulse width of 8 nsec, and a beam diameter of 2.7 mm. $KTiOPO_4$ single crystalline samples were oriented and fabricated with optical faces (flatness to one-eighth wave at 580 nm, parallelism within 5 seconds of arc, scratch/dig of 5/10) perpendicular to the second harmonic generating direction. Based on a convention where the unit cell dimensions are in the order $\vec{a} > \vec{b} > \vec{c}$, this direction lies in the $\vec{a} \cdot \vec{c}$ plane, 23° from $\vec{a}$ toward $\vec{c}$.

For a typical set of experiments performed on a prepared $KTiOPO_4$ specimen 8 x 8 mm^2 in cross-section and 3.5 mm in path length, the doubling efficiency was measured to be 25%, the wavefront distortion less than one-quarter wave, the temperature bandwidth 22 °C·cm, and the

angular bandwidth 26 mrad·cm in the $\vec{a} \cdot \vec{c}$ plane [72]. These values are roughly equivalent to the best reported for $KTiOPO_4$ grown by other techniques.

8.4 Ferroelectricity & Domains in $KTiOPO_4$

$KTiOPO_4$ is reported to undergo a paraelectric to ferroelectric phase transition on cooling, with a transition temperature of roughly 936 °C [73]. $KTiOPO_4$ single-crystalline specimens produced through other growth techniques have been found in many cases to contain multiple ferroelectric domains [74]. In general, the presence of such multiple domains severely degrades the performance of devices incorporating the crystals. In many instances, high-temperature poling can be performed, albeit involving the risk of potentially undesirable side effects on the material [74]. In instances where the domain structure is associated with a significant strain field, poling can be impossible [74]. As such, it is generally preferable for as-grown $KTiOPO_4$ crystals to consist of single-domain material.

A number of $KTiOPO_4$ crystals grown in the heat pipe furnace system were reportedly examined for the presence of multiple ferroelectric domains [74]. Without exception, all the crystals examined were reported to consist of single-domain material. It is not yet clear how or to what extent the growth process influences the presence or absence of multiple ferroelectric domains. Further investigation into the issue of ferroelectric domains in $KTiOPO_4$ grown in the heat pipe based furnace system is presently in progress [75].

Chapter 9

Summary, Conclusions, & Outlook

9.1 Project Synopsis

The development of a practical production process for single crystals of the important non-linear optical material $KTiOPO_4$ was undertaken as a case study in crystal growth from high-temperature solution. Following selection of the previously-reported high-temperature solvent composition $K_6P_4O_{13}$, a preliminary analysis was performed of the expected growth process kinetics. The results of the analysis were applied in establishing design criteria for a furnace system for growth of $KTiOPO_4$ from its solution in $K_6P_4O_{13}$.

Two identical furnace systems were built. They enabled top-seeded growth of $KTiOPO_4$ by a slow cooling process and each featured an annular heat pipe liner providing for a high degree of spatial temperature uniformity in the central furnace cavity. The achieved thermal field enabled avoidance of copious spurious nucleation, a common problem with other furnace systems used in previous attempts to grow $KTiOPO_4$ from solution.

A series of high-temperature viscosity and density measurements was made on $KTiOPO_4$-$K_6P_4O_{13}$ growth solutions employing one of the heat pipe based furnace systems. The gathered data were used in establishing a room-temperature flow visualization facility for experimental analysis of fluid convection patterns prevailing in the crystal growth process. Due to the high degree of spatial temperature uniformity throughout the growing crystal and surrounding solution in using the heat pipe based furnace systems, the possibility of natural buoyancy-driven convection could be neglected with the dynamic similarity flow visualization based strictly on forced convection effects due to imposed crystal rotation.

An extensive set of experiments was devoted to investigation of the effects of seed orientation and attachment, fluid convection, and bulk supersaturation on initial seeded growth using the furnace systems. The preferred seed attachment technique involved ultrasonically drilling and threading a small $KTiOPO_4$ crystal and screwing it onto the end of a threaded platinum seed rod. The achievement of initially uniform and flaw-free growth off a seed crystal was determined to require the controlled dissolution of the original seed surfaces prior to initiation of supersaturation and consequent growth.

An additional set of experiments was devoted to treatment of a chronic flawing problem whereby volumes of growth solution would become trapped and included in growing crystals. Room-temperature flow visualization analyses and crystal growth experiments in the heat pipe based furnace system were correlated through application of a recently-developed qualitative model of interfacial instability in crystal growth from solution. A crystal orientation configuration was thereby established enabling flaw-free growth of $KTiOPO_4$ crystals to sizes limited only by the dimensions of the furnace cavity.

The overall process developed through the project enables production of the largest flaw-free crystals of $KTiOPO_4$ growable on a routine basis from high-temperature solution. Crystalline plates 10 x 10 x 7 mm^3 oriented in the optimal direction for second-harmonic generation can be fabricated from crystals produced in 10-day growth runs with properties measured to be at least as good as $KTiOPO_4$ crystals grown by other methods.

9.2 Major Conclusions

As discussed in the Introduction, the research project presented in this thesis was directed toward two principal objectives. First, it was expected that the information acquired and techniques established would lead to improved capacity for producing high-quality single crystals of the important optical material $KTiOPO_4$. Second, it was intended that the work serve as a

well-developed case study in HTS crystal growth in general, involving the exploration of new growth technology, the examination of prevailing theory, and the application of novel heuristic approaches.

In the area of $KTiOPO_4$ crystal growth technology, the progress made through the present project is clear. The overall process developed, including the use of the heat pipe based furnace system, controlled seeding with initial surface dissolution, and the so-called 90° crystal orientation configuration, enables efficient, reproducible growth of flaw-free crystals of $KTiOPO_4$ to sizes never before achieved. Current plans call for the process to be on line in a commercial production mode by mid-1987 [76]. It is anticipated that the expanded capacity for $KTiOPO_4$ crystal production will have a significant impact on the extent of future applications of the material.

In the case of HTS crystal growth in general, the contributions of the present work are somewhat less tangible but probably more significant overall. First, the preliminary analysis of the crystallization kinetics in the system, although an uncommon undertaking in developing a growth process from HTS, proved to be especially fruitful. Despite its necessarily approximate and intuitive character, the analysis enabled insights that were extremely useful throughout the project, guiding the initial furnace design and pointing out the possibility of analogy with crystal growth operations from aqueous solution. Based on these observations, it appears that such preliminary kinetic analysis could profitably be considered a standard first step in similar future process development projects.

Second, the present work provided clear evidence of the importance of thermal field characteristics in HTS crystal growth operations. Historically, thermal field considerations have received little emphasis in HTS crystal growth process development. In the present project, careful attention to achievement and control of the thermal profile throughout the environment of the growing crystal enabled both the establishment of desirable thermal process conditions

and also meaningful and therefore useful modelling and analysis of additional aspects of the process. Also noteworthy is the first successful application of heat pipe technology in a bulk crystal growth operation from solution.

Third, the practical applicability of the qualitative theory of interfacial instability in crystal growth from solution was demonstrated for the first time in an HTS crystal growth operation. Solution inclusion flawing phenomena were modelled, analyzed, controlled, and eventually eliminated through a relatively small number of experiments guided by insights provided through this qualitative model.

Finally, to offer a general conclusion based on the entire project, the overall success of the work reported herein boldly underscores both the possibility and the potential benefit of attempting to replace experimentation based on trial and error with understanding of fundamental process mechanistics in approaching practical problems in crystal growth from high-temperature solution.

9.3 Further Issues Beyond this Work

It is appropriate as a final topic to consider some of the further issues suggested but not addressed through the project reported herein. A number of specific questions were raised directly in the course of the present work. First, although it was determined empirically that initial dissolution of original seed surfaces was required in order to achieve flaw-free growth immediately off a seed crystal, the mechanistic basis for the limitation was not clarified. Second, although measurements on crystals grown in the heat pipe furnace system showed them to consist of single ferroelectric domains, an explanation for this observation awaits further analysis. Third, the question of OH^- incorporation remains largely unsettled. It is not yet clear whether OH^- is necessarily to be avoided in $KTiOPO_4$ crystals. If it is, the source of OH^- incorporation in the present process requires clarification. Elimination of OH^- incorporation could

involve variation in the nature of the starting chemical components or even measures to control the atmosphere above the growth solution.

A final set of specific questions concerns the scale-up of the present process to enable growth of larger $KTiOPO_4$ crystals. Can a different approach to crystal orientation or supersaturation programming with the present furnace system enable the growth of larger flaw-free crystals from the same sized crucible? If not, will a purely geometric scale-up of the present furnace system result in a furnace system with adequate thermal field conditions to enable the growth of correspondingly scaled-up flaw-free crystals?

In addition to these immediate questions, several long-range issues can be identified as warranting investigation. First, the present project focused strictly on what may be termed "macroscopic" effects such as spurious nucleation and solution inclusion flawing. Following the progress herein reported in these areas, the stage is now set for detailed examination on a microscopic scale of processing/defect/property relationships in $KTiOPO_4$ directed toward further control over material properties and corresponding improvement in device performance. It can be anticipated that such examination would involve attention to such factors as dislocation structures, growth sector boundaries, and impurity incorporation effects.

A second area of long-range interest concerns the extension of the methods developed in the present project to other HTS crystal growth systems. A number of materials identified as possessing attractive properties suiting them for potentially important device applications are currently limited by their inability to be prepared as single crystals of sufficient size and quality via standard HTS growth techniques. Notable among these are the non-linear optical materials $KNbO_3$ and β-BaB_2O_4, and the solid-state laser host $KNdP_4O_{12}$. The potential benefits of focusing the present results on such longstanding HTS crystal growth problems may be enormous.

Finally, from a general perspective, it remains to be seen whether, through further efforts like the present project, the scientific and technological basis for HTS crystal growth can be

developed to the point where its current status as a "last resort" method can be displaced by a critical and respected position among standard materials processing techniques.

References

1. D. Elwell and H.J. Scheel, "Crystal Growth from High-Temperature Solutions", Academic Press, 1975.
2. R.D. Dawson et. al., J. Crystal Growth, 23 (1974) 65.
3. M.L. Ouvrard, Computes Rendu, 111 (1890) 177.
4. R. Masse and J.C. Grenier, Bull. Soc. Fr. Mineral. Cryst., 94 (1971) 437.
5. I. Tordjman et. al., Z. Fur Krist., 139 (1974) 103.
6. F.C. Zumsteg et. al., J. Appl. Phys., 47 (1976) 4980.
7 J.D. Bierlein and C.B. Arweiler, Appl. Phys. Lett., 49 (1986) 917.
8. T.E. Gier, U.S. Patent 4231838, 1980.
9. T.E. Gier, U.S. Patent 4305778, 1981.
10. G. Gashurov and R.F. Belt, in "Tunable Solid State Lasers for Remote Sensing", R.L. Byer et. al., eds., Springer-Verlag, 1985, 119.
11. R.F. Belt and G. Gashurov, U.S. Government Report AFWAL-TR-85-1185, 1986.
12. R.A. Laudise et. al., J. Crystal Growth, 74 (1986) 275.
13. J.C. Jacco et. al., J. Crystal Growth, 70 (1984) 484.
14. W. Tolksdorf and F. Welz, in "Crystals - Growth, Properties, and Applications", C.J.M. Rooijmans, ed., Springer-Verlag, 1978.
15. J.C. Jacco, private communication.
16. A.L. Aleksandrovskii et. al., Sov. J. Quantum Electron., 15 (1985) 885.
17. N.I. Pavlova et. al., Sov. Phys. Cryst., 31 (1986) 87.
18. Y.G. Liu et. al., MRS Meeting Abstracts, 1985.
19. D. Shen and C. Huang, MRS Meeting Abstracts, 1985.
20. A.A. Ballman et. al., J. Crystal Growth, 75 (1986) 390.
21. A.A. Ballman, private communication.
22. J.R. Van Wazer, "Phosphorous and Its Compounds", Interscience, 1958, 608.
23. J.C. Jacco and G.M. Loiacono, unpublished data.
24. J.C. Jacco and G.M. Loiacono, U.S. Government Report DAAK20-83-C-0139, 1986.
25. G.H. Gilmer et. al., J. Crystal Growth, 8 (1971) 79.
26. A.E. Nielsen, "Kinetics of Precipitation", Macmillan, 1964, 32.
27. E. Kirkova and R. Nikolaeva, Cryst. Res. and Tech., 18 (1983) 743.
28. J. Novotny and F. Moravec, J. Crystal Growth, 11 (1971) 329.
29. R. Janssen-Van Rosmalen et. al., J. Crystal Growth, 29 (1975) 342.
30. M. Rak, Zesz. Nauk.-Politech. Lodz. Fiz., 7 (1984) 25.
31. W.R. Wilcox, J. Crystal Growth, 65 (1983) 133.
32. Dynatherm, Inc., Cockeysville, MD.
33. S.W. Chi, "Heat Pipe Theory and Practice", Hemisphere, 1976.

34. E.P. Martin et. al., J. Electrochem. Soc., 126 (1979) 284.
35. T.J. Jasinski and A.F. Witt, U.S. Patent 4597949, 1986.
36. Thermal American Fused Quartz, Montville, NJ.
37. Mellen, Inc., Penacook, NH.
38. Zircar, Inc., Florida, NY.
39. Heraeus-Amersil, Inc., Sayreville, NJ.
40. Newport Research Co., Fountain Valley, CA.
41. Electronic Control Systems, Inc., Fairmont, WV.
42. Eurotherm Co., Reston, VA.
43. Hewlett-Packard Co., Palo Alto, CA.
44. Keithley Instruments, Inc., Cleveland, OH.
45. W.M. Rohsenow and H.Y. Choi, "Heat, Mass, and Momentum Transfer", Prentice-Hall, 1961, 108.
46. W.M. Rohsenow and H.Y. Choi, op. cit., 102.
47. W.M. Rohsenow and H.Y. Choi, op. cit., 524.
48. R.B. Bird, et. al., "Transport Phenomena", Wiley, 1960, 409.
49. J.R. Van Wazer, op. cit., 779.
50. Aldrich Chemical Co., Milwaukee, WI.
51. MCB Manufacturing Chemists, Inc., Cincinnati, OH.
52. Perkin-Elmer Co., Norwalk, CT.
53. Brinkmann Instruments, Inc., Westbury, NY.
54. Thermolyne Co., Dubuque, IA.
55. Lindberg Co., Watertown, WI.
56. Brookfield Engineering Laboratories, Stoughton, MA.
57. Scientech, Inc., Boulder, CO.
58. J. Bockris et. al., "Physicochemical Measurements at High Temperatures", Butterworths, 1959.
59. C.M. Lawrence, Thesis, Portsmouth Polytechnic, 1976.
60. W.D. Kingery, "Property Measurements at High Temperatures", Wiley, 1959.
61. C.F. Callis et. al., J. Am. Chem. Soc., 77 (1955) 1471.
62. J.C. Jacco, Mat. Res. Bull., 21 (1986) 1189.
63. F. Rosenberger and G. Muller, J. Crystal Growth, 65 (1983) 91.
64. J.C. Brice, "Crystal Growth Processes", Blackie, 1986, 147.
65. P.S. Chen et. al., J. Crystal Growth, 47 (1979) 43.
66. Creare, Inc., Hanover, NH.
67. S. Motakef, private communication.
68. M.H. Frommer and T.F. McGee, private communication.
69. R. Janssen-Van Rosmalen et. al., Cryst. Res. and Tech., 13 (1978) 17.
70. R. Janssen-Van Rosmalen and P. Bennema, J. Crystal Growth, 42 (1977) 224.

71. Ledoux Co., Teaneck, NJ.
72. R.A. Stolzenberger et. al., unpublished data.
73. V.K. Yanovskii et. al., Sov. Phys. Solid State, 27 (1985) 1508.
74. J.D. Bierlein, private communication.
75. G.M. Loiacono, private communication.
76. Ferroxcube, Inc., Saugerties, NY.

Biographical Note

Peter Bordui, a native of Sturgeon Bay, Wisconsin, entered the Massachusetts Institute of Technology as a freshman in September of 1978. He was graduated in May of 1983 with both Bachelor's and Master's of Science Degrees from the Department of Materials Science and Engineering. As an undergraduate, Bordui was elected to membership in the Phi Beta Kappa and Tau Beta Pi honor societies and the Sigma Xi scientific research society. He was also awarded the 1981 Professor Morris Cohen Materials Science Prize from the Boston Chapter of the A.I.M.E for superior performance in the study of materials science.

Bordui entered a doctoral program in M.I.T.'s Department of Materials Science and Engineering in June of 1983. His doctoral studies were supported in entirety by North American Philips Laboratories, Briarcliff Manor, New York. From June of 1984 through December of 1986, Bordui was in residence at Philips Laboratories as a Member of the Research Staff, pursuing research contained in this thesis document. He will be graduated in February of 1987 with the Degree of Doctor of Philosophy in Ceramics.

Bordui has authored or co-authored fifteen papers in the field of crystal growth and properties of non-linear optical materials. His professional affiliations include the American Association of Crystal Growth and the Materials Research Society.